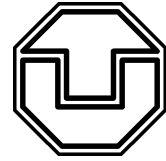


Institut für Theoretische Physik
Fachrichtung Physik
Fakultät Mathematik und Naturwissenschaften
der Technischen Universität Dresden



A theory of Plasma Membrane Calcium pump function and its consequences for presynaptic calcium dynamics

Diplomarbeit
zur Erlangung des akademischen Grades
Diplom - Physiker

vorgelegt von

Michael Graupner

geboren in Annaberg-Buchholz am 9. August 1977

Juli 2003

1. Gutachter: Prof. Dr. Gerhard Soff
2. Gutachter: Priv.-Doz. Dr. Markus Bär

Datum des Einreichens der Arbeit: 31. Juli 2003

Abstract

Towards a deeper understanding of long-term effects at the synapse, molecular mechanisms, capable to encode activity-dependent calcium elevations, become more interesting. The calcium- and calmodulin-dependent stimulation of the Plasma Membrane Calcium (PMCA) pump can sense the frequency and intensity of intracellular Ca^{2+} signals by its modifiable activity. The stimulation effect ranges on a time scale of minutes, which clearly exceeds the time period of the common synaptic signal transmission (ms) and could possibly be a link in the signal cascade towards long-term modifications. A new model of this calcium- and calmodulin-dependent PMCA pump stimulation process is introduced and analytical expressions for experimental observables are deduced in order to determine the model parameters on the basis of specific experiments. Furthermore a model for the pumping activity is developed. The conjunction of the description of calcium pumping and the stimulation model fully and correctly simulates PMCA pump function. Therewith the model enables to draw conclusions from and make propositions about the biological processes involved in PMCA pump activity and so far undone measurements. The presented model provides the possibility to characterise different pump isoforms by different type-specific parameter sets and can serve as a tool for calcium dynamics simulations. Implemented as module in the presynaptic calcium dynamics model, the consequences for the calcium dynamics and a theoretical proposition of a signature of the pump stimulation are acquired. This implementation calls for an investigation of the cooperating affinities of the calmodulin protein for calcium and the target proteins for the calmodulin-calcium complex. New insights in the concerted intracellular calcium - calmodulin - target protein interaction are revealed.

Zusammenfassung

Hin zu einem genaueren Verständnis möglicher Induktionsmechanismen von Lang-Zeit Effekten an der chemischen Synapse sind molekulare Mechanismen besonders interessant, welche die Fähigkeit besitzen, aktivitätsabhängige intrazelluläre Calcium Entwicklungen zu speichern. Die calcium- und calmodulinabhängige Stimulation der Plasma Membran Calcium (PMCA) Pumpe setzt die Frequenz und Intensität von Calcium-Signalen in erhöhte Pumpaktivität um. Dieser Stimulationseffekt findet auf einer Zeitskala von Minuten statt und überschreitet damit deutlich die Dauer einer einfachen synaptischen Signalübertragung (ms) und könnte eine mögliche Verbindung in der Signalkaskade hin zu synaptischen Lang-Zeit Veränderungen sein. Ein neues Modell des Stimulationsprozesses wird eingeführt und analytische Ausdrücke für experimentelle Observablen werden abgeleitet. Diese ermöglichen die Festlegung der Modellparameter auf der Basis spezifischer Experimente. Des Weiteren wird ein Modell für die Pumpaktivität entwickelt. Die Verbindung zwischen diesen beiden Modellen beschreibt die Funktion der PMCA Pumpe vollständig und korrekt. Das ermöglicht die Ableitung von Schlußfolgerungen über mögliche, der PMCA Pumpen Aktivität zugrundeliegende, biologische Vorgänge und Voraussagen für noch nicht vorgenommene Messungen. Das eingeführte Modell bietet die Möglichkeit, die verschiedenen Pumpisoformen in Parametersätzen zu charakterisieren, und kann als Modul in Calciumdynamiksimulationen eingesetzt werden. Die Einarbeitung in die präsynaptische Calciumdynamik ermöglicht die Herausarbeitung von Konsequenzen für die Dynamik und die theoretische Vorhersage einer Signatur der Pumpenstimulation. Diese Implementierung zieht eine Untersuchung der zusammenwirkenden Affinitäten des Calmodulinproteins für Calcium und der Zielproteine für den Calmodulin-Calciumkomplex nach sich, womit neue Einblicke in das abgestimmte intrazelluläre Zusammenspiel von Calcium - Calmodulin und Zielproteinen gewonnen werden.

Contents

1	Introduction	1
2	The base units of the nervous system - the neurons - and how they communicate	5
2.1	Structure of and signalling in and between Neurons	5
2.2	Synaptic Calcium dynamics	10
2.3	Long-term effects: LTP/LTD	17
3	A theory of Plasma Membrane Calcium pump function	21
3.1	The calmodulin protein	21
3.2	The Plasma Membrane Calcium pump	27
3.3	Current status of PMCA pump stimulation models	29
3.3.1	Measurement of Plasma Membrane Calcium pump activity	29
3.3.2	Previous models	31
3.4	The new Model of PMCA pump stimulation	33
3.4.1	Stimulation	36
3.4.2	Relaxation	41
3.4.3	Stimulation dynamics	45
3.5	Modelling the PMCA pump activity	48
3.5.1	Pumping activity and stoichiometry	49
3.5.2	Pumping parameter determination with steady-state pump activity	54
3.6	Comprehensive PMCA pump dynamics	58
3.7	Discussion of the PMCA pump model	61
4	PMCA pump stimulation in presynaptic calcium dynamics	69
4.1	PMCA pump affinity	69
4.2	Intracellular calcium - calmodulin - target protein homeostasis . .	74
4.3	Implementation in the presynaptic calcium dynamics model . . .	82
4.4	Consequences of the pump stimulation for the calcium dynamics .	86
5	Discussion and Conclusions	91
	Acknowledgement	95
	Bibliography	97

*If the Lord Almighty had consulted me
before embarking on creation I should have
recommended something simpler.*

Alphonso X (Alphonso the Wise), 1221-1284
King of Castile and Leon (attributed)

1 Introduction

The human brain consists of approximately 100 billion nerve cells (neurons), which are the functional base units of the nervous system. According to their size and shape, they can be classified into different types. However they comprise all the same constituents and similar functions. To understand how the complex processing and storage of perceptions and cognitions work one requires knowledge on several levels. On the basis of single cells the properties of neurons and how they interact are of interest. But due to the small structural and functional diversity of neurons, the complexity does not emerge from single cells but is founded in a sophisticated network structure. This is reflected in an average number of 10.000 synapses - the connections between neurons - per neuron. Moreover storage - meaning learning and memory - needs mechanisms within neurons and of the neuronal network which allow alterations of signal processing. In turn, these changes leading to states of cognition are consequences of signalling patterns to which the network of neurons are exposed. External perceptions cause these stimuli. Therewith the nervous system is capable to adapt the behaviour of organisms to their external environment.

On the basis of neurons the changeability has been attributed to long-lasting activity-dependent changes in the efficacy of synaptic communication. In 1972 experimental support for such an assumption was delivered. Repetitive activation of excitatory synapses in the hippocampus caused an increase in synaptic signal transmission strength that could last for hours or even days. The effect is known as Long-Term Potentiation (LTP) and has since been popular as an underlying cellular memory mechanism below the time scale of cell growth and differentiation. Over the past 30 years this long-lasting synaptic enhancement has been the object of intense investigations. It has been proven difficult to elucidate the detailed cellular and molecular changes forming the basis of LTP. Alongside with a consistent terminology in the current understanding some aspects of the involved molecular processes still remain unclear. One of the subjects of an ongoing debate is the question whether the modifications characterising LTP occur on the post-, pre- or extrasynaptic side.

Regarding the connection between induction conditions for long-lasting synaptic modifications and the expression state of these, processes provoke interest, which are capable to encode the intensity and frequency of intracellular calcium elevations. The Plasma Membrane Calcium (PMCA) pump can translate increased intracellular calcium concentrations into a higher persistent activity. The stimulation effect ranges on a time scale of minutes and therewith clearly exceeds the

time period of the single synaptic signal transmission. Though the stimulation is obviously not a significant expression form of long-term effects (> 60 min), it can constitute a sensitive link in the signal cascade leading to long-term modifications.

Caride *et al.* have published a model of the PMCA pump stimulation in conjunction with measurements of the dynamical stimulation behaviour [1]. The problems of that model call for further improvements. At first the stimulation parameter cannot be deduced from the measured data. Secondly, the stimulation rate of the pump can be arbitrarily increased by raising the calcium concentration in the model. Whereas converging experimentally measured stimulation constants call for a limitation by a maximum value at high calcium concentrations.

The model introduced here separates the stimulation as well as the relaxation into two steps and introduces rate limiting reactions. An analytical approach enables to deduce the required rate constants from measurements. Beside the stimulation model also the calcium pumping activity is considered. This joined model of stimulation and pumping is therefore capable to serve as a tool for simulations in a wide variety of systems such as membranes or single cells. For that purpose the same way of function is assumed for all pump isoforms and the different isoforms are characterised by type specific sets of parameters, which are classified to have universal or specific properties. Universal parameters are postulated to have system-independent properties. These parameters typically describe single pump protein properties, such as affinities for calcium or transport rates. Specific parameters depend on the pump under consideration or on the details of the experimental setup. This concerns the surface density of membrane proteins, for example.

The presented joined model of stimulation and pumping is in agreement with the available experimental data of the calcium- and calmodulin-dependent PMCA pump activity. Furthermore stimulation behaviour of so far undone measurements are predicted [2].

Special emphasis is placed on the consideration of the impact of the pump stimulation on presynaptic calcium dynamics. The modular architecture of the model and the distinction between specific and universal parameter provide appropriate preconditions to incorporate the model in various calcium dynamics simulations including PMCA pumps. For that purpose the interaction of calcium and calmodulin as well as the binding of the calmodulin-calcium complex to target proteins has to be adjusted to cytosolic conditions in order to account for the concerted interaction of all these participants.

With the implementation of the PMCA stimulation model in the presynaptic calcium dynamics this work enquires for a signature of the pump stimulation within neuronal calcium homeostasis. Furthermore the question whether the plasticity of the PMCA pumps is involved in the signal cascade leading towards long-term modifications or establishes an expression state of short-term effects is addressed in the investigations. And if so, it will be explored how that possible

integrations become prominent.

The first chapter of this diploma thesis is supposed to introduce the basics of nerve cell assembly and function. A short survey of signalling within neurons will be concluded with established mechanisms leading to and expressing long-term effects. In the second chapter the new model of Plasma Membrane pump function will be introduced and adapted to experimental data. The implementation of the developed model in presynaptic calcium dynamics is under consideration in the third chapter. Finally, the assumptions, achievements and outcomes are summarised and discussed at the end of the second chapter concerning the pump model and at the end of the thesis related to the synaptic calcium dynamics.

2 The base units of the nervous system - the neurons - and how they communicate

The nervous system consists of two different cells types: nerve cells (*neurons*) and glia cells (*neuroglia*). There are approximately 100 billion neurons in the nervous system whereas the number of glia cells exceeds the number of neurons about 10 to 50 times. Though glia cells are not involved directly in signalling they play critical rolls in controlling the environments of the nerve cells as well as being intimately involved in many of their functions. Glia cells support the nerve cells structure or serve as insulation of axons in form of myelin, for example.

The functional task of neurons is signalling. Their every aspect - their size, shape, cellular organisation, development, and organisation within the nervous system - is shaped by their specific functions of receiving, organising and transmitting informations. The connectivity within the network of about 100 billion neurons is provided by synapses, the points where the information is transmitted from one nerve cell to the other.

This chapter starts with a short introduction of the nerve cell structure and the signal transmission within neurons and at the synapse. Alongside with the signalling outline, the synaptic signal transmission model of the Research Group Theoretical Biophysics at the Technische Universität Dresden will be presented [3, 4]. Finally, possible induction and expression mechanisms of activity-dependent changes of synaptic signal transmission efficacy are explored.

2.1 Structure of and signalling in and between Neurons

Structure Although neurons have various morphologies, they all share similar constituents, which identify them as neurons (see figure 2.1). The neuron, like all other mammalian cells, is bound by a plasma membrane. Across the membrane exists an electrical potential of about 60-70 mV (see “Signal transduction” paragraph on page 7). The membrane encloses the cytoplasm with the nucleus, which accommodates the genes, consisting of the DNA and its associated proteins. The cell body - *the soma* - contains beside the nucleus the membrane organelles responsible for the synthesis and processing of cellular proteins. Depending on the processes emerging from the cell body the extentions from it can be classified in *axons* and *dendrites*.

On average, one to nine dendrites emerge from the soma and then divide successively to a highly branched dendritic tree with specific characteristics for each

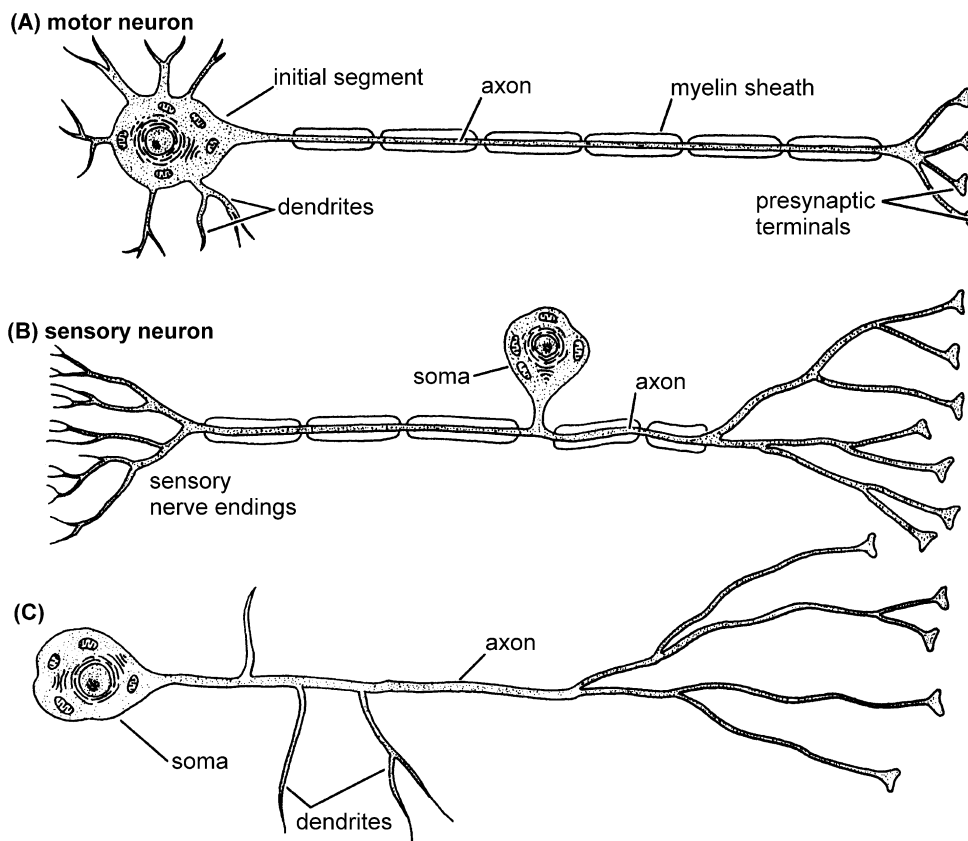


Figure 2.1: Diverse forms of neurons

(A) A conventional neuron form the vertebrate central nervous system in which both axons and dendrites extend from the cell body.

(B) A vertebrate sensory neuron in which the proximal regions of the axon and dendrite are fused into a single process.

(C) A invertebrate neuron in which the cell body is connected to an extensively branched dendritic tree from which the axon arises (picture taken from [5]).

neuronal population. They are morphologically distinct from axons by their irregular outline, by their diameter which decreases along their branches, by the acute angles between the branches and by their ultrastructural characteristics [6]. The differences between dendrites and axons in signal transport will be discussed in the “Signal transduction” paragraph.

The number of connections that a neuron makes can be extraordinarily large. Single neurons can receive signals from over 10,000 synapses on the surface of dendrites and the soma. This part therefore constitutes the main receptive area of neurons. In order to respond to afferent information dendrites either have direct junctions with the previous neuron (electrical synapse) or express receptors and other proteins necessary to convert the incoming chemical signal into an electrical signal (chemical synapse). The synaptic signal transmission process will be discussed in more detail in section 2.2. Electrical signals mean small depolarisations or hyperpolarisations of the membrane potential that are transported along the dendrites and integrated from all input channels at the soma.

Axons are distinguished from dendrites by their smooth appearance, their uniform diameter along their entire extent and their ultrastructural characteristics. They generally emerge at the level of a conical expansion of the soma but sometimes at the level of a primary dendrite (see neuron (C) in figure 2.1). Axons can transport electrical signals over a range from 0.1 millimetre up to 2 metres to the *presynaptic terminal*. Over that range axons are divided into one or several collaterals which form right angles with the main axon and give rise to multiple terminals. The axon and its collaterals may be surrounded by a sheath, the myelin sheath. Myelin sheaths are formed by glia cells and act as an isolator.

In spite of the general plan of cellular organisation that most neurons share, they exist in an extraordinary variety of sizes and shapes. This diversity allows flexibility in the signalling patterns and sites of synaptic connections.

Signal transduction As a consequence of the unequal distribution of ions across the membrane and because of the selective permeability of the membrane to them a difference in electrical potential across the surface membrane exists. The same principles underlie the complex signal processing of neurons. The *resting potential* across the membrane is about 60 - 70 mV negative to the extracellular fluid outside. Proteins in the membrane called transporters and pumps use metabolic energy to actively transport ions in and out of the cell, resulting in ion concentration gradients across the membrane responsible for the resting potential. The intracellular and extracellular concentration of the main ions involved are shown in table 2.1. These gradients represent a form of stored energy used by neurons to generate electrical signals. Attention should be drawn to the marked difference in cytosolic and extracellular calcium concentration. Though calcium is present in the cytosol at very low concentration (0.01-0.1 μM) and as bound Ca^{2+} ions

ion	intracellular concentration (mM)	extracellular concentration (mM)
K ⁺	140	3
Na ⁺	7	140
Cl ⁻	7	140
Ca ²⁺	0.0001	1.5

Table 2.1: Asymmetric concentration distributions of ions across the plasma membrane (terrestrial vertebrates) [6]

to proteins it is also distributed in organelles able to sequester calcium. These organelles include endoplasmatic reticulum, calciosome and mitochondria.

The signals in a neuron result from the opening and closing of *ion channels*. These are transmembrane proteins which facilitate the passive flow of specific ions across the membrane along their electrochemical gradient. The flow of ions through the channels constitute a current that changes the membrane potential resulting in *depolarisations* or *hyperpolarisations* of the resting potential. These changes vary in time and space and represent electrical signals.

In the following, a rough scheme of a signal transport in a single neuron will be outlined. Auxiliary to the text, a demonstrative sketch of the signalling in the respective part of the neuron is shown in figure 2.2.

The signalling connections between neurons are formed by synapses, which can be divided in two subtypes. *Chemical synapses* use neurotransmitter in order to bridge the synaptic cleft and provide the signal transmission. In contrast, *electrical synapses* or gap junctions are characterised by the apposition of the plasma membrane of the connected neurons. In this case, the ions flow directly from one cell to another without the use of transmitter. This work will deal with chemical synapses since they display a plasticity.

Preliminarily to the postsynaptic side can either be an upstream neuron, which expels neurotransmitter in the synaptic cleft or the terminal is exposed directly to a physical input signal such as arising from the expansion of a muscle, for example. However, in both cases the sensoric stimuli are transferred by the receptive surface to the extracellular space into either a depolarisation or a hyperpolarisations of the transmembrane potential, referred to as *synaptic potential*. The resulting signal encodes the input informations in its size and shape and is therefore an analog signal. The synaptic potential travels along the dendrite and decreases in size due to its passive transport. All incoming signals are propagated towards the *initial segment* at the soma and are integrated there. If at any moment the local potential at the initial segment exceeds a certain depolarisation threshold, an action potential is triggered, which travels down the axon. Depolarisations increase the probability of generating an action potential and are therefor called excitatory, whereas hyperpolarisations have an opposite effect and act inhibitory.

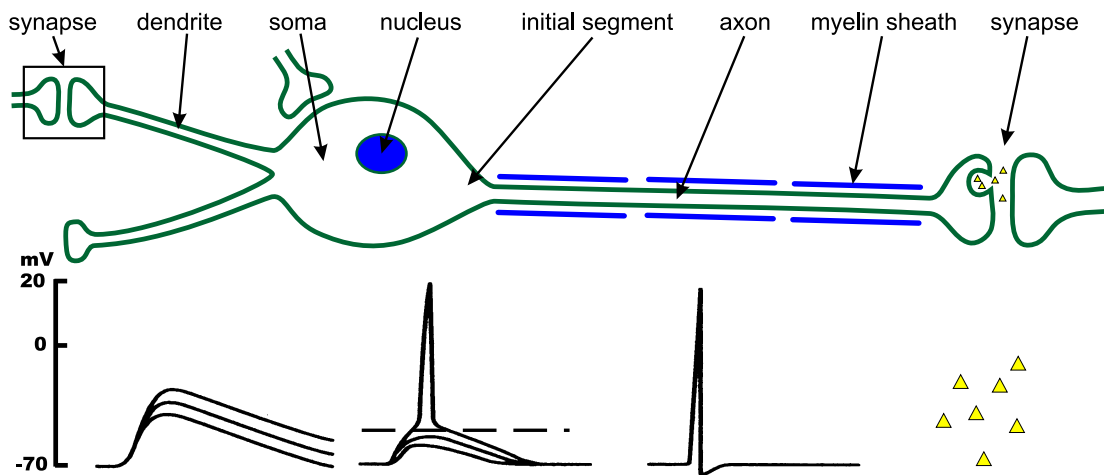


Figure 2.2: Main constituents and signalling of a neuron

The sketch depicts the main constituents comprised by all neurons. The kind of signals occurring in the respective part are shown in the lower half of the picture. A synaptic or physical input signal evokes a gradual synaptic potential. If all incoming integrated exceed a certain threshold at the initial element, an action potential is triggered which travels along the axon. At the axon terminal of the synapse the action potential increases the probability of neurotransmitter release into the synaptic cleft. See text for more details.

Action potentials are brief, stereotyped depolarisations of amplitudes up to 110 mV which convey signals rapidly and efficiently over long distances. In contrast to the graduated input signal - the synaptic potential, action potentials are actively self-propagating. The stereotyped property of all action potential is achieved by an “all-or-none” reaction at the initial segment once the threshold is passed. In a digital manner, action potentials encode information by their frequency. They mostly do not exceed durations of 1 ms. The propagation into nerve terminals triggers a signal cascade which finally leads to transmitter secretion. The signal transmission at the synapse is considered in more detail in the following sections. Inhibitory synaptic potentials are mainly mediated by chloride (Cl^-) ions and excitatory synaptic potentials as well as action potentials are mediated by sodium (Na^+) and potassium (K^+) ions. The alternating chain of electrical and chemical signals (see the lower part of figure 2.2) provides the capacity of efficient, fast information transport and simultaneously accessibility for activity-dependent changes in transmission efficacy.

With regard to learning and memory, what are the underlying neuronal cellular and molecular mechanisms? The ability of neurons to form new processes and new synaptic connections results in an ongoing modification of the synaptic circuit. Anyhow, this developmental form of plasticity acts on a large time scale

and the accessibility for changes below the time scale of cellular growth has to be assured. The whole signal transport from the synaptic potential to the action potential happens in a more or less deterministic manner. It has been suggested that the generation of action potentials at the initial segment undergoes modifications but substantiated experimental support for that assumption is lacking so far. Whereas many experiments have been performed investigating short- and long-term modifications of the synaptic response. Since the synapse displays the only well approved cellular plasticity it will be of special interest in the following considerations. An introduction in the synaptic signalling cascade in section 2.2 will be followed by the presentation of possible long-term effects at the synapse in section 2.3.

It should be noticed that the purpose of this section is to provide a general and short overview of the composition and function of neurons within the nervous system. The above described process of neuronal functioning is applicable to the vast majority of neurons. However, it is not accurate in detail for all neurons. The picture presented here has to be seen as a simplification of the neuronal diversity but is sufficient as preparation to understand the subsequent text. The books of Hall [5], Hammond [6] and Kandel [7] should be mentioned here for further readings.

2.2 Synaptic Calcium dynamics

This section introduces the biochemical mechanisms that have been identified to provide the signal transmission at the chemical synapse. Among the events leading to neurotransmitter release into the synaptic cleft, the connection between the local rise of the intracellular calcium concentration and the probability of vesicular exocytosis has been clearly established. Referring to this and since calcium is the main messenger for a vast array of processes involved in synaptic signalling the following introduction and investigation will concentrate on calcium dynamics of the pre- and the postsynaptic terminal. Herein the emphasis is laid on a signal cascade inducing an excitatory post-synaptic response. Accompanying to the text see also figure 2.3, which provides a summary of the basic steps involved in excitatory synaptic signal transmission.

The Research Group Theoretical Biophysics at the Technische Universität Dresden has developed a model of the signal transmission at the synapse [3, 4]. Physiological single protein descriptions of proteins involved in synaptic signal transmission are the basic principle of the model. The conjunction of these modules is used in order to simulate the synaptic signal cascade. For that purpose one distinguishes between universal and specific classes of parameters. Universal parameters are postulated to have neuron-independent properties. These parameters typically describe single membrane protein properties, such as affinities for calcium

or transport rates. Specific parameters depend on the neuron under consideration or on the details of the experimental setup. This concerns the surface density of membrane proteins as well as type and concentration of calcium indicators, for example. Concluding from the separation, the model provides a tool to quantitatively compare and simulate the results of different experiments and setups. The model contains no abstract parameters but only parameters which express physiological properties.

Simultaneously to the introduction in synaptic signalling, the presynaptic part of the theoretical synapse model is introduced. This work restricts to the presynaptic calcium dynamics model since the later developed theory of the Plasma Membrane Calcium pump will be applied there.

Presynaptic calcium dynamics An incoming action potential at the presynaptic terminal causes *Voltage Dependent Calcium channels* (VDCC) to open and therewith evokes an influx of calcium along its electrochemical gradient [8]. Recall that the intracellular Ca^{2+} concentration is at least 10.000 times smaller then the extracellular calcium concentration. The calcium influx current density J_v can be described with

$$J_v(U(t), Ca) = \rho_v O_v(U(t)) I_v(U(t), Ca). \quad (2.1)$$

The influx current is weighted by the surface density of VDCC pores ρ_v . $I_v(U(t), Ca)$ is the calcium current through a single pore, which is driven by the electrochemical gradient, reflected in the dependence on the transmembrane potential $U(t)$.

Note that the free intracellular concentration of Ca^{2+} ions, $[\text{Ca}^{2+}]_{\text{free}}$, is referred to as Ca in italic style. For simplicity this notation is applied throughout the whole work, *i.e.* roman style symbols refer to elements or proteins whereas italic style symbols denote concentrations or probabilities of the respective elements or proteins.

The voltage dependent opening probability is described by $O_v(U(t))$. The underlying gating mechanism is modelled by a minimal Markov model



including the probability of one open state O_v and one closed state C_v of the VDCC. The voltage dependent transition rates k are described as Boltzmannfactors. Utilising the probability conservation $C_v + O_v = 1$, the reaction scheme (2.2) can be translated in a differential equation of the opening probability

$$\frac{dO_v}{dt} = (O_\infty - O_v) \frac{1}{\tau}, \quad (2.3)$$

with the time constant $\tau = 1/(k_+ + k_-)$ and the asymptotic opening probability $O_\infty = k_+/(k_+ + k_-)$. This results in a single exponential time behaviour of

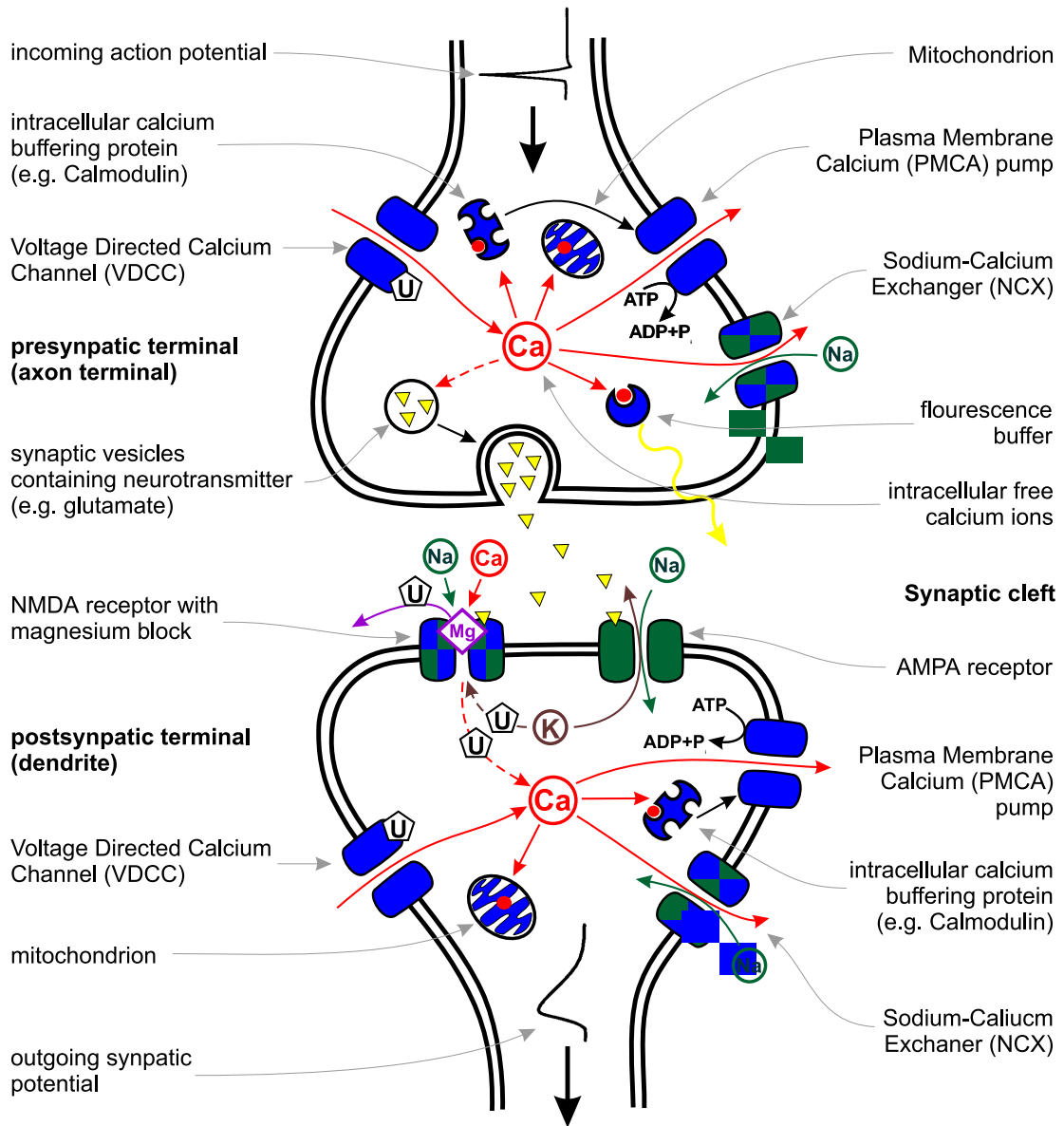


Figure 2.3: Signal transduction pathway at a chemical synapse

The major components involved in the signalling pathway are depicted. Note that due to place restrictions the respective charges of the ions Na^{+} , K^{+} , Ca^{2+} and Mg^{2+} are not shown. See text for a detailed explanation of the shown transduction process.

the opening probability O_v and accounts therewith for the delayed opening of the voltage-gated calcium channels. The voltage dependence of the asymptotic opening probability O_∞ is determined by the Boltzmannfactors k_+ and k_- and has a sigmoidal characteristic given by

$$O_\infty = \left(\exp \left((U_H - U) \frac{1}{\kappa} \right) + 1 \right)^{-1}. \quad (2.4)$$

U_H is the the half activation voltage and κ describes the steepness of the asymptotic opening probability. Although τ is also defined by the Boltzmannfactors k_+ and k_- it is treated to be constant justified by measurements of Magee *et al.* (1995) investigating the dynamical opening properties of VDCC's [9]. The influx current $I_v(U(t), Ca)$ is simplified to be linear of the form

$$I_v(U(t), Ca) = \bar{g}_v (\bar{U}_{Ca}(Ca) - U(t)), \quad (2.5)$$

where \bar{U}_{Ca} denotes the reversal potential of calcium corrected for the linear approximation and \bar{g}_v is the open pore conductivity.

In contrast to other descriptions of VDCC pores this ansatz involves only two possible states, C_v and O_v . In order to reproduce experimental data on time scales smaller than ms the implementation of intermediate steps is required. Bezanilla states a minimum of six sequential steps in order to account for the details of activation and reproduce gating current recordings [10]. For the purpose of the model presented here, this simplification is sufficient (for more informations see [10, 11]).

Within the cytosol, calcium is bound via intracellular calcium buffering proteins including parvalbumin, calmodulin, calretinin, calcineurin and calbindin-D_{28k}. Collectively, these mobile buffers absorb nearly 95 - 99 % of the total cellular calcium load, leaving the rest available as free calcium ions [6, 12]. On account of its importance for the Ca²⁺-dependent regulation of the activities of a vast array of different target proteins, the model includes calmodulin as buffer. Calmodulin has four high affinity calcium binding sites ($K_a = 10^6 - 10^7 \text{ M}^{-1}$ at low ionic strength [13]). The buffering of calcium by calmodulin will be considered in the next chapter since the fully liganded calmodulin-calcium complex also stimulates the Plasma Membrane Calcium pump.

Other neuronal calcium clearance mechanisms include calcium transport across the membrane into the extracellular space and calcium uptake by the plasma membrane of organelles and sequestration in intracellular organelles, e.g. by sacro/endo- plasmic reticulum calcium Adenosine Triphosphate (ATP)-dependent (SERCA) sequestration into the Endoplasmatic Reticulum, or mitochondrial uptake by a H⁺/Ca²⁺ uniporter [5, 12]. The here presented model does not include intracellular uptake in organelles. Moreover, it is one outcome of the model that with the components included in the model it is possible to correctly reproduce

measured presynaptic calcium dynamics [3], indicating that the implementation of intracellular uptake is not necessarily required on the examined time scale. However, the effect of intracellular calcium storage within organelles resembles the buffering of calcium by intracellular buffer proteins, except for the time scales of calcium release after sequestration. As the cytosolic concentration falls, the storage compartment slowly releases Ca^{2+} to be transported out of the cell [5]. It has been suggested by Schiegg *et al.* (1995) that the slow decay of intracellular calcium due to the slow release kinetics of intracellular stores plays an important role in the induction of LTP in the dendritic spine [14] (see section 2.3).

Two efflux pathways reduce the calcium concentration within the cytosol by ejection into the extracellular space. Calcium is expelled from the cytoplasm by the ATP-driven Plasma Membrane Calcium (PMCA) pump and the Sodium-Calcium Exchanger (NCX), which utilises the electrochemical potential of sodium in order to actively transport calcium out of the cell. Together, the calcium efflux current density is

$$J(\text{Ca}) = \rho_x g_x(\text{Ca}) I_x + J_p(\text{Ca}), \quad (2.6)$$

with

$$J_x(\text{Ca}) = \rho_x g_x(\text{Ca}) I_x. \quad (2.7)$$

$J_x(\text{Ca})$ describes the efflux current density through Sodium-Calcium Exchanger only. ρ_x is the surface density of the NCX membrane proteins and I_x is the maximum rate through a single NCX pore. The calcium dependence of the NCX-kinetics g_x is assumed to follow a Hill equation with Hill coefficient $n_x = 1$ of the form

$$g_x(\text{Ca}) = \frac{\text{Ca}^{n_x}}{H_x^{n_x} + \text{Ca}^{n_x}}. \quad (2.8)$$

H_x refers to the half activation concentration. Note that the efflux current through the NCX protein is a quasi-steady-state expression, meaning an immediate answer to the present intracellular free calcium concentration. A new model of the PMCA pump stimulation and activity will be developed in the second chapter of this diploma thesis, hence the calcium current density transported by PMCA channels $J_p(\text{Ca}, t)$ will be introduced and discussed there.

The conjunction of every sink and source contribution to the free intracellular calcium concentration can be represented by an ordinary differential equation in the calcium concentration Ca :

$$\frac{d\text{Ca}}{dt} = \frac{G}{zF} \{J_v(U(t), \text{Ca}) - J_x(\text{Ca}) - J_p(\text{Ca}) + L\} + B_{\text{buffered}}(\text{Ca}). \quad (2.9)$$

The geometry factor $G = S/V$ is the surface to volume ratio and accounts for the localisation of the channels at the surface rather than in the described volume. F and z are the Faraday constant and the valence charge of calcium ions ($z_{\text{Ca}} = 2$), respectively. G/zF translates the current densities $J_v(U(t), \text{Ca})$, $J_x(\text{Ca})$, $J_p(\text{Ca})$

and L into changes of free intracellular calcium concentration. The leakage surface current density L represents the residual conductivity of the plasma membrane. B_{buffered} denotes the calcium sink term due to buffering by calmodulin or other calcium buffering proteins. Based on the realistic assumption that the buffering of calcium occurs fast, this binding is treated to be in quasi-steady-state. The quasi-steady-state approximation for the calcium buffering implies that the bound calcium concentration Ca_{bound} is adapted instantaneously to the free calcium concentration Ca at each time point t . Therefore, we have

$$B_{\text{buffered}}(Ca) = -\frac{dCa_{\text{bound}}}{dt} = -\frac{dCa_{\text{bound}}}{dCa} \cdot \frac{dCa}{dt}. \quad (2.10)$$

This is generally known as fast buffer approximation. With equation (2.10) the calcium dynamics expression (2.9) becomes

$$\frac{dCa}{dt} = \frac{G}{zF} \{J_v(U(t), Ca) - J_x(Ca) - J_p(Ca) + L\} \frac{1}{1 + \frac{dCa_{\text{bound}}}{dCa}}. \quad (2.11)$$

This expression will be specified in more detail once the PMCA pump efflux density and the calmodulin buffer term have been introduced. Therefore, the discussion of equation (2.9) will be continued chapter 4.

Note that the spatiotemporal diffusion of calcium ions and buffers is not resolved in that model. Since presynaptic terminals are small, *i.e.* having a diameter of the order of microns [15], we assume the diffusion of calcium ions to be fast enough to reach equilibrium distribution on a time scale of one ms. With a calcium diffusion constant of $D_{Ca} = 0.6 \frac{\mu\text{m}^2}{\text{ms}}$ and an investigated volume with a radius of $r = 0.5 \mu\text{m}$ one gets a characteristic spreading time of $t_{Ca} = 0.2 \text{ ms}$, hence the neglect of calcium diffusion is reasonable. This argumentation does not hold for the calmodulin protein, which exhibits a diffusion constant of about $D_{CaM} \approx 5 \cdot 10^{-4} \frac{\mu\text{m}^2}{\text{ms}}$ [16, 17]. The characteristic spreading time of about $t_{CaM} \approx 250 \text{ ms}$ cannot be neglected during calcium elevations lasting only for about 100 ms. This calls for an implementation of the spatiotemporal diffusion in the model which is currently in progress. In this work the diffusion will not be considered.

However, due to the high intracellular calmodulin concentration of $CaM_0 = 30 \mu\text{M}$ [14, 18, 19] the impact of the diffusion might be lowered during low concentration calcium elevations, *i.e.* $0.1 \mu\text{M} \leq Ca \leq 10 \mu\text{M}$. In such a range the calmodulin concentration can be considered as thermodynamical bath due to the higher quantity. Furthermore, calcium buffering by calmodulin happens dominantly at the influx pathways of calcium, *i.e.* at the cell membrane. Simultaneously, this is the intracellular domain where the target activation of the PMCA pumps by calmodulin-calcium complexes takes place which might also lessens the relevance of diffusion for the PMCA pump stimulation.

Attention should be drawn to the fact that all introduced model parameter can be classified either into universal and specific parameters. The surface densities

relate to the investigated specific cell and are thus specific parameters, for example. Whereas the maximum rates through single pores are assumed to apply to all channels of the same type but in different systems. For more details concerning the presynaptic calcium dynamics model please refer to [3, 4].

Postsynaptic response Depolarisation-induced calcium entry in the presynaptic terminal triggers a second-messenger cascade leading to exocytosis of neurotransmitters [7]. Activated proteins promote the calcium-dependent probabilistic fusion of vesicles with the plasma membrane. Little is known about the details of the second-messenger signal cascade leading to exocytosis. The common neurotransmitters that mediate signalling at the chemical synapse are *glutamate* and *acetylcholine* (ACh), which are usually excitatory neurotransmitters, and *glycine* and *gamma-aminobutyric acid* (GABA), which are usually inhibitory neurotransmitters [5]. Following the release of the neurotransmitters, they diffuse across the synaptic cleft to act on postsynaptic receptors. Basal conditions in the synaptic cleft are restored by transmitter reuptake, generally known as *endocytosis*, and synaptic vesicle recycling.

The neurotransmitters act directly on receptor proteins in the postsynaptic membrane. The response evoked by a single stimulus is predominantly mediated by the glutamate acting on α -amino-3-hydroxy-5-methyl-4-isoxazolepropionate (AMPA) receptors. The therewith evoked increase in the AMPA channel conductance allows a passive sodium ion inflow and potassium ion outflow along their respective electrochemical gradients. Basically, the dynamical description of the postsynaptic site comprises the same components as the presynaptic terminal extended by the sodium- and potassium conducting AMPA channels as well as N-methyl-D-aspartate (NMDA) channels, which are permeable for sodium, potassium and calcium ions. The opening of both is promoted by the neurotransmitter Glutamate whereas the Mg^{2+} block at the NMDA channel prohibits calcium influx below a certain depolarisation threshold and thus delays the influx. Therefore NMDA receptors contribute little to the synaptic response to single stimuli because of their relatively slow activation kinetics [20]. The depolarisation of the transmembrane potential at the postsynaptic compartment is mainly mediated by a passive flow of sodium and potassium ions through AMPA and NMDA channels. Chloride ions are predominately involved in inhibitory postsynaptic hyperpolarisations. The net current of calcium ions across the postsynaptic membrane through NMDA and voltage-directed calcium channels contributes little to the de- or hyperpolarisation.

Again, this chapter does not account for the complexity and whole diversity of signal transmission at the chemical synapse. For further readings please refer to the books of Hall [5], Hammond [6] and Kandel [7].

2.3 Long-term effects: LTP/LTD

Up to this point the pathway of signal transmission at the synapse has been introduced. As indicated before, synapses display activity-dependent short- and long-term modifications in their postsynaptic response and are thus interesting on the quest for cellular mechanisms underlying neuronal plasticity. Two related topics will be reviewed in the following section: possible induction pathways for changes in synaptic transmission efficacy and the expression forms of the potentiated or depressed state. The engagement with the Plasma Membrane Calcium pump stimulation in the main part of this diploma thesis is motivated with regard of mechanisms leading to plasticity. Developmental forms of plasticity are not discussed here.

Activity-dependent synaptic potentiation occurs within milliseconds and can persist for hours, or even up to days in the intact animal [6, 20]. Generally, different forms of plasticity have to be distinguished according to their time range. Post-tetanic potentiation (PTP), short-term potentiation (STP) and long-term potentiation (LTP) not only differ in their persistence time but also in the incorporated mechanical temporal components. This section will focus on long-term potentiation (LTP) and long-term depression (LTD), which denote a long-term increase in the synaptic efficacy and long lasting depression of synaptic efficacy, respectively. Whereas long-lasting changes are characterised to last for at least 60 min.

Activity-dependent changes of synaptic efficacy It is well accepted that an increase in the postsynaptic calcium concentration is required for triggering LTP [20, 21]. Therewith related is the activation of postsynaptic N-methyl-D-aspartate (NMDA) receptors. This requires a sufficient depolarisation of the postsynaptic membrane in order to expel the Mg^{2+} block of the NMDA channel. Only a repetitive tetanic stimulation can evoke a sufficient depolarisation mediated by an inward sodium and outward potassium current through AMPA channels to reduce the level of the Mg^{2+} block of the NMDA channel. Experiments indicate that also the replacement of calcium influx through NMDA channels by induced calcium release from intracellular stores can evoke LTP. Hence the rise in the calcium concentration within the postsynaptic cytosol plays a key role in the induction of LTP rather than the activation of NMDA receptors. It remains unclear whether the influx of Ca^{2+} alone is adequate or an amplification due to calcium release from intracellular stores is required for triggering LTP. In this regard, one possible mechanism is calcium-induced calcium release from $Ca^{2+}/InsP_3$ -sensitive intracellular calcium stores which amplifies the calcium signal from NMDA channels and dendritic voltage-dependent calcium channels.

However, the level of the postsynaptic calcium concentration and its duration may profoundly influence the form of the resulting synaptic plasticity. If the

postsynaptic calcium concentration does not reach the threshold and duration to induce LTP, it can generate either short-term potentiation (STP) or long-term depression (LTD) [21]. Long-term depression, a long-lasting decrease in synaptic strength is assumed to be a reversal of the mechanisms underlying LTP.

Experiments which block the elevation of postsynaptic calcium by calcium chelators prohibit the induction of LTP, indicating that an increase in postsynaptic calcium is required. However, it remains unclear, whether this provides a sufficient trigger for the induction [20].

Expression of the potentiated state A closely related question to the induction of long-term effects is the expression of the potentiated or depressed state. There is an ongoing debate whether the increase of synaptic strength is due to pre-, post- or extrasynaptic modifications. Experiments indicate two likely forms of expression of LTP: the presynaptic increase of neurotransmitter release and the increase in AMPA receptor-mediated excitatory current [21]. Whereas the possible increase in neurotransmitter release and the pathways leading to it are controversially discussed.

Since AMPA and NMDA receptor channels are colocalised at individual synapses, manipulations that increase the probability of transmitter release would cause an equal increase in the synaptic response of both receptor channels. Most investigators find, however, that LTP only increases the AMPA receptor-mediated excitatory postsynaptic current. This is used as argument against an presynaptic expression of the potentiated state. This argumentation does not account for the possible fact, that all NMDA receptors could be already saturated by Glutamate and hence not be accessible to changing neurotransmitter concentrations (for a review see [22]). This hypothesis is supported by the extremely high equilibrium affinity for glutamate of NMDA receptors [23]. However, recent studies contradict the saturation assumption [24]. Another question related to presynaptic modifications leading to an increase in neurotransmitter release is whether the amount of vesicles available and able to fuse is increased or the amount of neurotransmitter within the available vesicles.

On the postsynaptic side, the increase of AMPA receptor mediated current can either be due to a higher single-channel conductance by phosphorylation of the AMPA receptor subunit GluR1 or to a possible increase of the total number of AMPA channels within the membrane.

Connection between induction and expression of LTP/LTD What biochemical pathways are activated by postsynaptic Ca^{2+} and are required for translating the calcium signal into an increase in synaptic strength? A link between a postsynaptic calcium accumulation and the alteration of AMPA receptor conductance or number or both is suggested by experiments which indicate the calcium-

calmodulin-dependent protein kinase II (CaMKII) as a key component of the molecular machinery of LTP [25]. Inhibition or genetic deletion of CaMKII blocks the ability to generate LTP [21]. The protein kinase is activated by the calmodulin-calcium complex whereas a subsequent autophosphorylation prolongs its activity independent of the present calcium concentration. Experiments further provide strong evidence that the phosphorylation of the AMPA receptor subunit GluR1 by CaMKII increases the single channel conductance. CaMKII is also believed to influence the localisation of AMPA receptors, namely it can deliver more AMPA receptor to the plasma membrane.

Several other protein kinases have been suggested to contribute to LTP. The evidence in support of critical roles for these kinases is, however, considerably weaker than that for CaMKII.

A possible connection between postsynaptic calcium elevations and presynaptic modifications could be provided by retrograde messengers. They are required since the initial triggering of LTP clearly resides in the postsynaptic cell. Molecules that have received the most attention as possible retrograde messenger include nitric oxide (NO), carbon monoxide, arachidonic acid and platelet-activating factor [20, 21, 26].

The Ca^{2+} /calmodulin-dependent protein kinase II (CaMKII) is involved in phosphorylation mechanisms also at the presynaptic side. In an axon terminal only a small proportion of vesicles, which is located in a readily releasable pool, is available for fast calcium-induced exocytosis. The majority of vesicles is sequestered in a filamentous network. Phosphorylation by CaMKII disengages the vesicles from this reserve pool and provides them for the active zone [27]. In this regard the time course of presynaptic calcium accumulations is relevant for the calcium-dependent activity of the CaMKII and therewith for the vesicle placement.

A number of fundamental properties of synaptic plasticity in the mammalian brain have been introduced in that section. Many secondary processes involved in the molecular machinery have not been mentioned here, since often little is known about their mechanisms or meaning and it was aimed to restrict to basic and experimental profound findings. Two interesting review articles concerning LTP are: Bliss *et al.* (1993) [20] and Malenka *et al.* (1999) [21].

3 A theory of Plasma Membrane Calcium pump function

It was pointed out in the last chapter that calmodulin-kinase II has time-dependent kinetic properties, which enables the kinase to relate Ca^{2+} signals to long-term potentiation [25]. Another component involved in synaptic calcium dynamics displaying a memory property is the Plasma Membrane Calcium pump. The calcium- and calmodulin-dependent stimulation of this transmembrane protein can sense the frequency and intensity of the Ca^{2+} signal. The stimulation effect ranges on a time scale of minutes, which clearly exceeds the time period of the synaptic signal transmission (ms) and might be significant for short-term effects (min). The PMCA stimulation can possibly be a link in the signal cascade towards long-term effects (> 60 min).

The chapter starts with the introduction of the calmodulin protein in section 3.1 and the Plasma Membrane Calcium (PMCA) pump in section 3.2. Chapter 3.3.2 will be devoted to the existing PMCA pump model of Caride *et al.* [1]. This is utilised as a starting point for the presentation and discussion of a new theory of Plasma Membrane Calcium pump stimulation and activity [2] in the main part of the chapter.

3.1 The calmodulin protein

Calmodulin is a mobile, intracellular calcium buffering protein. It belongs to the EF-hand protein family with the helix-loop-helix conformation. These calcium buffering proteins include parvalbumin, calretinin, calcineurin, calbindin- D_{28k} and calmodulin [12]. Together they have a high capacity to buffer calcium ions. Collectively, these mobile buffers absorb nearly 95-99 % of the total intracellular calcium load, leaving only a minor fraction as free calcium ions [6, 12]. Therefore the mobile buffering proteins play an important role for the trans-cellular diffusion of calcium ions and the spatial propagation of calcium within the cytoplasm.

The EF-hand motif can accommodate calcium and magnesium with subtle differences in affinities [28]. The classical EF-hand is a helix-loop-helix motif characterised by a sequence of, usually, 12 residues with the pattern $\text{X}\bullet\text{Y}\bullet\text{Z}\bullet - \text{Y}\bullet - \text{X}\bullet\bullet - \text{Z}$ [28]. This sequence of spatial 3-dimensional interacting coordinates forms a loop that can accommodate calcium or magnesium (see figure 3.1). The dots (\bullet) in this sequence represent intervening residues of the protein polypeptide chain which are not involved in the ion binding. The participating residues com-

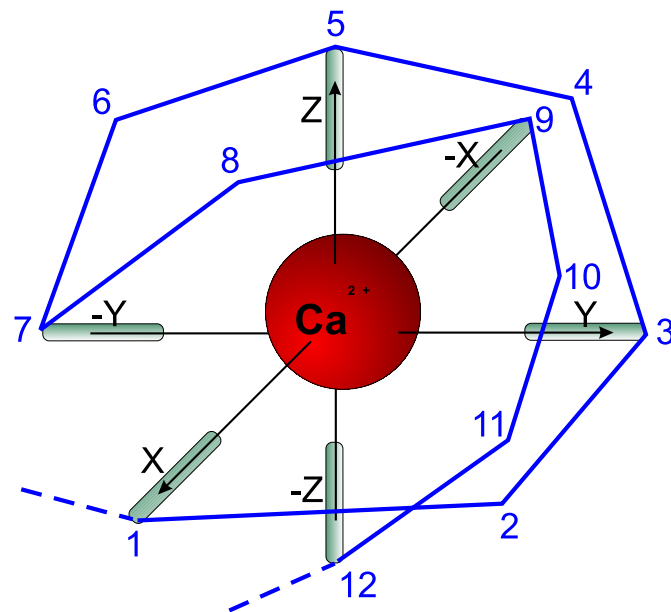


Figure 3.1: Spatial ion binding by an EF-hand motif

The spatial interacting points between calcium and the protein residues are characterised by the 3-dimensional coordinates X , $-X$, Y , $-Y$, Z and $-Z$. The green bars depict the polar residues, which extend from the polypeptide chain, involved in the ion binding. The polypeptide chain of the EF-hand motif is shown by the blue line. Each numbered corner of the chain represents a residues. Important and characteristic is the number of intervening residues between the respective interacting points which are not involved in the binding of calcium.

prise exposed polar binding sites in order to interact with the two-fold charged calcium ion Ca^{2+} . The further consideration here is focused on the binding of calcium, since the calcium mediated process is of special interest in this work.

Calmodulin contains four EF-hand motifs allowing itself to bind four calcium ions. The first two EF-hands combine to form a globular amino-terminal (N-terminal) domain. The highly homologous carboxyl-terminal (C-terminal) consisting of the second pair of EF-hand motifs is connected with the N-terminal domain by a flexible linker - a α -helix [29]. The tertiary structure of calmodulin is shown in figure 3.2. Calmodulin has a molecular weight of 16690 Da¹, the total number of residues is 148 and it contains 9 α -helices, four in each globular domain forming the two EF-hand motifs and one flexible α -helix linker, and 4 β -sheets².

EF-hands occurring together within one protein can have different binding affinities for metal ions. Pairs of EF-hands display cooperativity as a functional conse-

¹Da refers to Dalton, which is a frequently used mass measure in molecular biology; 1 Da = 1 u = $1.6605 \cdot 10^{-27}$ kg

²data from the online protein data bank: <http://www.rcsb.org/pdb/index.html>

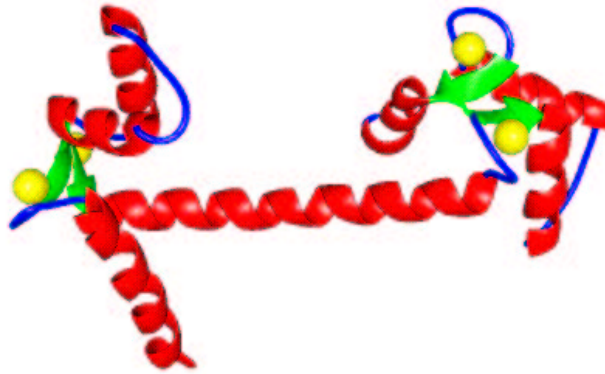


Figure 3.2: Tertiary structure of the calmodulin protein

The red spirals depict α -Helices, blue lines are random coils and green arrows represent β -sheets. Yellow dots are calcium ions bound by the EF-hands in the C-terminal as well as in the N-terminal domain (picture taken from http://www.sidwell.edu/~bio21/images/calm_lg.gif).

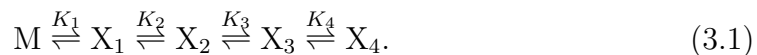
quence of calcium binding, as it is the case within the globular N- and C-terminal domains of calmodulin. In contrast, the calcium-binding between the globular domains happens in a independent, non-cooperative manner [13]. When calcium binds, one helix of the EF-hand motif moves from a closed to an open conformation. This is a first step of larger, subsequent conformational changes within the C-terminal and the N-terminal domain as well as for the whole calmodulin protein. This rearrangement of the helices leads to the exposure of several hydrophobic residues [30, 31]. The calmodulin protein liganded with four calcium ions, referred to as X_4 , is capable for Ca^{2+} -dependent regulation of the activities of a vast array of different target proteins, including enzymes, ion pumps and channels [18]. The dissociation constants of these target proteins and the calmodulin-calcium complex range from 1 nM to greater than 100 nM [32]. Among those with high affinity to the calmodulin-calcium complex is the Plasma Membrane Calcium pump ($K_d \approx 9$ nM for the hPMCA4b isoform [32, 33, 34, 35]), which will be presented in section 3.2.

In order to describe the buffering of calcium by calmodulin, one has to differentiate between macroscopic and microscopic dissociation constants. In the case of calmodulin, the first calcium ions can choose freely between four binding sites, namely the four EF-hand motifs. For protein occupied with one calcium ion X_1 four possible forms with four microscopic dissociation constants are available, accordant to the respective occupied binding cite at the protein. The second calcium ion may still choose between three possible binding sites. This step results in twelve microscopic binding constants. The binding of the third ion yields further twelve dissociation constants, while four equilibria lead to the saturated

<i>KCl</i> (mM)	K_1 (μM)	K_2 (μM)	K_3 (μM)	K_4 (μM)
Low	0.1	0.025	0.32	0.40
10	0.63	0.04	1	1
25	1.58	0.1	3.98	2.00
50	3.98	0.20	25.1	3.16
100	12.6	0.25	39.8	2.51
150	20.0	0.63	100	5.01

Table 3.1: Macroscopic binding constants of calmodulin taken from Linse *et al.* [13].

calmodulin protein. Altogether $4 + 12 + 12 + 4$ dissociation constants describe the successive binding of four Ca^{2+} ions to calmodulin on the microscopic level. The difference between the microscopic and the macroscopic binding constants can be shown best with the following reaction scheme



M is free intracellular calmodulin and X_i ($i = 1, 2, 3, 4$) refers to the calmodulin-calcium complex with the respective number (i) of calcium ions bound. In reaction scheme (3.1) only the number of bound calcium ions to calmodulin is of interest with no regard to the occupied microscopic binding sites. X_1 stands for the four possible forms of one calcium ion bound to calmodulin, for example. K_1 , K_2 , K_3 and K_4 are the macroscopic dissociation constants related to equilibria with one

$$K_1 = \frac{Ca \cdot M}{X_1}, \quad (3.2)$$

two, three and four calcium ions bound, respectively. These dissociation constants are strongly dependent on the present KCl concentration. The K_i ($i = 1..4$) measured by Linse *et al.* at various KCl concentrations are quoted in table 3.1. The binding sites in the C-terminal domain exhibit a higher calcium affinity than those in the N-terminal domain [13]. And within each domain the binding happens in a cooperative manner. Two successive cooperative steps are reflected in the binding constants shown in table 3.1. $4K_1 > 3K_2/2$ indicates the increase in affinity upon the binding of the first calcium ion, which can be applied to the binding of the third and the fourth ion, respectively, since $2K_3/3 > K_4/4$. The numbers multiplied by the binding constants result from the possible free binding sites at the respective step. This is expressed by a lower affinity in step 1 compared to step 2 in reaction scheme (3.1) with equal affinities of all microscopic binding sites, for example [36]. The interaction of the binding sites between the two globular domains cannot clearly be deduced from the macroscopic binding constants. However, Linse *et al.* indicate that the calcium affinities of the sites in the C-terminal

domain are on average 6-fold higher than those of the sites in the N-terminal domain [13]. Beside the dependence of K_i (with $i = 1, 2, 3, 4$) to the present KCl concentration a relation to the pH value is pointed out.

Of further interest is the concentration of X_4 at a given calcium concentration, since it is assumed that only the saturated calmodulin-calcium complex X_4 plays a key role in PMCA stimulation [29, 37, 38, 19]. In equivalence to equation (3.2) an equilibrium for the saturated calmodulin protein exists

$$X_4 = \frac{Ca \cdot X_3}{K_4} = \frac{Ca \cdot M}{K_1 K_2 K_3 K_4}, \quad (3.3)$$

resulting from the last equilibrium in reaction scheme (3.1) and the successive replacement of X_i ($i = 3, 2, 1$) by their equilibrium equations (corresponding to equation (3.2) for X_1). Using the calmodulin concentration conservation $M_0 = M + X_1 + X_2 + X_3 + X_4$ leads to

$$X_4 = \frac{M_0}{1 + \frac{K_4}{Ca} + \frac{K_3 K_4}{Ca^2} + \frac{K_2 K_3 K_4}{Ca^3} + \frac{K_1 K_2 K_3 K_4}{Ca^4}}. \quad (3.4)$$

The choice of the binding constants in order to describe the relationship between free fully liganded calmodulin-calcium complexes and free calcium ions in the cytosol is discussed in section 4.1.

Some remarks to the cooperativity in the C-terminal as well as in the N-terminal domain shall conclude this section. In order to demonstrate the described effects, three different binding scenarios are shown in figure 3.3.

1. The blue line displays the real calcium dependent formation of X_4/M_0 at low ionic strength. A crosscheck with measurements of Persechini *et al.* [39, 40] confirms the quasi-steady-state buffering equation (3.4) (data not shown).
2. In the case of simultaneous binding of all the four calcium ions, the relation X_4/M_0 is described by the red line in figure 3.3. The law of mass action for this reaction equilibrium leads to a Hill function with Hill coefficient $n = 4$

$$X_4 = \frac{Ca^4 M_0}{K_1 K_2 K_3 K_4 + Ca^4}, \quad (3.5)$$

where $K_1 K_2 K_3 K_4 = K_{1/2}^4$ represents an analogon to a half maximum concentration. This equation can be deduced from equation (3.4) by assuming a highly cooperative binding between all binding sites, *i.e.* $K_4 \ll K_3 \ll K_2 \ll K_1$, meaning instantaneous attachment of all the four calcium ions [36].

3. Calmodulin comprises four identical binding sites which are independent of each other. This implies equal microscopic binding constants K_{mic} . For

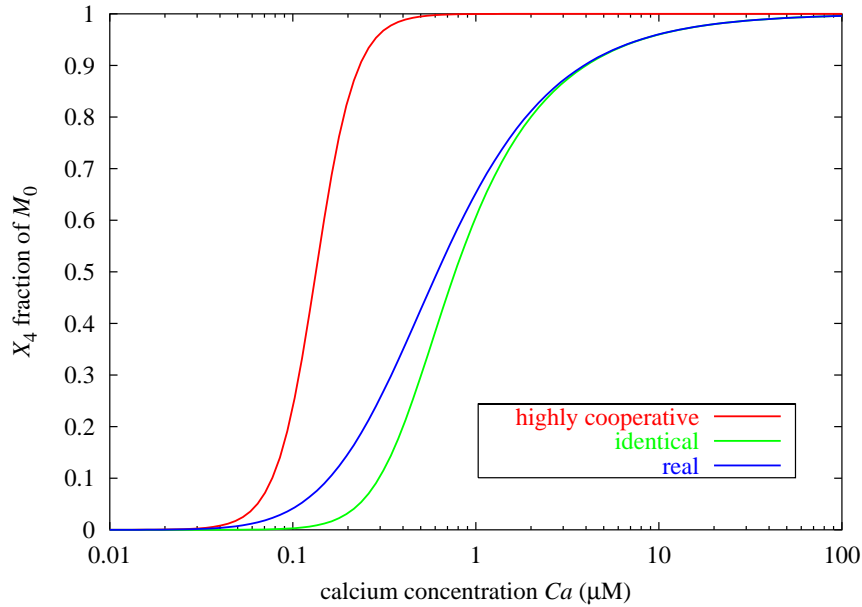


Figure 3.3: Different calcium buffering scenarios at low ionic strength

The fraction X_4/M_0 is shown for the real calmodulin protein (blue line), an assumed highly cooperative binding between all the four binding sites (red line) and identical, independent binding sites (green line). The microscopic dissociation constant K for the identical binding sites case is taken to be $K_{\text{mic}} = 4K_1$. The binding constants at low ionic strength are taken from table 3.1 for the different scenarios.

the accordant macroscopic dissociation constants one gets $K_1 = K_{\text{mic}}/4$, $K_2 = 2K_{\text{mic}}/3$, $K_3 = 3K_{\text{mic}}/2$ and $K_4 = 4K_{\text{mic}}$ [36] and therewith the quasi-steady-state buffering expression (3.4) becomes

$$X_4 = \frac{M_0}{1 + 4\frac{K_{\text{mic}}}{Ca} + 6\left(\frac{K_{\text{mic}}}{Ca}\right)^2 + 4\left(\frac{K_{\text{mic}}}{Ca}\right)^3 + \left(\frac{K_{\text{mic}}}{Ca}\right)^4}. \quad (3.6)$$

With regard to the relations between the microscopic and macroscopic binding constants we use $K_{\text{mic}} = 4K_1$ in figure 3.3.

With its functional, molecular structure, the real calmodulin protein is able to place the steepest rise of the sigmoidal saturation curve (blue line in figure 3.3) in the physiological range of the accordant intracellular free calcium concentration $0.1 < Ca < 10 \mu\text{M}$ (see section 4.1 for further investigations). Within that range the calmodulin protein can react most sensitively to concentration changes. Note that in contrast to identical, independent binding sites, cooperative binding in the C-terminal and in the N-terminal domain enables the protein to form calmodulin-calcium complex at lower calcium concentrations. Beside that gap, the real calmodulin and the identical binding sites case display similar behaviours.

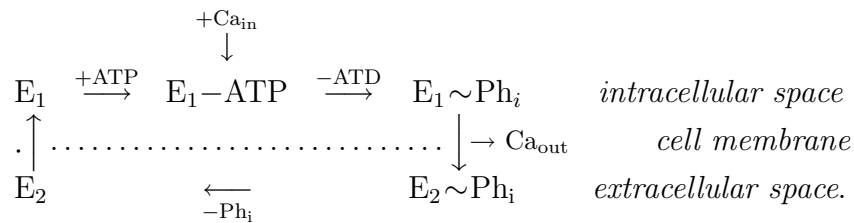
Another fact can be a reason for the special domain structure of calmodulin. As measured by Linse *et al.* the calcium affinities of the binding site in the C-terminal are on average 6-fold higher than in those of the sites in the N-terminal domain [13]. For the high affinity C-terminal this results in a faster saturation. Together with the approximately 10.000-fold greater affinity of the PMCA pump to the C-terminal domain of calmodulin ([31], see the following section for more details) this might improved the ability and sensitivity of calmodulin for PMCA stimulation.

3.2 The Plasma Membrane Calcium pump

Calcium efflux from cells occurs through two main systems, the $\text{Na}^+/\text{Ca}^{2+}$ exchanger (NCX) and the ATP-driven Plasma Membrane Calcium pump (PMCA) [41, 42]. The $\text{Na}^+/\text{Ca}^{2+}$ exchanger protein utilises the electrochemical potential of the sodium ions, which travel passively along their electrochemical gradient into the cell. The so provided energy is used in order to transport calcium against its electrochemical gradient out of the cell. The NCX protein comprises a low affinity for cytosolic calcium ($H_x \approx 0.6\text{-}3\text{ mM}$) with a high calcium transport rate ($I_x \gg 1000\text{-}5000\text{ Hz}$) [41, 42]. On the contrary the Plasma Membrane Calcium pump displays a high calcium affinity ($K_d < 0.5 - 1\ \mu\text{M}$ [37, 38, 42]) and a low transport rate ($\approx 30\text{ Hz}$, [41] and private communication). Both are important for the maintenance of calcium homeostasis. The NCX is suited for rapid recovery from high levels of cytosolic calcium. Due to its high affinity and low transport rate compared to the NCX, the PMCA pump is of crucial importance for the fine tuning of cytosolic calcium ion concentration [41, 42]. At resting level the cytosolic free Ca^{2+} concentration is maintained at $Ca = 0.05 - 0.1\ \mu\text{M}$ [12, 42].

The PMCA pump protein has been found in all mammalian cells [43], where the expression level does not exceed 0.1% of the total membrane protein [29, 42, 44, 45]. An exception is the brain where this value is up to 10 times higher than in non-excitabile cells [42, 43]. The pump belongs to the P-type ATPase family the members of which are able to utilise the energy stored in ATP to transport calcium ions against their electrochemical gradient across the plasma membrane [37]. ATP apparently interacts with the pump at two sites with different affinities, $K_m^1 = 1 - 2.5\ \mu\text{M}$ and $K_m^2 > 100\ \mu\text{M}$ [38, 45]. The transport cycle involves the formation and degradation of phosphorylated intermediate states. Carafoli

suggested the following cycle [38]



The enzyme can exist in two different states - called E1 and E2, which further appear in different phosphorylation states. The translocation step of calcium across the membrane, depicted as $\text{E}_1\sim\text{Ph}_i \rightarrow \text{E}_2\sim\text{Ph}_i$ is related to a transformational change [38, 43]. More informations related to the transformational change can be found in Carafoli (1991) [38].

In contrast to the Ca^{2+} pump of the sarcoplasmic reticulum (SERCA) the stoichiometry between transported Ca^{2+} and hydrolysed ATP of the PMCA pump is most likely 1:1 [12, 38, 42, 45]. The SERCA pump works with a calcium:ATP ratio of 2:1 [12, 45, 46]. This will be discussed further in section 3.5.1, since the deduced theoretical expression for a Ca^{2+} :ATP stoichiometry of 1:1 does not reproduce experimental measured uptake behaviour.

The four different PMCA pump isoforms are encoded by four independent genes, which are indicated by numbers 1-4. PMCA1 and PMCA4 are expressed in practically all tissues, whereas in all human tissues PMCA1 is present in higher concentration than PMCA4 [42, 44]. PMCA2 and PMCA3 have been shown to occur in highly specialised tissues such as brain and heart [42, 44]. The diversity of pump forms is further increased by alternative mRNA splicing variants, characterised by small letters. There exist more than 26 transcripts which differ in their regulatory properties, for instance in their affinity to calmodulin, and are distributed in a tissue specific manner [38, 42]. The origin animal of the pump genes is indicated by a small letter, *e.g.* r stands for rat and h relates to human. Referring to the available data form Caride *et al.* [1], isoforms hPMCA2b and hPMCA4b will be investigated in this work.

The PMCA-ATPase is stimulated by direct interaction with calmodulin. Beside this, the pump can be stimulated by alternative pathways such as kinase-mediated effects (protein kinase A, protein kinase C) or exposure to acidic phospholipids or polysaturated fatty acids [37, 45]. This stimulation effects predominately change the calcium affinity, whereas calmodulin changes the affinity to calcium and the maximum calcium turnover rate of the pump [19, 29, 37, 38].

The free CaM-binding domain of the PMCA pump interacts with the pump at two sites. It acts as a repressor of pump activity since it covers the ATP-binding site of the pump [40, 45]. The relieving of that autoinhibitory domain segment after the binding of X_4 causes a stimulation of pump function by increasing the

affinity to calcium and the maximum calcium turnover rate [19, 29, 37, 38]. The stimulation and the relaxation to the initial unstimulated state happens on a time scale of minutes [1, 37]. Since the stimulation and relaxation process depends on the present calmodulin- and the calcium concentration, it responds to intracellular calcium elevations. At resting level almost no calmodulin-calcium complexes are formed, whereas higher calcium concentrations cause an accumulation of X_4 which leads to a stimulation of the pump. Due to the gradual decay of stimulated pump form the pump remains stimulated even after recovery to the resting calcium level. This effect enables the pump to display a memory to previous calcium transients since it can react immediately with a higher activity at subsequent calcium elevations [1].

3.3 Current status of PMCA pump stimulation models

Having introduced the participating proteins, the following sections will deal with already available realisations of the biological processes in a theoretical model. As preparation, the measurement of the PMCA activity is explained in section 3.3.1. The model of Caride *et al.* is introduced in section 3.3.2 as a starting point for the new theory of PMCA pump function, comprising both, stimulation and activity, presented in section 3.4.

3.3.1 Measurement of Plasma Membrane Calcium pump activity

In order to determine the parameters of the PMCA stimulation model the stimulation and relaxation constants k_{stim}^{exp} and k_{relax}^{exp} , measured in experiments, will be used. It will be explained how these stimulation constants are obtained from measurements of PMCA pump activity in this section.

The pumping rate can be determined by measuring the kinetics of inorganic phosphate Ph_i release (whereas sub- i refers to inorganic) [47]. The total amount of produced Ph_i by hydrolysing ATP during a single turnover of the pump is proportional to the optical density at 360 nm [47]. Caride *et al.* in 2001 [1] used this in order to measure the total amount of produced Ph_i . It is rather likely that during a single turnover of the PMCA pump one ATP is hydrolysed as well as one calcium ion transported [38, 42, 45]. Due to the stoichiometry of 1 Ph_i : 1 Ca^{2+} the rate of the Ph_i production directly corresponds to the calcium pumping rate.

Stimulation of the PMCA pump means an increase of the calcium turnover rate, hence an increase in the Ph_i production rate. Actually the affinity to calcium and the maximum turnover rate are increased, but both combined results in an increase of the net turnover rate. The total production of Ph_i during the stimulation

procedure between t_0 and t is given by

$$\text{Ph}_i(t) = \text{Ph}_0 + \int_{t_0}^t [f_{\text{unstim}} \cdot v_{\text{unstim}}(\text{Ca}) + f_{\text{stim}} \cdot v_{\text{stim}}(\text{Ca})] dt. \quad (3.7)$$

Where v_{unstim} and v_{stim} represent the production rates of Ph_i , as well as the calcium pumping rates, at the present intracellular calcium concentration in unstimulated and stimulated state, respectively. Ph_0 refers to the amount of Ph_i at t_0 . f_{unstim} and f_{stim} represent the fractions of unstimulated and stimulated pumps of the investigated system, respectively. Equation (3.7) describes the Ph_i production of a whole system which comprises an ensemble of PMCA pumps. According to this the fractions $f_{\text{unstim}}/f_{\text{stim}}$ and the production rates $v_{\text{unstim}}/v_{\text{stim}}$ summarise the stimulation and pumping properties of the whole ensemble of PMCA pumps. More details concerning the Ph_i production rate expression are found in section 3.5.1 (see equation (3.55)).

The production rates are multiplied by the fraction of unstimulated or stimulated pump form. As a first approximation the alteration during the progress of the stimulation of these fractions is assumed to follow single exponential functions

$$f_{\text{unstim}} = \exp(-k_{\text{stim}}^{\text{exp}} t), \quad (3.8)$$

$$f_{\text{stim}} = 1 - \exp(-k_{\text{stim}}^{\text{exp}} t), \quad (3.9)$$

where $k_{\text{stim}}^{\text{exp}}$ denotes the stimulation constant. The total amount of Ph_i becomes therewith

$$\text{Ph}_i(t) = \text{Ph}_0 - \Delta v/k_{\text{stim}}^{\text{exp}} + v_{\text{stim}}t + \Delta v/k_{\text{stim}}^{\text{exp}} \cdot e^{-k_{\text{stim}}^{\text{exp}} t} \quad (3.10)$$

with $\Delta v = v_{\text{stim}} - v_{\text{unstim}}$ and $t_0 = 0$.

An equivalent approach is used in the relaxation case. The relaxation constant $k_{\text{relax}}^{\text{exp}}$ is introduced as an approximation to describe the decay of stimulated pump form by single exponential functions

$$f_{\text{stim}} = \exp(-k_{\text{relax}}^{\text{exp}} t), \quad (3.11)$$

$$f_{\text{unstim}} = 1 - \exp(-k_{\text{relax}}^{\text{exp}} t). \quad (3.12)$$

This ansatz delivers from equation (3.7)

$$\text{Ph}_i(t) = \text{Ph}_0 + \Delta v/k_{\text{relax}}^{\text{exp}} + v_{\text{unstim}}t - \Delta v/k_{\text{relax}}^{\text{exp}} \cdot e^{-k_{\text{relax}}^{\text{exp}} t}. \quad (3.13)$$

The single exponential approximations (3.8), (3.9) and (3.11), (3.12) do not take the steady-state distribution into account, hence they reproduce experimentally measured Ph_i production only in the beginning of the stimulation or relaxation process. The steady-state behaviour will be considered in section 3.5.2.

The fit of equation (3.10) and (3.13) to the measured Ph_i production during stimulation and relaxation, respectively, yields the stimulation constant $k_{\text{stim}}^{\text{exp}}$ and the relaxation constant $k_{\text{relax}}^{\text{exp}}$, respectively, as single exponential fit parameter (for further details please refer to [47, 35]). Caride *et al.* have determined these fit constants for various calcium concentrations. As a measure of stimulation or relaxation velocity a relation between the rate constants introduced by the stimulation model in section 3.4 and $k_{\text{stim}}^{\text{exp}}/k_{\text{relax}}^{\text{exp}}$ will be deduced.

3.3.2 Previous models

During intensive studies of literature only one model describing the stimulation of the Plasma Membrane Calcium pump could be found. In the publication “The plasma membrane calcium pump displays memory of past calcium spikes” Caride *et al.* in 2001 presented the measurement of the stimulation of the PMCA pump by calmodulin [1]. Not only the steady-state activities in the absence and the presence of calmodulin are examined, also the temporal stimulation behaviour has been measured. In this paper the group presents a simple model which describes their experimentally measured stimulation data. As a starting point for further considerations and improvements this model is presented here.

The stimulation is based on a system of rate equations, which describes the calcium and calmodulin dependent transition from unstimulated to stimulated pump form and vice versa. The stimulation dynamics of an ensemble of PMCA pumps is characterised by the following equations



M is free calmodulin, Ca is free calcium and X_4 denotes the free calmodulin-calcium complex. P is referred to as free PMCA pump, whereas P_X^* is calmodulin-calcium complex X_4 bound to the PMCA pump and P_M^* is PMCA pump complexed with calmodulin. The asterisk denotes stimulated pump forms. The superior (c) refers to rate constants of the Caride model. Since the buffering of calcium by calmodulin is fast compared to the stimulation of the PMCA pump, the binding (3.14) and the dissociation (3.16) are treated as being in equilibrium. This is a realistic assumption since the buffering within milliseconds does not affect the

temporal behaviour of the stimulation which happens on a time scale of minutes. Note that Caride *et al.* assumes a highly cooperative binding of all the four calcium ions, which corresponds to case two on page 25. Thus the used association constant $K_1^{(c)}$ (see table 3.2) for reaction (3.14) is calculated from the dissociation constants of Linse [13] with

$$K_1^{(c)} = \frac{1}{K_1 K_2 K_3 K_4}. \quad (3.18)$$

The values of K_i ($i = 1..4$) at $KCl = 150$ mM from the publication of Linse *et al.* (1991) fit best the experimental conditions of 30 mM Tes-TEA, pH 7.2 and 120 mM KCl of Caride *et al.* (for more details see [1, 13]).

P_X^* and P_M^* are considered to be stimulated pump forms, accordingly P is unstimulated PMCA pump form. By reversible binding of the calmodulin-calcium complex to the pump, the PMCA pump protein is stimulated (step (3.15)). The assumption, that calcium dissociates first from the stimulated PMCA pump bound with calmodulin-calcium P_X^* (step (3.16)), should be remarked since it will be described in a different way in the new stimulation model. After this detachment the pump complexed with calcium-free calmodulin, P_M^* , remains stimulated. The irreversible relaxation is described with step (3.17).

Only species of calmodulin (M) bound with four calcium ions are included in the stimulation model. This is in contrast to the observation, that the isolated N- and C-terminal domain of calmodulin are both able to fully activate the PMCA pump [31]. However, the amount of the single CaMN- or CaMC-domain necessary for half-maximal stimulation is 1500- or 400-fold higher than for complete calmodulin protein, comprising the N- and the C-terminal domain [31]. This justifies the simplification of including only native calmodulin in the stimulation, which comprises the carboxyl-terminal domain connected with the amino-terminal by the central α -helix. This α -helix enables the difference to sole domain stimulation by facilitating a specific, cooperative binding of both domains to the PMCA pump [31].

Two problems arise with that model. Firstly the quoted parameter sets shown in table 3.2 ([1] and private communication) cannot be deduced from the measured stimulation constants. Secondly they correctly describe one specific experiment but there is a lack of generality for differing experimental conditions, such as modified calcium or calmodulin exposures.

The experiments were performed with the h2b and h4b isoforms of the PMCA pump. The process of stimulation is assumed to be the same for both isoforms, hence differences in the temporal stimulation behaviour are expressed by different parameter sets, which are shown in table 3.2. The quasi-steady-state treatment of the calcium buffering by calmodulin reduces the rate constants $k_1^{(c)}$ and $k_{-1}^{(c)}$ to the dissociation constant of that reaction $K_1^{(c)} = k_{-1}^{(c)}/k_1^{(c)}$ which is taken from Linse *et al.* [13] (see equation (3.18)). Note that $K_1^{(c)}$ is related to the buffering

parameter	2b	4b	unit
$K_1^{(c)} = k_{-1}^{(c)}/k_1^{(c)}$	$1.58 \cdot 10^{-4}$	$1.58 \cdot 10^{-4}$	$1/\mu\text{M}^4$
$k_2^{(c)}$	$5 \cdot 10^3$	$2.2 \cdot 10^3$	$1/(\mu\text{M} \cdot \text{s})$
$k_{-2}^{(c)}$	0.0005	0.001	1/s
$k_3^{(c)}$	1	1	1/s
$k_{-3}^{(c)}$	$1 \cdot 10^4$	$1 \cdot 10^4$	$1/(\mu\text{M}^4 \cdot \text{s})$
$k_4^{(c)}$	0.014	0.034	1/s

Table 3.2: Pump specific rate constants used by Caride *et al.* 2001 ([1] and private communication).

of calcium by free calmodulin, whereas $k_3^{(c)}$ and $k_{-3}^{(c)}$ are related to the attachment and detachment of calcium to and from calmodulin bound by the PMCA pump, respectively. It can be seen that the dissociation constant for step (3.16), $K_3^{(c)} = 1 \cdot 10^4 \mu\text{M}^{-4}$, is substantially larger compared to $K_1^{(c)} = 1.58 \cdot 10^{-4} \mu\text{M}^{-4}$.

As already mentioned, the parameters in table 3.2 reproduced the stimulation behaviour measured under the experimental conditions in [1]. In figure 3.4 the temporal stimulation behaviour under different calcium exposures is shown. The total concentration of available PMCA pumps P_0 is taken from Caride *et al.* to be $0.005 \mu\text{M}$ [1]. It can be seen, that the stimulation velocity can be arbitrarily increased by increasing the calcium concentration. This is in contradiction with the saturation of the stimulation constant at high calcium concentrations as suggested by the measured data (see experimental data shown in figure 3.5 and 3.6), *i.e.* increasing the calcium concentration cannot further accelerate the stimulation. In the reaction scheme (3.14) - (3.17) the forward direction velocity of step (3.15) is directly connected with the present calcium concentration, since the buffering (step (3.14)) is treated of being in equilibrium. This connection results in an arbitrarily increase of the stimulation velocity accompanying with the increasing calcium concentration.

3.4 The new Model of PMCA pump stimulation

On the basis of Caride's model and with the knowledge of the problems there, a new model is presented in this section [2]. The new transition from unstimulated to

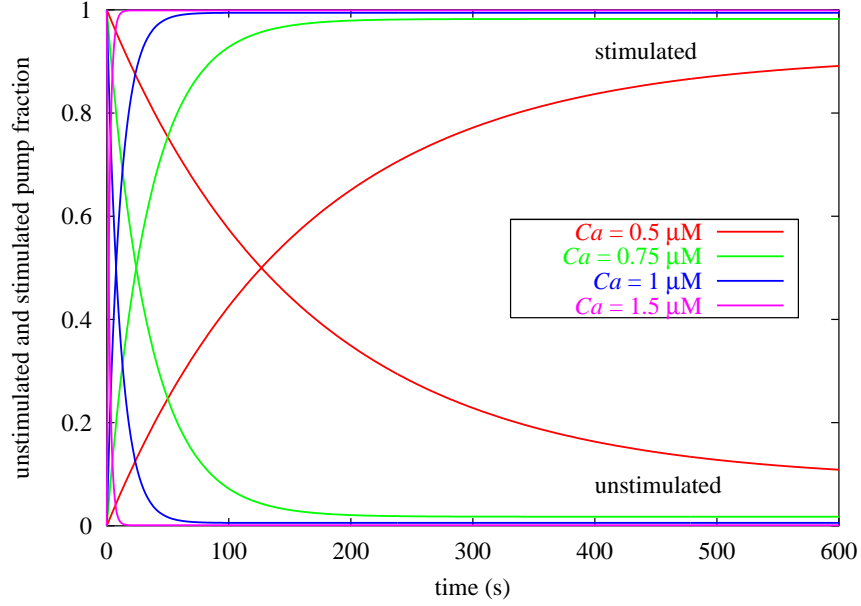


Figure 3.4: Stimulation of the 2b isoform at $\text{CaM} = 0.117 \mu\text{M}$

For different calcium concentration the temporal change of the fractions P/P_0 for unstimulated pump and $(P_X^* + P_M^*)/P_0$ for stimulated pump form are shown. The calmodulin concentration at all simulations is $0.117 \mu\text{M}$ and the total pump concentration $P_0 = 0.005 \mu\text{M}$. The stimulation started with only unstimulated pump form to be present, *i.e.* $P/P_0 = 1$.

stimulated pump form and vice versa is described by the following rate equations:



M and Ca is free calmodulin and calcium within the cell which form the calmodulin-calcium complex X_4 (see equation (3.3)). P denotes free PMCA pump, PMCA pump bound with X_4 is denoted by P_X . The asterisk denotes stimulated pump forms. The k_i 's ($i = \pm 1, \pm 2, 3, \pm 4, 5$) are the rate constants of the accordant equation and direction.

The formation of the calmodulin-calcium complex X_4 is described with equation (3.3) which accounts for the cooperative binding in the C-terminal as well as in the N-terminal domain of calmodulin. Based on the realistic assumption that the buffering of calcium occurs faster than the PMCA pump stimulation, which

happens on a time scale of minutes, we treat this binding to be in quasi-steady-state, generally referred to as fast buffer approximation.

The free PMCA pump P and the PMCA pump complexed with calmodulin-calcium, P_X , will be referred to as unstimulated pump forms. The stimulation in equation (3.20) is assumed to be irreversible. P_X^* is the stimulated PMCA pump form bound with X_4 whereas P^* is free stimulated pump. After the detachment of the calmodulin-calcium complex (equation (3.21)) from the stimulated pump the recovery to unstimulated PMCA pump is again irreversible. The assumption of irreversible steps (3.20) - stimulation - and (3.22) - relaxation - mean, the pump can only be stimulated after X_4 has attached to the pump, whereas recovery to the unstimulated pump form only occurs in the absence of X_4 . It will be seen later on that these irreversible steps cause a limiting of the stimulation and relaxation rate, *i.e.* both cannot exceed the rates k_3 or k_5 , respectively. Note this as distinction to the model of Caride, where a additional stimulation step, apart from the attachment of the calmodulin-calcium complex, is lacking.

In contrast to step (3.16) in Caride's model the calmodulin-calcium complex dissociates as a whole from the pump in step (3.21). The lack of experimental data considering that process allows both assumptions. Here the binding of calcium to calmodulin is treated as being tighter compared to the association of calmodulin with the pump protein.

Different pathways for the stimulation (equations (3.19) and (3.20)) and the relaxation process (equations (3.21) and (3.22)) are introduced. This enables to describe the temporal behaviour of these two processes independently. Since the underlying transformational changes are considered as discriminative processes this assumption is rather realistic.

With respect to the PMCA pump mass conservation $P_0 = P + P_X + P_X^* + P^*$ with P_0 as total pump concentration and the calmodulin mass conservation $M_0 = M + X_1 + X_2 + X_3 + X_4 + P_X + P_X^*$ with M_0 as total intracellular calmodulin concentration the stimulation routine introduced by reactions (3.19) - (3.22) can be translated into a system of three differential equations by using the law of mass action:

$$\begin{aligned} \frac{dP}{dt} &= -\frac{k_2 P (M_0 - P_X - P_X^*)}{A} + k_{-2} P_X + k_5 (P_0 - P - P_X - P_X^*), \\ \frac{dP_X}{dt} &= \frac{k_2 P (M_0 - P_X - P_X^*)}{A} - (k_{-2} + k_3) P_X, \\ \frac{dP_X^*}{dt} &= k_3 P_X - k_4 P_X^* + k_{-4} (P_0 - P - P_X - P_X^*) \frac{M_0 - P_X - P_X^*}{A}, \end{aligned} \quad (3.23)$$

with

$$A = 1 + \frac{K_4}{Ca} + \frac{K_3 K_4}{Ca^2} + \frac{K_2 K_3 K_4}{Ca^3} + \frac{K_1 K_2 K_3 K_4}{Ca^4}. \quad (3.24)$$

To describe the relation between free calcium, free calmodulin and free calmodulin-calcium complexes X_1 , X_2 , X_3 as well as X_4 equation (3.3) is employed by simul-

taneously respecting the calmodulin mass conservation. The transition between the four pump states is completely described therewith. P^* is determined via $P^* = P_0 - P - P_X - P_X^*$. Equations (3.23) - (3.23) describe a system of coupled inhomogeneous ordinary differential equations of first order which cannot be solved analytically. The subsequent section considers the determination of the rate constants k_i with $i = \pm 2, 3, \pm 4, 5$. Once these are fixed the transition dynamics can be simulated numerically, which is shown in section 3.4.3.

3.4.1 Stimulation

An analytical expression for k_{stim} corresponding to $k_{\text{stim}}^{\text{exp}}$ from equation (3.10) will be deduced in this section from the above presented stimulation model (equations (3.19) - (3.22)) in order to determine the rate constants k_i ($i = \pm 2, 3, \pm 4, 5$).

Suppose only unstimulated pump form P to be present and calmodulin is added. In the beginning stage the stimulation model can be reduced to the rate equations (3.19) and (3.20)



During the beginning of the stimulation the finite calmodulin concentration puts no restriction to the process, since only a minor fraction of free X_4 will be bound. Therefore the calmodulin concentration conservation is reduced to $M_0 = M + X_1 + X_2 + X_3 + X_4$ by neglecting bound calmodulin in form of P_X and P_X^* . Equation (3.4) describes the quasi-steady-state formation of X_4 for this calmodulin conservation equation. The calcium concentration in this expression is treated as thermodynamical bath, which is justified by the experimental procedure. Caride *et al.* state that enough calcium was added to obtain the concentration of free Ca^{2+} indicated in the figures [1]. The macroscopic binding constants K_i with $i = 1, 2, 3, 4$ are taken from Linse *et al.* at a KCl concentration of 150 ml [13], since this fits best the experimental conditions. See page 32 in section 3.3.2 and [1] for more details concerning the experimental setup.

With this assumption and the pump mass conservation $P_0 = P + P_X + P_X^*$, note that P^* is not involved here, reaction equations (3.19) and (3.20) can be rewritten by applying the law of mass action into a system of three linear homogeneous ordinary differential equations of first order

$$\frac{dP}{dt} = -k_2 X_4 P + k_{-2} P_X, \quad (3.26)$$

$$\frac{dP_X}{dt} = k_2 X_4 P - (k_{-2} + k_3) P_X, \quad (3.27)$$

$$\frac{dP_X^*}{dt} = k_3 P_X. \quad (3.28)$$

Attention should be drawn to the fact that the consideration of the exact calmodulin concentration conservation yields a system of three coupled inhomogeneous or-

dinary differential equations of first order which cannot be solved analytically (see equations (3.23) - (3.23)). In contrast, the system (3.26) - (3.28) can be solved via the ansatz $P = D \cdot \exp(-k_{\text{stim}}t)$, $P_X = E \cdot \exp(-k_{\text{stim}}t)$ and $P_X^* = F \cdot \exp(-k_{\text{stim}}t)$. The characteristic equation

$$\begin{vmatrix} -k_2 X_4 + k_{\text{stim}} & k_{-2} & 0 \\ k_2 X_4 & -(k_{-2} + k_3) + k_{\text{stim}} & 0 \\ 0 & k_3 & k_{\text{stim}} \end{vmatrix} = 0 \quad (3.29)$$

leads to three solutions for k_{stim} : $k_{\text{stim}}^{(1)} = 0$ and

$$k_{\text{stim}}^{(2/3)} = \frac{k_{-2} + k_3 + k_2 X_4}{2} \pm \sqrt{\left(\frac{k_{-2} + k_3 + k_2 X_4}{2}\right)^2 - k_2 k_3 X_4}. \quad (3.30)$$

With the boundary conditions of $P(0) = P_0$, $P(\infty) = 0$, $P_X(0) = 0$, $P_X(\infty) = 0$, $P_X^*(0) = 0$, $P_X^*(\infty) = P_0$ and the pump mass conservation $P_0 = P(t) + P_X(t) + P_X^*(t) \forall t$, the exact solution for the stimulated pump form becomes

$$P_X^*(t) = P_0 \left[1 + \left(\frac{k_{\text{stim}}^{(2)}}{k_{\text{stim}}^{(3)}} - 1\right)^{-1} e^{-k_{\text{stim}}^{(2)}t} - \left(1 - \frac{k_{\text{stim}}^{(3)}}{k_{\text{stim}}^{(2)}}\right)^{-1} e^{-k_{\text{stim}}^{(3)}t} \right]. \quad (3.31)$$

At the first stage of the stimulation the pump exhibits a single exponential behaviour of the form

$$P_X^*(t) = P_0(1 - e^{-k_{\text{stim}}t}) \quad (3.32)$$

as described in the section 3.3.1 by equation (3.8). The exact solution for $P_X^*(t)$ in equation (3.31) can be reduced to an equivalent expression of the form

$$P_X^*(t) = P_0(1 - e^{-k_{\text{stim}}^{(3)}t}) \quad (3.33)$$

with $k_{\text{stim}}^{(2)} \gg k_{\text{stim}}^{(3)}$. In order to yield a single exponential behaviour, the stimulation constants $k_{\text{stim}}^{(2)}$ and $k_{\text{stim}}^{(3)}$ have to fulfil this relation. Note that $k_{\text{stim}}^{(2)}$ does not appear in equation (3.33), which is reduced to be only dependent on $k_{\text{stim}}^{(3)}$.

With equation (3.33) an expression is found analogous to the single exponential fit function (3.8) for the temporal behaviour for the stimulated pump form during the stimulation process. Both expressions were deduced with the restriction to describe only the beginning stage of the stimulation. In the stimulation model the fractions of unstimulated f_{unstim} and stimulated pump forms f_{stim} in equations (3.8) and (3.9) correlate to $(P(t) + P_X(t))/P_0$ and $P_X^*(t)/P_0$, respectively. $k_{\text{stim}}^{(3)}$ directly corresponds to the stimulation constant $k_{\text{stim}}^{\text{exp}}$. Therewith an connection between the observable $k_{\text{stim}}^{\text{exp}}$ and the rate constants of the stimulation model in form of the expression for $k_{\text{stim}}^{(3)}$ in equation (3.30) is established. This is used in order to determine the parameter of the model.

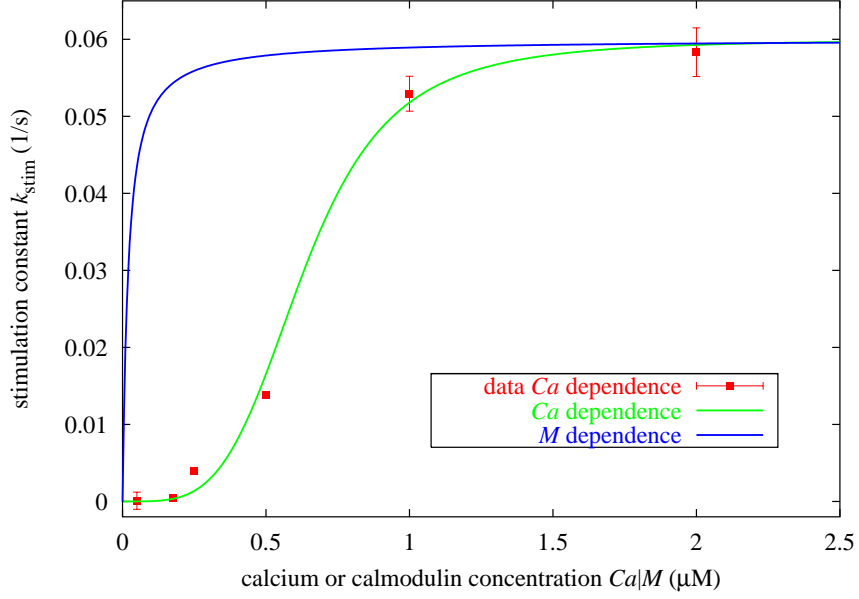


Figure 3.5: Theoretical and experimentally measured stimulation constant of the h2b isoform

$k_{\text{stim}}^{(3)}$ according to equation (3.30) is plotted against calcium (green line) at constant calmodulin concentration of $0.117 \mu\text{M}$. The blue lines represent the $k_{\text{stim}}^{(3)}$ dependence on calmodulin at fixed calcium concentration of $1 \mu\text{M}$. The stimulation rate data (red squares) has been measured at various calcium concentrations with constant calmodulin concentration of $0.117 \mu\text{M}$ (with kind permission of Caride [1]).

The data points in figure 3.5 and 3.6 depict $k_{\text{stim}}^{\text{exp}}$. In addition $k_{\text{stim}}^{(3)}$ from equation (3.30) is plotted against calcium or calmodulin concentration whereas calmodulin or calcium, respectively, is kept constant. Both display a sigmoidal behaviour. Therefore it is possible to adapt the theoretical curve to the experimental data in order to fix the stimulation parameter. The single exponential fit constants $k_{\text{stim}}^{\text{exp}}$ (squares in figure 3.5 and 3.6) determined by experiments [1] can be correctly fitted by the Hill equation

$$k_{\text{stim}}^{\text{exp}}(Ca) = \frac{k_{\text{stim}}^{\text{max}} \cdot Ca^4}{Ca_{\text{stim}}^{(1/2)4} + Ca^4}, \quad (3.34)$$

with the Hill coefficient $n = 4$, the maximal stimulation constant $k_{\text{stim}}^{\text{max}}$ and the half activation concentration $Ca_{\text{stim}}^{(1/2)}$. Fitting equation (3.34) to the experimental data shown in figure 3.5 and 3.6 yields $k_{\text{stim}}^{\text{max}} = 0.0603 \text{ 1/s}$, $Ca_{\text{stim}}^{(1/2)} = 0.653 \mu\text{M}$ for the h2b isoform and $k_{\text{stim}}^{\text{max}} = 0.0243 \text{ 1/s}$, $Ca_{\text{stim}}^{(1/2)} = 1.1 \mu\text{M}$ for the h4b isoform.

In order to find a correspondent for $k_{\text{stim}}^{\text{max}}$ the limes of $k_{\text{stim}}^{(3)}$ for $X_4 \rightarrow \infty$, meaning high calcium or calmodulin concentrations, in the case of real and positive rate

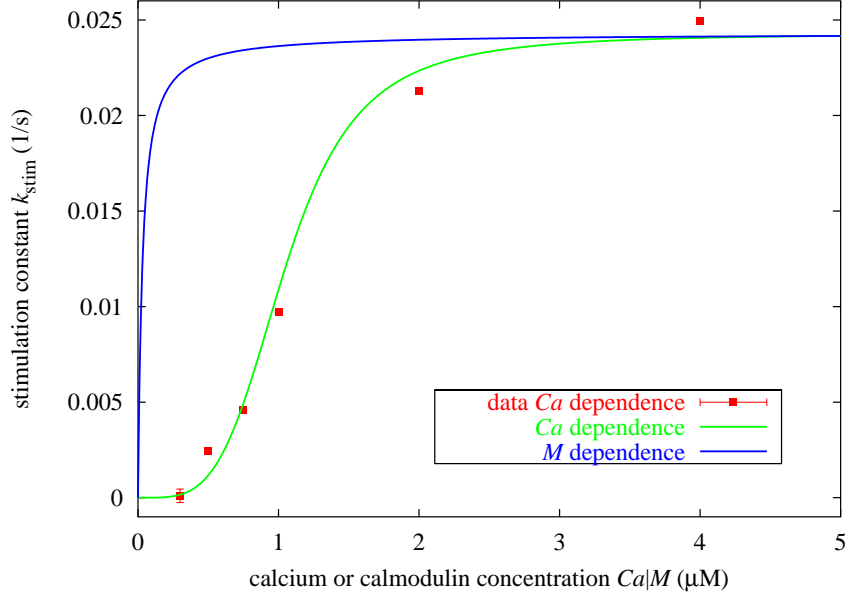


Figure 3.6: Theoretical and experimentally measured stimulation constant of the h4b isoform

$k_{\text{stim}}^{(3)}$ according to equation (3.30) is plotted against calcium (green line) at constant calmodulin concentration of $0.117 \mu\text{M}$. The blue lines represent the $k_{\text{stim}}^{(3)}$ dependence on calmodulin at fixed calcium concentration of $1.5 \mu\text{M}$. The stimulation rate data (red squares) has been measured at various calcium concentrations with constant calmodulin concentration of $0.117 \mu\text{M}$ (with kind permission of Caride [1]).

constants k_2 , k_{-2} and k_3 is considered.

$$\begin{aligned}
 \lim_{X_4 \rightarrow \infty} k_{\text{stim}}^{(3)} &= \lim_{C \rightarrow \infty} \frac{k_{-2} + k_3 + k_2 X_4}{2} - \sqrt{\left(\frac{k_{-2} + k_3 + k_2 X_4}{2}\right)^2 - k_2 k_3 X_4} \\
 &= \lim_{X_4 \rightarrow \infty} \frac{1 - \sqrt{1 - \frac{4k_2 k_3 X_4}{(k_{-2} + k_3 + k_2 X_4)^2}}}{\frac{2}{k_{-2} + k_3 + k_2 X_4}} \quad (3.35)
 \end{aligned}$$

In the limes $X_4 \rightarrow \infty$ this expression becomes undetermined. Using the rule of de l'Hospital leads to:

$$\begin{aligned}
 \lim_{X_4 \rightarrow \infty} k_{\text{stim}}^{(3)} &= \lim_{X_4 \rightarrow \infty} -k_3 \frac{\left(\frac{k_{-2}}{X_4} + \frac{k_3}{X_4} - k_2\right)}{\left(\frac{k_{-2}}{X_4} + \frac{k_3}{X_4} + k_2\right)} \frac{1}{\sqrt{1 - \frac{4k_2 k_3 X_4}{(k_{-2} + k_3 + k_2 X_4)^2}}} \\
 &= k_3. \quad (3.36)
 \end{aligned}$$

$k_{\text{stim}}^{(3)}$ converges to k_3 for large calcium or calmodulin concentrations, hence k_3 confines the maximum stimulation rate and can be identified with $k_{\text{stim}}^{\text{max}}$. This corresponds to the introduction of equation (3.20) with which it is aimed to get a limitation of the stimulation rate. Knowing that, setting equation (3.30) equal to $k_3/2$ and using (3.4), an expression for $X_{4Ca_{\text{stim}}^{(1/2)}}$ corresponding to the calmodulin-calcium complex concentration X_4 at the half maximum calcium concentration $Ca_{\text{stim}}^{(1/2)}$ (from fit equation (3.34)) can be deduced

$$X_{4Ca_{\text{stim}}^{(1/2)}} = \frac{M_0}{1 + \frac{K_4}{(Ca_{\text{stim}}^{(1/2)})} + \frac{K_3K_4}{(Ca_{\text{stim}}^{(1/2)})^2} + \frac{K_2K_3K_4}{(Ca_{\text{stim}}^{(1/2)})^3} + \frac{K_1K_2K_3K_4}{(Ca_{\text{stim}}^{(1/2)})^4}} = \frac{k_{-2} + k_3/2}{k_2}. \quad (3.37)$$

Here the calmodulin concentration is kept constant. With the knowledge of k_3 the value of $X_{4Ca_{\text{stim}}^{(1/2)}}$ determines a relation between k_2 and k_{-2} . Further limitations of both rate constants will be discussed below.

Presently, only measurements of the calcium dependence of k_{stim} are available. For the determination of the model parameters data of the calmodulin dependence would not provide further informations. But with equation (3.30) and the so far determined parameters it is possible to quote the calmodulin dependence of the stimulation constant. In figure 3.5 and 3.6 the proposed behaviour of $k_{\text{stim}}^{(3)}(M)$ is shown. Provided the experimental data have a similar behaviour, they can be fitted by

$$k_{\text{stim}}^{\text{exp}}(M) = \frac{k_{\text{stim}}^{\text{max}} \cdot M}{M_{\text{stim}}^{(1/2)} + M}. \quad (3.38)$$

In analogy to the calcium case the maximum stimulation constant $k_{\text{stim}}^{\text{max}}$ yields k_3 and the half activation concentration $M_{\text{stim}}^{(1/2)}$ provides a relation between k_2 and k_{-2} given by

$$X_{4M_{\text{stim}}^{(1/2)}} = \frac{M_{\text{stim}}^{(1/2)}}{1 + \frac{K_4}{(Ca_0)} + \frac{K_3K_4}{(Ca_0)^2} + \frac{K_2K_3K_4}{(Ca_0)^3} + \frac{K_1K_2K_3K_4}{(Ca_0)^4}} = \frac{k_{-2} + k_3/2}{k_2}, \quad (3.39)$$

with a constant calcium concentration of Ca_0 .

Each fit, for the calcium- (equation (3.34)) and the calmodulin-dependent (equation (3.38)) case delivers two fit parameter $k_{\text{stim}}^{\text{max}}$ and $Ca_{\text{stim}}^{(1/2)}$ or $M_{\text{stim}}^{(1/2)}$, respectively, which determine k_3 and a relation between k_2 and k_{-2} . The calmodulin dependence fit cannot provide further informations since $X_{4Ca_{\text{stim}}^{(1/2)}} = X_{4M_{\text{stim}}^{(1/2)}}$ (see equations (3.37) and (3.39)). But this equivalence allows to predict the stimulation constant behaviour which is done in figure 3.5 and 3.6. Currently, no data are available to verify the predictions in figure 3.5 and 3.6.

3.4.2 Relaxation

The same procedure as for the stimulation process is applied to the relaxation of the stimulated PMCA pump in this section. It is aimed to find a connection between the experimental data in form of $k_{\text{relax}}^{\text{exp}}$ and the rate constants k_i with $i = \pm 4, 5$ introduced by the stimulation model.

Suppose only stimulated pump form P_X^* to be present. The beginning stage of the relaxation can be reduced to equations (3.21) and (3.22)

$$P_X^* \xrightleftharpoons[k_{-4}]^{k_4} P^* + X_4, \quad (3.40)$$

$$P^* \xrightarrow{k_5} P. \quad (3.41)$$

Neglecting the calmodulin concentration conservation causes no problem since the changes in calmodulin concentration in the beginning of the relaxation are small. Again the calmodulin conservation does not include the calmodulin bound to the pump. With that simplification the remaining reaction scheme (3.40) and (3.41) can be translated into a system of three linear homogeneous differential equations of first order by applying the law of mass action. Again the neglect of the exact calmodulin conservation provides the solubility of the differential equations system. With the general ansatz $P_X^*(t) = M \cdot \exp(-k_{\text{relax}}t)$, $P^*(t) = N \cdot \exp(-k_{\text{relax}}t)$ and $P(t) = O \cdot \exp(-k_{\text{relax}}t)$, for the linear homogeneous system, the characteristic equation leads to three solutions for the relaxation constant k_{relax} : $k_{\text{relax}}^{(1)} = 0$ and

$$k_{\text{relax}}^{(2/3)} = \frac{k_4 + k_5 + k_{-4}X_4}{2} \pm \sqrt{\left(\frac{k_4 + k_5 + k_{-4}X_4}{2}\right)^{(2)} - k_4k_5}. \quad (3.42)$$

With the boundary conditions $P_X^*(0) = P_0$, $P_X^*(\infty) = 0$, $P^*(0) = 0$, $P^*(\infty) = 0$, $P(0) = 0$, $P(\infty) = P_0$ and the pump mass conservation $P_X^*(t) + P^*(t) + P(t) = P_0$, the exact solution for the temporal accumulation of unstimulated pump form becomes

$$P(t) = P_0 \left[1 - \left(1 - \frac{k_{\text{relax}}^{(2)}}{k_{\text{relax}}^{(3)}}\right)^{-1} e^{-k_{\text{relax}}^{(2)}t} + \left(\frac{k_{\text{relax}}^{(3)}}{k_{\text{relax}}^{(2)}} - 1\right)^{-1} e^{-k_{\text{relax}}^{(3)}t} \right]. \quad (3.43)$$

Again, to get a single exponential behaviour, as suggested by experiment, the solutions in equation (3.42) have to fulfil $k_{\text{relax}}^{(2)} \gg k_{\text{relax}}^{(3)}$. Therewith the solution for the unstimulated pump form becomes

$$P(t) = P_0(1 - e^{-k_{\text{relax}}^{(3)}t}), \quad (3.44)$$

where $k_{\text{relax}}^{(2)}$ does not appear. This expression is similar to the single exponential fit function for the unstimulated pump form during relaxation (3.12) which is used

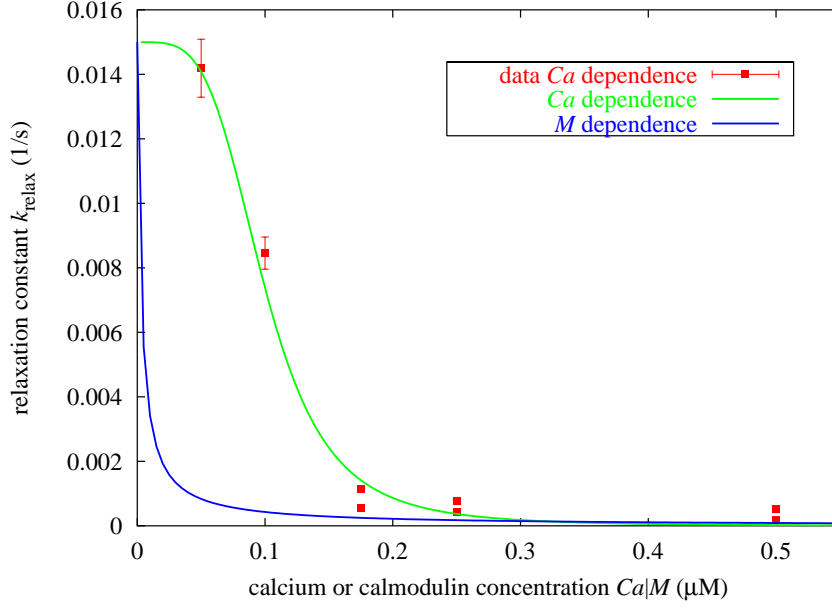


Figure 3.7: Theoretical and experimentally measured relaxation constant of the h2b isoform

The relaxation constant $k_{\text{relax}}^{(3)}$ according to equation (3.42) is plotted for changing calcium (green line) and calmodulin (blue line) concentrations whereas calmodulin ($M_0 = 0.117 \mu\text{M}$) and calcium ($Ca = 0.25 \mu\text{M}$) are kept constant. The theoretical behaviour at changing calcium concentrations is fitted to the experimental data (red squares) at $M = 0.117 \mu\text{M}$ (with kind permission of Caride [1]).

in order to determine $k_{\text{relax}}^{\text{exp}}$. The fraction f_{unstim} in that model is characterised by $P(t)/P_0$, whereas f_{stim} during relaxation becomes $(P_X^*(t) + P^*(t))/P_0$. Both, the single exponential fit functions (3.11), (3.12) and equation (3.44) claim to describe the temporal behaviour of an ensemble of pumps during relaxation only in the beginning stage. However, the correspondence of $k_{\text{relax}}^{\text{exp}}$ in equation (3.12) with $k_{\text{relax}}^{(3)}$ in (3.44) allows to determine the relaxation parameter.

In figure 3.7 and 3.8 $k_{\text{relax}}^{(3)}$ is plotted in conjunction with experimental measured relaxation constants $k_{\text{relax}}^{\text{exp}}$ by Caride *et al.* [1]. Both exhibit a sigmoidal behaviour. Thus, the adaption of the theoretical expression for the relaxation constant $k_{\text{relax}}^{(3)}$ in equation (3.42) allows to make statements about the relaxation rate constants introduced by the stimulation model equations.

The experimental data can be correctly fitted by the reverse Hill equation

$$k_{\text{relax}}^{\text{exp}}(Ca) = \frac{k_{\text{relax}}^{\text{max}}}{1 + \left(\frac{Ca}{Ca_{\text{relax}}^{(1/2)}}\right)^4}. \quad (3.45)$$

The fit delivers $k_{\text{relax}}^{\text{max}} = 0.0152 \text{ 1/s}$, $Ca_{\text{relax}}^{(1/2)} = 0.102 \mu\text{M}$ for the h2b isoform and

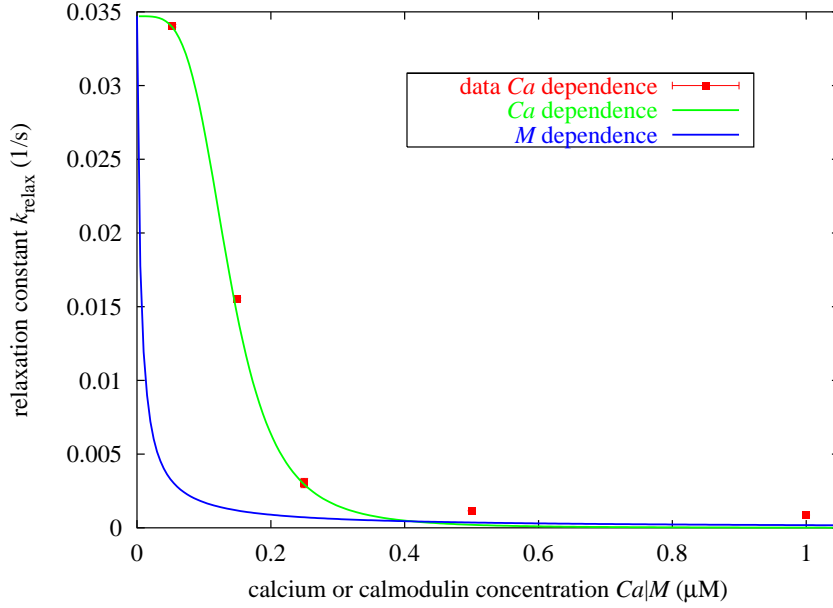


Figure 3.8: Theoretical and experimentally measured relaxation constant of the h4b isoform

The relaxation constant $k_{\text{relax}}^{(3)}$ according to equation (3.42) is plotted for changing calcium (green line) and calmodulin (blue line) concentrations whereas calmodulin ($M_0 = 0.117 \mu\text{M}$) and calcium ($Ca = 0.3 \mu\text{M}$) are kept constant. The theoretical behaviour at changing calcium concentrations is fitted to the experimental data (red squares) at $M_0 = 0.117 \mu\text{M}$ (with kind permission of Caride [1]).

$k_{\text{relax}}^{\text{max}} = 0.0347 \text{ 1/s}$, $Ca_{\text{relax}}^{(1/2)} = 0.142 \mu\text{M}$ for the h4b isoform.

For $Ca = 0 \mu\text{M}$ the maximal relaxation rate $k_{\text{relax}}^{(3)}$ is k_5 with $k_4 > k_5$. Hence the maximum relaxation fit parameter $k_{\text{relax}}^{\text{max}}$ is identified with k_5 . Setting equation (3.42) equal to $k_5/2$ yields a relation for the half maximum concentration $Ca_{\text{relax}}^{(1/2)}$

$$X_4 Ca_{\text{relax}}^{(1/2)} = \frac{M_0}{1 + \frac{K_4}{(Ca_{\text{relax}}^{(1/2)})} + \frac{K_3 K_4}{(Ca_{\text{relax}}^{(1/2)})^2} + \frac{K_2 K_3 K_4}{(Ca_{\text{relax}}^{(1/2)})^3} + \frac{K_1 K_2 K_3 K_4}{(Ca_{\text{relax}}^{(1/2)})^4}} = \frac{k_4 - k_5/2}{k_{-4}}, \quad (3.46)$$

where $X_4 Ca_{\text{relax}}^{(1/2)}$ is the calmodulin-calcium complex concentration at $Ca_{\text{relax}}^{(1/2)}$. There-with and with $k_{\text{relax}}^{\text{max}} = k_5$ a relation between k_4 and k_{-4} is established.

Data at various calmodulin concentrations have not been reported. But with the data obtained from the calcium dependence it is possible to provide a theoretical proposition from equation (3.42) (see blue lines in figure 3.7 and 3.8). Such data could be described with

$$k_{\text{relax}}^{\text{exp}}(M) = \frac{k_{\text{relax}}^{\text{max}}}{1 + \frac{M}{M_{\text{relax}}^{(1/2)}}}. \quad (3.47)$$

parameter	h2b	h4b	unit	source
K_1	20.0		μM	[13]
K_2	0.63			
K_3	100			
K_4	5.01			
k_2	> 9500	> 516	$1/(\mu\text{M} \cdot \text{s})$	equation (3.37)
k_3	0.06	0.024	1/s	$k_{\text{stim}}^{\text{max}}$
k_{-4}	$> 3.8 \cdot 10^6$	$> 2.33 \cdot 10^6$	$1/(\mu\text{M} \cdot \text{s})$	equation (3.46)
k_5	0.015	0.0347	1/s	$k_{\text{relax}}^{\text{max}}$

Table 3.3: General values and ranges of the rate constants for the h2b and h4b isoform

Pump specific rate constants determined using experimental data from Caride *et al.* (2001) [1].

Both fit parameter, the half maximum concentrations $M_{\text{relax}}^{(1/2)}$ and the maximum relaxation constant $k_{\text{relax}}^{\text{max}}$ would not provide additional informations compared to the calcium behaviour fit parameter. $k_{\text{relax}}^{\text{max}}$ corresponds to k_5 with $k_4 > k_5$ and $M_{\text{relax}}^{\text{exp}}$ delivers a relation between k_4 and k_{-4} via

$$X_{4M_{\text{relax}}^{(1/2)}} = \frac{M_{\text{relax}}^{(1/2)}}{1 + \frac{K_4}{(Ca_0)} + \frac{K_3K_4}{(Ca_0)^2} + \frac{K_2K_3K_4}{(Ca_0)^3} + \frac{K_1K_2K_3K_4}{(Ca_0)^4}} = \frac{k_4 - k_5/2}{k_{-4}}. \quad (3.48)$$

$X_{4M_{\text{relax}}^{(1/2)}}$ is the accordant complex concentration at the half maximum calmodulin concentration $M_{\text{relax}}^{(1/2)}$.

As before the lack of data for the calmodulin dependence of the relaxation process restricts to the quantitative determination of k_5 and a relation between k_4 and k_{-4} out of the calcium fit parameter only. The prediction of the calmodulin dependence is possible since $X_{4Ca_{\text{relax}}^{(1/2)}} = X_{4M_{\text{relax}}^{(1/2)}}$ (see equations (3.46) and (3.48)).

With the data provided by Caride *et al.* and the described procedure we can quote parameter sets for the two investigated isoforms h2b and h4b, which are shown in table 3.3. Attention should be drawn to the fact, that Ca^{2+} is bound by polar amino acids of calmodulin and therefore the affinities represented by K_i with $i = 1..4$ strongly depend on the ionic strength of the experimental solution. The here used value for the K_i 's at 150 mM KCl fit best the experimental conditions of 30 mM Tes-TEA, pH 7.2 and 120 mM KCl of Caride *et al.* (for more details see [1, 13] and section 3.1).

Equations (3.37) and (3.46) do not allow to fix k_2, k_{-2}, k_4 and k_{-4} , therefore the theoretical possible ranges of values for k_2 and k_{-4} are shown in table 3.3. The informations of the stimulation and relaxation constant measurements relate k_{-2} and k_4 to k_2 and k_{-4} via equations (3.37) and (3.46), respectively. The lower

parameter	h2b	h4b	unit	source
k_2	$1 \cdot 10^5$	$5 \cdot 10^3$	$1/(\mu\text{M} \cdot \text{s})$	equation (3.37)
k_{-2}	0.286	0.101	1/s	
k_4	2.03	7.47	1/s	equation (3.46)
k_{-4}	$1 \cdot 10^9$	$1 \cdot 10^9$	$1/(\mu\text{M} \cdot \text{s})$	

Table 3.4: Fixed rate constants for the h2b and h4b isoform

Reasonable values for k_2, k_{-2}, k_4 and k_{-4} are chosen by using additional informations (see text for more details).

bounds of k_2 and k_{-4} are delivered from $0 > k_{-2}$ and $k_4 > k_5$, respectively. $k_4 > k_5$ is required in order to assure step (3.22) to be the limiting reaction. In the opposite case ($k_4 < k_5$), k_4 would be the limiting relaxation constant which is not conflicting with the model but will not be considered here.

In addition, further informations are related to the choice of k_{-2}, k_4, k_2 and k_{-4} . Note that equations (3.30) and (3.42) are derived only by concerning the beginning of the stimulation or the relaxation. Without that simplification the velocity of the exact stimulation and relaxation process, if measured, would further confine the range of these parameter. The steady-state graph, which will be discussed in section 3.5.2, and also the slopes of the raising faces in figures 3.5, 3.6, 3.7 and 3.8 are correlated with k_{-2}, k_4, k_2 and k_{-4} . So far, informations from the steady-state graph and the slopes in the figures are used to quote the parameter set in table 3.4, which will be used for all further calculations. Attention should be drawn to the fact, that the exact stimulation and relaxation velocity provides the most relevant additional information in order to restrict the ranges in table 3.3, *i.e.* the choice of k_i , with $i = \pm 2, \pm 4$ significantly influences how fast stimulated pump form is provided or degraded. The effect of differing k_{-2}/k_2 ratios can be seen and is discussed in section 3.4.3 in regard of the difference between the two considered isoforms.

3.4.3 Stimulation dynamics

Based on the stimulation model (3.19) - (3.22) and with the isoform specific rate constants in table 3.3 and 3.4, the pumping state dynamics of the PMCA pump can be simulated, *i.e.* the transition from unstimulated f_{unstim} to stimulated pump fraction f_{stim} and vice versa.

With the obtained parameters, precise statements on dynamical stimulation and relaxation differences are possible. The 2.5 times higher value for k_3 of the h2b isoform compared to h4b suggests a faster stimulation, whereas the decay of stimulated pump form occurs faster for the h4b isoform since $k_5^{\text{h4b}} > k_5^{\text{h2b}}$. These results suggest that the hPMCA2b pump exhibits memory of the previous

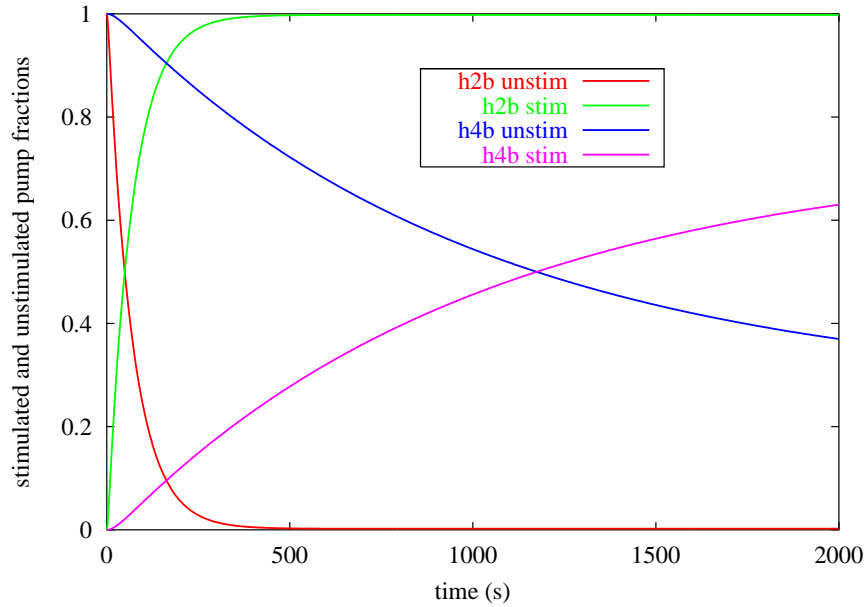


Figure 3.9: Stimulation of the h2b and h4b isoforms at $Ca = 0.5 \mu\text{M}$

The fractions $f_{\text{unstim}} = \frac{P(t)+P_X(t)}{P_0}$ (red line for h2b, blue line for h4b) and $f_{\text{stim}} = \frac{P^*(t)+P_X^*(t)}{P_0}$ (green line for h2b, purple line for h4b) are shown during the stimulation. The simulation is done with a total calmodulin concentration of $0.117 \mu\text{M}$ and $P_0 = 0.005 \mu\text{M}$. The present calcium concentration is $0.5 \mu\text{M}$. At $t = 0$ only unstimulated pump form P is present $P(0) = P_0$.

Ca^{2+} for a longer time than the hPMCA4b pump. This is in agreement with the measurements and results of Caride *et al.* [1].

With the reaction rates shown in table 3.3 and 3.4 the system of coupled differential equations (3.23), (3.23) and (3.23) is solved numerically with a fourth order Runge-Kutta method. This has been implemented in a C++ program. The stimulation and relaxation dynamics of both isoforms can be seen in figure 3.9 and 3.10, respectively. In figure 3.9 no stimulated pump form $f_{\text{stim}} = 0$ is present at t_0 and the pump is exposed to a calcium concentration of $0.5 \mu\text{M}$, *i.e.* $P(0) = P_0$. Whereas in the relaxation graph 3.10 only stimulated pump form $f_{\text{stim}} = 1$ is available at t_0 and the calcium concentration is decreased to $0.1 \mu\text{M}$, *i.e.* $PC^*(0) = P_0$. The differences in the stimulation and relaxation behaviour between h2b and h4b, namely fast stimulation but slower relaxation of the h2b isoform compared to the h4b isoform, can clearly be seen.

In figure 3.11 the unstimulated h2b isoform, meaning $P(0) = P_0$, is exposed to different calcium concentrations and a constant calmodulin concentration of $M_0 = 0.117 \mu\text{M}$. In contrast to figure 3.4 where the same case for the Caride model is simulated, the stimulation velocity does not exceed a maximum possible formation

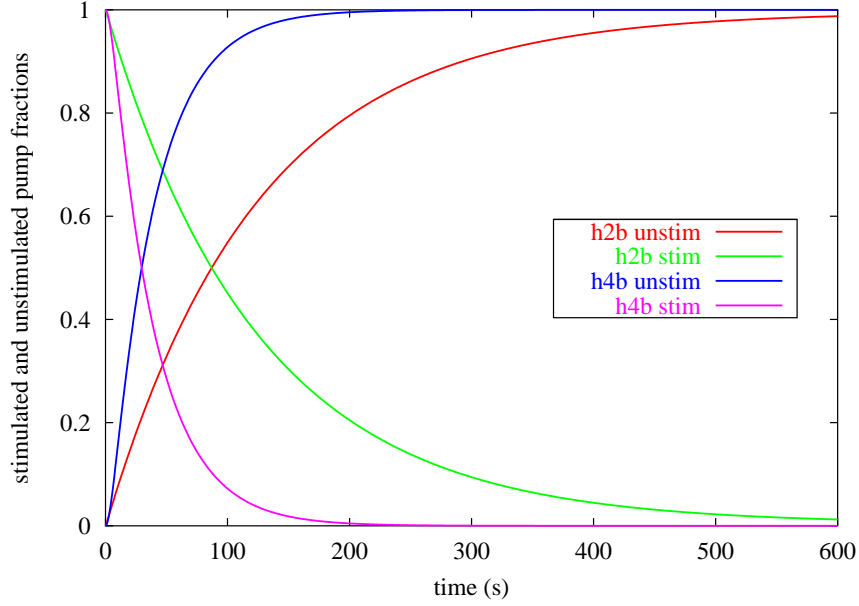


Figure 3.10: Relaxation of the h2b and h4b isoforms at $Ca = 0.1 \mu\text{M}$

The fractions $f_{\text{unstim}} = \frac{P(t)+P_X(t)}{P_0}$ (red line for h2b, blue line for h4b) and $f_{\text{stim}} = \frac{P^*(t)+P_X^*(t)}{P_0}$ (green line for h2b, purple line for h4b) are shown during the relaxation. The simulation is done with a total calmodulin concentration of $0.117 \mu\text{M}$ and $P_0 = 0.005 \mu\text{M}$. The present calcium concentration is $0.1 \mu\text{M}$. $PC^*(0) = P_0$ is the starting point of the simulation.

velocity of stimulated pump form. Regarding the theoretical expression for the stimulated pump fraction (3.32), $k_{\text{stim}}^{(3)}$ converges for large calcium or calmodulin concentrations, *i.e.* large X_4 , to k_3 . It can be seen in figure 3.11 that

$$(P_X^*(t) + P^*(t))/P_0 = 1 - \exp(-k_3 t) \quad (3.49)$$

describes the maximum possible stimulation velocity. This expression was originally deduced to describe the beginning stage of the stimulation. In comparison with the model of Caride described by (3.14) - (3.17), it becomes evident that this limitation is achieved with the introduction of reaction (3.20) in the new stimulation model.

Regarding the maximal possible formation velocity of stimulated pump form in equation (3.49), it is possible to quote a minimum half stimulation time $t_{\text{minstim}}^{(1/2)}$ which quantitatively expresses stimulation behaviour differences between the isoforms. Solving $1/2 = 1 - \exp(-k_3 t_{\text{minstim}}^{(1/2)})$ leads to 11.6 s for the h2b isoform and 28.5 s for h4b. The same approach can be applied to the relaxation, setting equation (3.44) equal to $P_0/2$ delivers a minimum relaxation time $t_{\text{minrelax}}^{(1/2)}$ as a measure of temporal relaxation behaviour (45.6 s for h2b, 20.0 s for h4b). Though the minimum half stimulation time for h4b is only twofold compared to

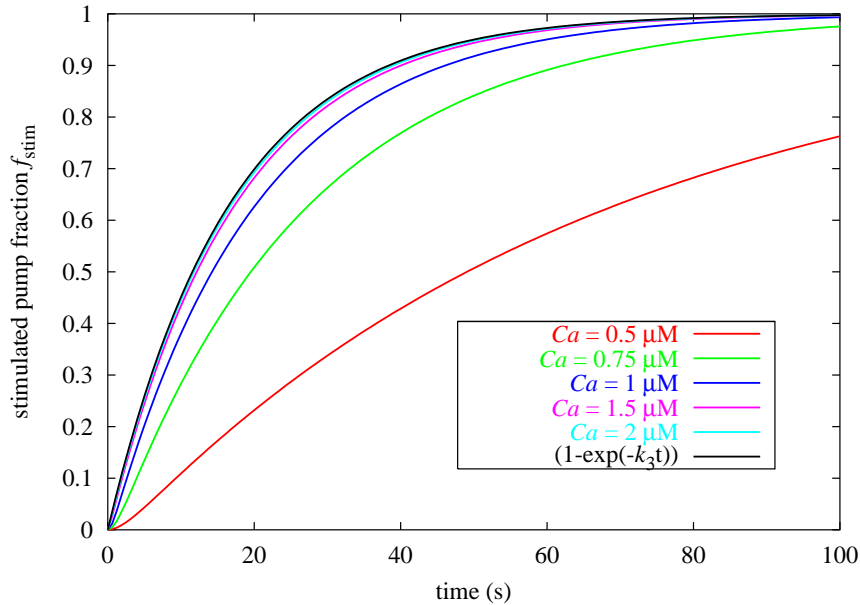


Figure 3.11: Stimulation of the 2b isoform at $M_0 = 0.117 \mu\text{M}$ and various calcium concentrations

For different calcium concentrations the temporal change of the stimulated pump fraction $(PC^*(t) + P^*(t))/P_0$ is shown. The calmodulin concentration at all simulations is $0.117 \mu\text{M}$ and the total pump concentration $P_0 = 0.005 \mu\text{M}$. The stimulation started with only unstimulated pump form to be present, *i.e.* $P(0) = 1$. Additionally the theoretical fastest possible stimulation $(PC^*(t) + P^*(t))/P_0 = 1 - \exp(-k_3t)$ (black line) is plotted.

h2b, the h2b isoform is stimulated much faster (see figure 3.9). The reason for that are the different affinities of the isoforms to the calmodulin-calcium complex, *i.e.* $K_d = 0.00286 \text{ nM}$ for the h2b isoform and $K_d = 0.0202 \text{ nM}$ for the h4b isoform. K_d refers to the dissociation constant between calmodulin-calcium complex (X_4) and PMCA pump and is defined as $K_d = k_{-2}/k_2$. The dissociation constant of the h4b isoform is about 10 times higher as the value of K_d for the h2b isoform, which is in agreement with experimental data [19, 32, 37, 43, 48]. The question concerning the affinity of the PMCA pump for the calmodulin-calcium complex will be discussed further in section 3.7 and section 4.1.

3.5 Modelling the PMCA pump activity

Up to this point the temporal transition between unstimulated and stimulated pump forms has been described. This section will consider the mathematical description how the Plasma Membrane Calcium pump transports calcium ions through the membrane in dependence on the intracellular calcium concentration.

The transport process is treated to be in quasi-steady-state, *i.e.* the pump activity reacts immediately on the intracellular calcium concentration. This is in contrast to the stimulation dynamics, where the stimulation and the relaxation occurs over a time scale of minutes and therefore the formation or decomposition of stimulated pump form has a time dependence related to the present calcium and calmodulin concentration. The quasi-steady-state simplification for the calcium transport process is justified, since the adaption of the pumping activity to different calcium concentrations happens within milliseconds and the stimulation/relaxation on a time scale of minutes.

3.5.1 Pumping activity and stoichiometry

In contrast to the Ca^{2+} pump of the sarcoplasmic reticulum (SERCA) the stoichiometry between transported Ca^{2+} and hydrolysed ATP of the PMCA pump is most likely 1:1 [38, 42, 45]. The SERCA pump works with a calcium:ATP ratio of 2:1 [45, 46]. The resulting pumping cycle, including the different phosphorylation states, is shown in chapter 3.2 on page 28. The translocation step of calcium across the membrane, depicted as $\text{E}_1 \sim \text{Ph}_i \rightarrow \text{E}_2 \sim \text{Ph}_i$ is related to a transformational change [38, 43]. For a simple approach, we neglect the different conformation - and phosphorylation states of the PMCA pump during transport. Then the transport cycle expressed in rate equations becomes



which is similar to the Michaelis and Menten enzyme model (1913). Note, that all the subtleties of diffusion of calcium to and from the intracellular binding site and the time resolution of the calcium transport through the membrane are replaced by rate constants. Since ATP is highly available in cells we treat the ATP concentration as thermodynamical bath, meaning ATP is always sufficiently disposable to hydrolyse the pump. Using the law of mass action, the steady-state expression for the calcium transport rate $I^{(1)}$ in the outward direction is

$$I^{(1)} = \frac{r_2 \cdot Ca}{\frac{r_{-1} + r_2}{r_1} + Ca} \equiv \frac{I_{\text{max}}^{(1)} \cdot Ca}{H_p^{(1)} + Ca}. \quad (3.51)$$

Ca is the free intracellular calcium concentration $[\text{Ca}^{2+}]_{\text{in}}$. This equation of the transport rate $I^{(1)}$ has the same form as a Hill equation with Hill coefficient $n = 1$. The corresponding transmembrane current $\frac{dQ}{dt}$, is given by $\frac{dQ}{dt} = z_{\text{Ca}} F I^{(1)}$, where F is the Faraday constant and z_{Ca} the valence charge of calcium ($z_{\text{Ca}} = 2$). r_2 can be identified with the maximal pump rate $I_{\text{max}}^{(1)}$. Since the maximum rate of the reaction is limited by the dissociation reaction $\text{P}_{\text{Ca}} \xrightarrow{r_2} \text{P} + \text{Ca}_{\text{out}}$, $r_2 = I_{\text{max}}^{(1)}$ stands for the saturating properties of the pumping process. Biologically, this means the

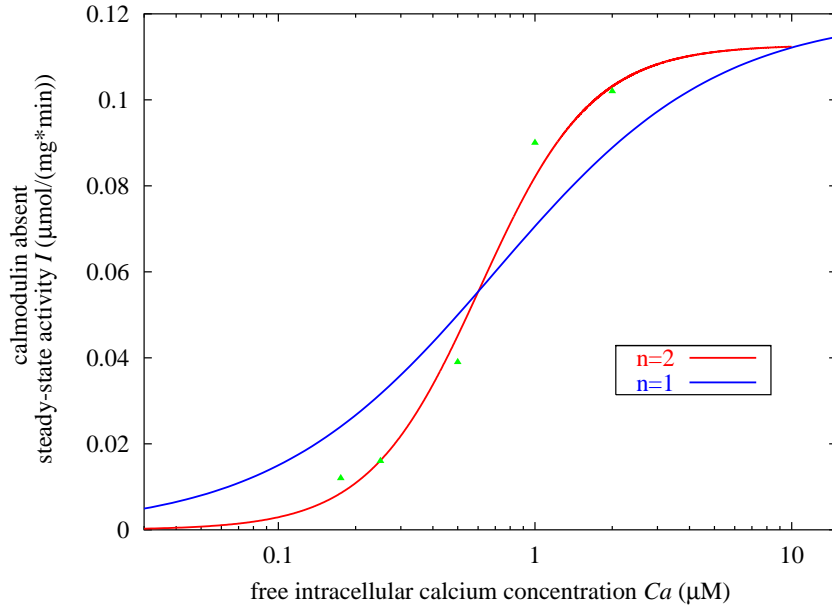


Figure 3.12: Steady-state activity of the h2b isoform in the absence of calmodulin

For different calcium concentration in the absence of calmodulin the measured steady-state activity (green triangles) is shown (with kind permission of Caride [1]). These data has been fitted by equation (3.51) (blue line), *i.e.* Hill equation with Hill coefficient $n = 1$, and by equation (3.52) (red line), *i.e.* Hill equation with Hill coefficient $n = 2$.

limitation by the confined transformational change velocity of the pump during the $E_1 \sim Ph_i \rightarrow E_2 \sim Ph_i$ transition. $H_p = \frac{r_{-1} + r_2}{r_1}$ is referred to as half activation concentration and is a measure for the affinity of the pump to calcium.

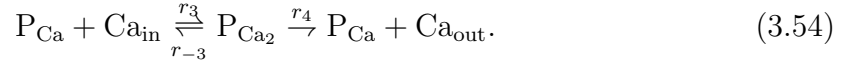
Considering the experimentally measured transport rate in the absence of calmodulin, equation (3.51) fails to reproduce the slope of the raising face between almost no pump activity and saturated pump activity (see figure 3.12). The steady-state calcium-dependent PMCA pump activity shows a sigmoidal behaviour, which is confirmed in experiments performed by Elwess *et al.* [19] or by Verma *et al.* [49]. As demonstrated in figure 3.12, such behaviour can be described better by a Hill equation with Hill coefficient $n = 2$,

$$I^{(2)} = \frac{I_{\max}^{(2)} \cdot Ca^2}{H_p^{(2)2} + Ca^2}. \quad (3.52)$$

At the moment there exists no biological justification for equation (3.52). Theoretically this equation can be deduced from a transport cycle with a stoichiometry 2:1 of Ca:ATP and by assuming the binding of the two calcium ions to be cooperatively. But as mentioned above, stoichiometry 2:1 is not the case for the PMCA

pump [37, 38, 42].

Considering the case of stoichiometry 2:1 of transported calcium to hydrolysed ATP, with the neglect of different phosphorylation and transformation pump states the pump cycle can be expressed by the following rate equations



Due to the different possible relations between the rate constants r_1 , r_{-1} and r_3 , r_{-3} , *i.e.* the binding of the first calcium ion affects the binding of the subsequent one, different pumping rate behaviours are possible [50]:

- The binding sites of the PMCA pump are independent and identical (see green line in figure 3.13), then $r_1 = 2r_3$ and $2r_{-1} = r_{-3}$. The attachment of the second calcium ion, step (3.54), occurs with half of the rate of the first calcium ion, step (3.53), since one site is already occupied.
- The red line in figure 3.13 depicts the case of positive cooperativity, *i.e.* the binding of the first calcium ion is slow, but that of the second is fast, meaning an increase in affinity upon the binding of the first ion. In terms of the rate constants, this can be expressed by $r_1 \rightarrow 0$ and $r_3 \rightarrow \infty$.
- In the opposite extreme, the binding of the first calcium ion decreases the rate of the subsequent ion binding. This case is referred to as negative cooperativity (blue line in figure 3.13) and can be modelled by $r_1 \gg r_3$.

The plots of all the three cases in figure 3.13 differ only in the relations between r_1 , r_{-1} and r_3 , r_{-3} , *i.e.* the rate constants r_2 and r_4 remain equal for all graphs.

Positive cooperativity provides the possibility for the pump to shift its range of sensitivity into a physiological relevant range of intracellular calcium concentration as the PMCA pump does. The steep raise of the sigmoidal function, describing positive cooperative calcium binding (green line in figure 3.12), lies within 0.2 and 3 μM free calcium concentration. Note that at resting state the intracellular calcium concentration is 0.1 μM . A similar phenomenon could be observed by considering the calcium binding of calmodulin in section 3.1 (see figure 3.3).

On the contrary, for the transported calcium to ATP ratio of 1:1 the pumping behaviour is determined by equation (3.51) and is plotted in figure 3.12. One possible way in this case to fit differing calcium dependent uptake scenarios is a calcium dependent reaction rate $r_1 = r_1(\text{Ca})$ (see equation (3.51)). But since all calcium dependencies should be intrinsic to the pumping cycle (3.50), a justification for this does not exist.

Concerning the contradiction between the calcium-dependent pumping behaviour and the stoichiometry between transported Ca^{2+} and hydrolysed ATP, Carafoli

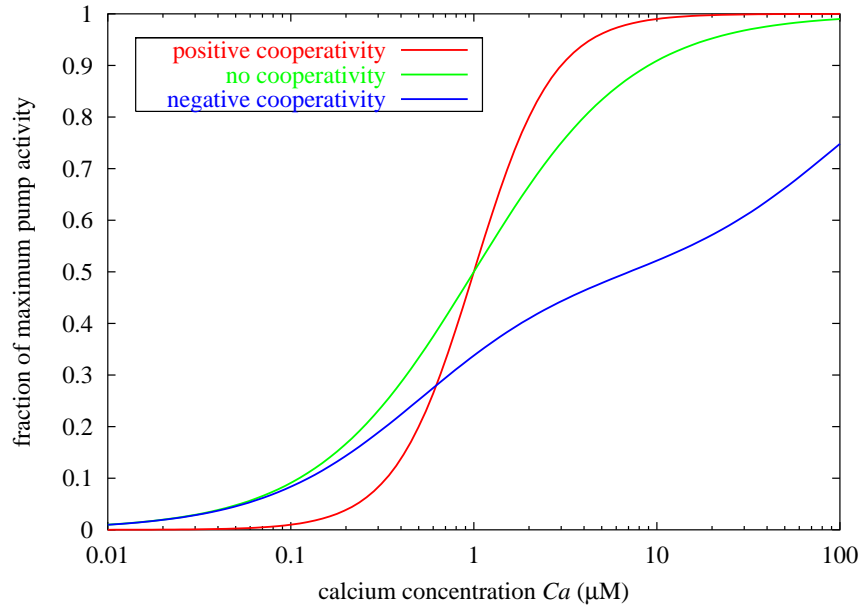


Figure 3.13: Different steady-state pumping scenarios for stoichiometry $1\text{ATP}:2\text{Ca}^{2+}$

In dependence of the intracellular calcium concentrations three different calcium uptake behaviours of the PMCA pump are shown: the pump comprises two identical and independent binding sites (green line), positive cooperativity (red line), *i.e.* the binding of the first calcium ion increases the rate for the subsequent one and the opposite case where the binding of the first ion decreases the rate of the second calcium ion, referred to as negative cooperativity (blue line). Note that r_2 and r_4 remain equal for all the three cases.

already pointed out that the saturation of the pump and its rate change with the square of the calcium concentration in the cytosol, *i.e.* Hill coefficient $n = 2$ [38]. As shown in figure 3.12, this observation can be confirmed and a Hill coefficient of $n = 2$ (equation (3.52)) is used here. However, only evidence for a $\text{Ca}^{2+}:\text{ATP}$ stoichiometry of 1:1 for the PMCA pump is found in literature [42, 38, 45]. As a possible explanation Carafoli describes a separation of the binding and the transduction of the calcium ions. The pump can bind two Ca^{2+} ions with high affinity but the transport step, related to the $\text{E}_1 \sim \text{Ph}_i \rightarrow \text{E}_2 \sim \text{Ph}_i$ transition, can involve only one calcium ion.

Even if there is no obvious biological explanation for equation (3.52), this expression will be used in order to adequately describe experimental pumping activity (see discussion in section 3.7 on page 61).

So far only the calcium-dependent pump activity in the absence of calmodulin has been looked at without considering the pump stimulation. One single PMCA pump can exist in two states, either unstimulated or stimulated. The transition

dynamics is given by the stimulation model in equations (3.19) - (3.22). Incorporating this, the total pumping rate of a system of PMCA pumps becomes

$$I_p = f_{\text{unstim}}(t) \cdot \frac{I_{\text{max}} \cdot \text{Ca}^2}{H_p^2 + \text{Ca}^2} + f_{\text{stim}}(t) \cdot \frac{I_{\text{max}}^* \cdot \text{Ca}^2}{H_p^{*2} + \text{Ca}^2}, \quad (3.55)$$

where f_{unstim} and f_{stim} are the time-dependent fractions of unstimulated and stimulated pumps with $f_{\text{unstim}} = \frac{P(t)+P_X(t)}{P_0}$ and $f_{\text{stim}} = \frac{P^*(t)+P_X^*(t)}{P_0}$. I_{max} and H_p refer to the maximum pumping rate and the half maximum concentration in unstimulated pump state. The asterisk denotes the accordant stimulated values. Note that this expression has been used already in equation (3.7) for the dynamical Ph_i production rate, since the calcium transport is directly connected with the hydrolysis of ATP. The transport rate expressions I_{unstim} and I_{stim} in equation (3.55) describe separately the quasi-steady-state uptake behaviour of all pumps in the unstimulated and stimulated state, respectively. These are multiplied by the fractions of the actual distribution between unstimulated and stimulated pumps within the system. f_{unstim} and f_{stim} are dependent on the intracellular calcium and calmodulin concentration and adapt over a time scale of minutes as shown in figure 3.9 and 3.10.

One input parameter of the stimulation model is the total pump concentration P_0 . This concentration P_0 is taken from Caride *et al.* to be $0.005 \mu\text{M}$ [1]. In contrast to the stimulation model, the total pump concentration is irrelevant for the pumping model since we use a probabilistic interpretation in equation (3.51) and (3.52). P is the probability to have a calcium-free pump, P_{Ca} is the probability of a pump to have bound one calcium ion and P_{Ca_2} is the probability of two calcium ions attached. The pump mass conservation becomes for the pumping cycle (3.50): $1 = P + P_{Ca}$ and for the pumping cycle (3.53) and (3.54): $1 = P + P_{Ca} + P_{Ca_2}$. The same interpretation cannot be applied to the stimulation model since the proportion between total calmodulin concentration and total pump concentration is significant, *i.e.* two mass conservations has to be respected that of the PMCA pump $P_0 = P + P_X + P_X^* + P^*$ and that of calmodulin $M_0 = M + X_1 + X_2 + X_3 + X_4 + P_X + P_X^*$. If for example the amount of PMCA pumps exceeds the number of available calmodulin proteins not all pumps could be stimulated.

For simulations the surface density of PMCA pumps has to be transferred into the concentration P_0 . This implies the neglect of diffusion of the calmodulin-calcium complex to and from the pump. This simplification becomes more profoundly the larger the investigated compartment becomes (see discussion in section 2.2 on page 2.2). However, a space resolving model with a local pump concentration has to be utilised. Considering a spherical cell with radius R the PMCA pumps are located at the surface of the volume which has to be implemented by a local pump concentration in the outer circles $P(R) = P_0$. Within that spherical system no extrusion pathway by PMCA pumps is available, *i.e.* $P(r) = 0$ for $r < R$.

3.5.2 Pumping parameter determination with steady-state pump activity

In the previous section the fit of equation (3.52) to the steady-state uptake behaviour of the PMCA in the absence of calmodulin is shown in figure 3.12. There-with the parameters of the unstimulated pumping activity I_{\max} and H_p can be determined. This section focuses on the determination of the stimulated pump parameters I_{\max}^* and H_p^* that complete the introduced set of parameters required to fully describe PMCA pump function.

By setting all differential equations (equations (3.23)) of the stimulation model (3.19) - (3.22) to zero, *i.e.* no more time-dependent change of the stimulation pump states, one gets the steady-state distribution of the different pump forms P, P_X , P_X^* and P^* . In dependence of the calcium and calmodulin concentration and of the rate constants k_i ($i = \pm 2, 3, \pm 4, 5$) and K_i ($i = 1 - 4$) the stimulation scenario which the system approaches after a sufficient long time can be calculated. This gives a cubic equation for P_X

$$\begin{aligned}
 0 = & P_X^3 \cdot \left[-\frac{k_3^2(k_3 + k_4)k_{-4}}{Ak_5^2} + \frac{k_3^2(k_3 + k_{-2})k_{-4}^2}{Ak_2k_5^2} \right] \\
 & + P_X^2 \cdot \left[-k_4(k_3 + k_4) - \frac{k_3k_4(k_3 + k_4)}{k_5} + \frac{M_0k_3^2k_4k_{-4}}{Ak_5^2} + \frac{2k_3k_4(k_3 + k_{-2})k_{-4}}{k_2k_5} \right. \\
 & \quad \left. - (k_3 + k_4) \left(k_3 + \frac{M_0k_3k_{-4}}{Ak_5} \right) + \frac{k_3(k_3 + k_4)k_{-4}P_0}{Ak_5} \right] \\
 & + P_X \cdot \left[M_0k_4^2 + \frac{M_0k_3k_4^2}{k_5} + \frac{Ak_4^2(k_3 + k_{-2})}{k_2} \right. \\
 & \quad \left. + M_0k_4 \left(k_3 + \frac{M_0k_3k_{-4}}{Ak_5} \right) + k_4(k_3 + k_4)P_0 - \frac{M_0k_3k_4k_{-4}P_0}{Ak_5} \right] \\
 & - M_0k_4^2P_0
 \end{aligned} \tag{3.56}$$

with

$$A = 1 + \frac{K_4}{Ca} + \frac{K_3K_4}{Ca^2} + \frac{K_2K_3K_4}{Ca^3} + \frac{K_1K_2K_3K_4}{Ca^4}, \tag{3.57}$$

and for the remaining pump states it follows

$$\begin{aligned}
 P &= \frac{\frac{A(k_{-2} + k_3)k_4}{k_2}P_X + \frac{(k_{-2} + k_3)k_3k_{-4}}{k_2k_5}P_X^2}{M_0k_4 - (k_3 + k_4)P_X}, \\
 P^* &= \frac{k_3}{k_5}P_X, \\
 P_X^* &= P_0 - P - P_X - P^*.
 \end{aligned} \tag{3.58}$$

The cubic equation (3.56) gives three solutions for $P_X(t \rightarrow \infty)$. Only with the real and positive solution which fulfils the restriction $0 \leq P_X \leq P_0$ is proceeded.

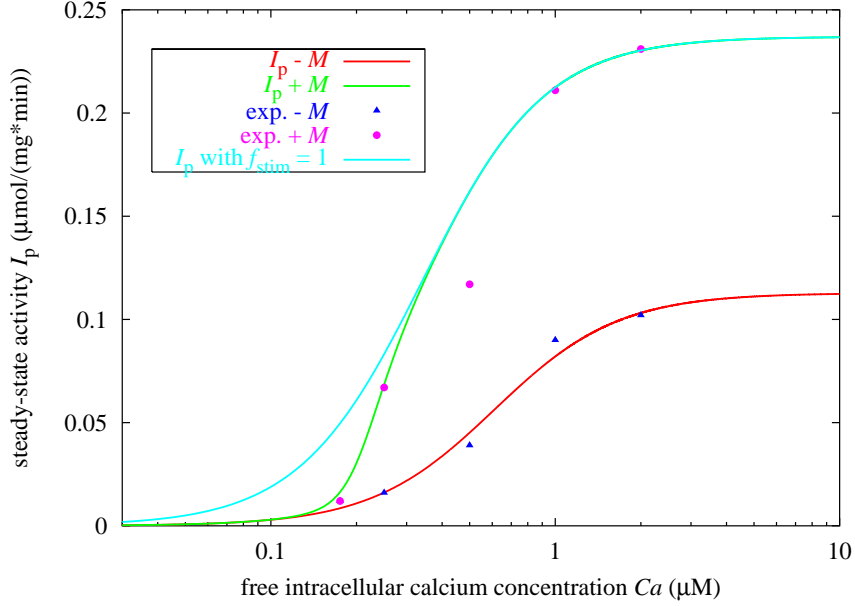


Figure 3.14: Steady-state calcium dependent pump activity of the h2b isoform

The measurements in the absence (blue triangles) and in the presence (purple circles) of $0.117 \mu\text{M}$ calmodulin have been kindly provided by Caride [1]. The total pump concentration P_0 is taken from [1] to be $0.005 \mu\text{M}$. The cyan line depicts the pump activity with the assumption that only stimulated pump form is present at all calcium concentrations, *i.e.* $f_{\text{stim}} = 1$ and $f_{\text{unstim}} = 0$. Whereas the green line shows the realistic case, *i.e.* $f_{\text{stim}} \simeq 0$ for low calcium concentrations. The red line shows the fit of equation (3.55) to the measurement in the absence of calmodulin ($f_{\text{unstim}} = 1$ and $f_{\text{stim}} = 0$).

This approach enables to calculate the asymptotic steady-state fractions f_{unstim} and f_{stim} in equation (3.55) for $t \rightarrow \infty$, which transfers equation (3.55) into an expression of the steady-state pumping activity in the presence of calmodulin. Many measurements of this activity in the presence and the absence of calmodulin has been performed [1, 34, 49, 48, 51]. The adaption of equation (3.55) to one of these experiments delivers I_{max} , I_{max}^* , H_p and H_p^* . In figure 3.14 and 3.15 the steady-state activity measurements done by Caride *et al.* [1] are used.

With $f_{\text{unstim}} = 1$ and $f_{\text{stim}} = 0$ equation (3.55) reduces to (3.52) with which the steady-state activity measurement in the absence of calmodulin is fitted, *i.e.* no stimulated pump form is available. This fit can be seen already in figure 3.12 and supplies I_{max} and H_p . Note that this is an immediate answer of the pump to different calcium concentrations, since the quasi-steady-state rate expression for the pump activity is used (equation (3.52)) and the stimulation is switched off due to the lack of calmodulin.

In the calmodulin present case the complete equation (3.55) is used in order to

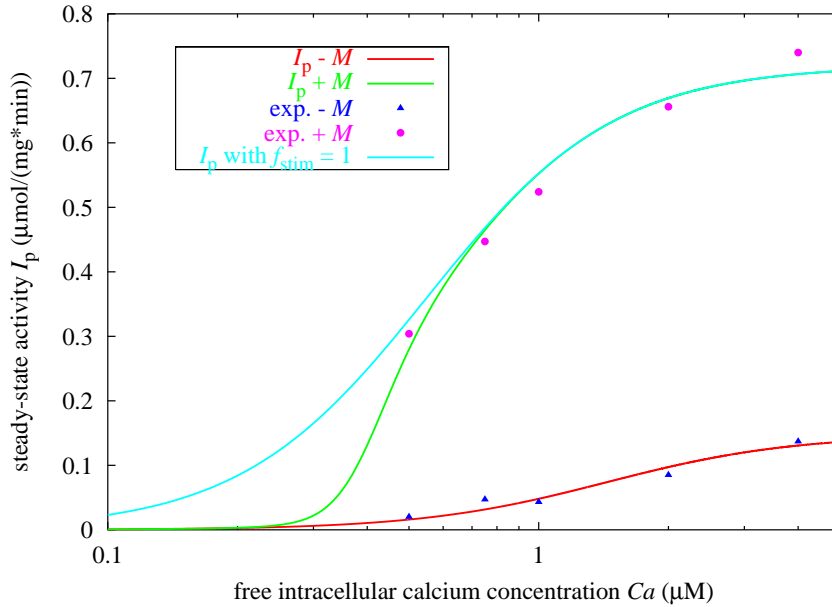


Figure 3.15: Steady-state calcium dependent pump activity of the h4b isoform

For details see description of figure 3.14.

fit the data (see green lines in figure 3.14 and 3.15). I_{\max}^* and H_p^* are determined with that fit, whereby the asymptotic steady-state fractions f_{unstim} and f_{stim} are given by equations (3.56) - (3.58). These calculated fractions respect the fact, that at lower calcium concentrations in the presence of calmodulin no stimulated pump form is available ($f_{\text{stim}} \simeq 0$). This can be seen in comparison with the cyan line in figure 3.14 and 3.15, which is plotted with the virtual assumption only stimulated pump form ($f_{\text{stim}} = 1$) to be present for all calcium concentrations. The gap between this virtual line (cyan) and the fit of equation (3.55) (green line) at low calcium concentrations is determined by the choice of the stimulation parameterset in table 3.3 and 3.4. Although I_{\max}^* and H_p^* are determined with that fit, changes in I_{\max}^* and H_p^* only alter the slope and the saturation value whereas the gap at low calcium concentrations is not influenced by these changes. That is, I_{\max}^* and H_p^* do not have influence in equation (3.55) at $f_{\text{stim}} \simeq 0$. This provides an indication that the parameter set in table 3.3 and 3.4 determined via $k_{\text{stim}}^{\text{exp}}$ and $k_{\text{relax}}^{\text{exp}}$ is in good agreement with these experiments.

The so obtained parameters I_{\max} and I_{\max}^* refer to the investigated system, *i.e.* they are determined by the ensemble of investigated pumps. In contrast to the pump rate, the affinity to calcium expressed by H_p or H_p^* is an universal parameter since it does not depend on the surface density. With the knowledge of the expression level of PMCA pumps within the system and the average protein mass one can calculate out of I_{\max} and I_{\max}^* the maximum unstimulated I_{single} and stimulated pumping rate I_{single}^* of a single PMCA pump, respectively. This

parameter	h2b	h4b	unit	characteristics
I_{\max}	0.113	0.147	$\frac{\mu\text{mol}}{\text{mg}\cdot\text{min}}$	system specific
I_{single}	4.9 (48% of I_{single}^*)	6.3 (20% of I_{single}^*)	Hz	universal
I_{\max}^*	0.237	0.72	$\frac{\mu\text{mol}}{\text{mg}\cdot\text{min}}$	system specific
I_{single}^*	10.3	31.3	Hz	universal
H_{p}	0.612	1.438	μM	universal
H_{p}^*	0.34	0.55	μM	universal

Table 3.5: Parameter of the steady-state pump activity

The values have been determined with the help of steady-state pumping activity measurements of Caride *et al.* 2001 [1].

single pumping rates are treated to be characteristic for the accordant isoform and therefore an universal parameter for all PMCA pumps of the same isoform. In order to separate between universal and system dependent values equation (3.55) can be rewritten

$$I_{\text{p}} = \frac{\eta}{m_{\text{Protein}}} \left[f_{\text{unstim}}(t) \cdot \frac{I_{\text{single}} \cdot \text{Ca}^2}{H_{\text{p}}^2 + \text{Ca}^2} + f_{\text{stim}}(t) \cdot \frac{I_{\text{single}}^* \cdot \text{Ca}^2}{H_{\text{p}}^{*2} + \text{Ca}^2} \right]. \quad (3.59)$$

where η is the expression level of PMCA pumps in respect to the total membrane protein in % and m_{Protein} is the overall average protein mass ($m_{\text{Protein}} = 130$ kDa) [45, 52]. Within the brackets on the right hand site in equation (3.59) only isoforms specific, system independent parameter occur. Whereas the expression level η differs between experiments and has to be adapted.

Caride *et al.* achieved with the baculovirus expression system an amount of 5% PMCA pumps of the total membrane protein, *i.e.* $\eta = 0.05$ (private communication). Knowing that and with the overall average protein mass m_{Protein} a turnover rate of 10.3 Hz out of $I_{\max}^* = 0.237 \mu\text{mol}/(\text{mg} \cdot \text{min})$ for the h2b isoform and 31.3 Hz out of $I_{\max}^* = 0.72 \mu\text{mol}/(\text{mg} \cdot \text{min})$ for the stimulated h4b rate are deduced.

The collection of all pumping parameters obtained from the steady-state curves in figure 3.14 and 3.15 is shown in table 3.5. The impact of stimulation by calmodulin on PMCA pump function, namely increase in both, the affinity to calcium H_{p} and the maximum pump rate I_{\max} or I_{single} , can be affirmed.

With the use of these parameters and the rate constants of the stimulation model (table 3.3 and 3.4) it is possible to calculate the calmodulin dependence of the steady-state activity, which is shown in figure 3.16 for the h4b isoform. The calcium dependent Hill equations which describe the pumping activity remain constant here since the calcium concentration is fixed. Only the fraction f_{unstim} and f_{stim} , calculated via equations (3.56) - (3.58), alter at changing calmodulin

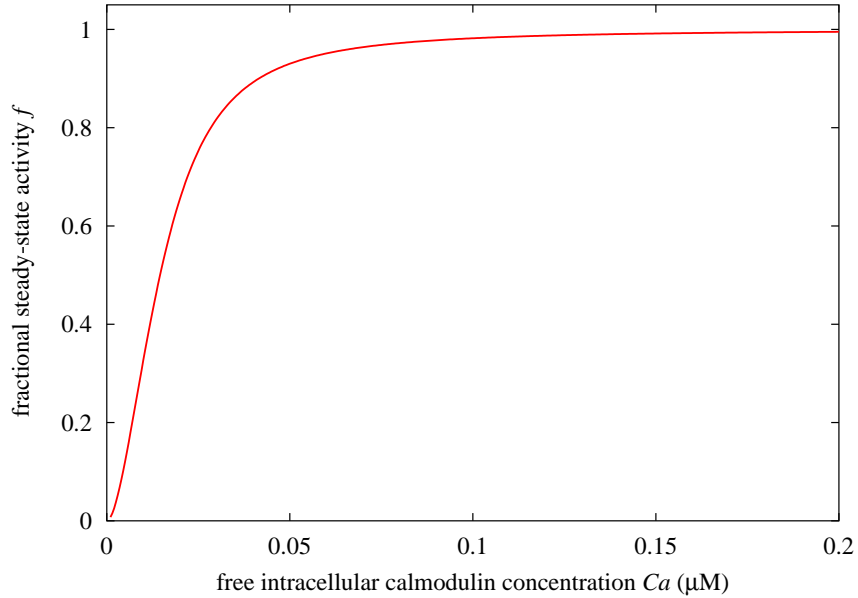


Figure 3.16: Steady-state calmodulin dependent pump activity of the h4b isoform

The fractional steady-state calmodulin dependent pump activity f (equation (3.60)) of the h4b isoform at $Ca_0 = 0.7 \mu\text{M}$ is shown. The calculation is done with a total pump concentration P_0 of $0.005 \mu\text{M}$.

concentrations. The displayed fractional steady-state activity f with

$$f = \frac{I_p - I_{p_{\max}}}{I_{p_{\max}}^* - I_{p_{\max}}} \quad (3.60)$$

is an universal description for equal M_0/Ca_0 ratios, since η , *i.e.* P_0 , does not appear in the expression of f . $I_{p_{\max}}$ is the activity in the absence of calmodulin and $I_{p_{\max}}^*$ is the steady-state activity in the presence of saturating calmodulin, both at the accordant calcium concentration. The quantitative behaviour of that theoretical plot in figure 3.16 is confirmed by figure 3 in [33] (data not shown). Note that f is calculated out of the available data without further fitting routines.

3.6 Comprehensive PMCA pump dynamics

With the knowledge of both the stimulation parameter from table 3.3, 3.4 and the pumping properties in table 3.5 the comprehensive time dependent behaviour of the calcium pumping rate of the PMCA pump including the stimulation can be simulated.

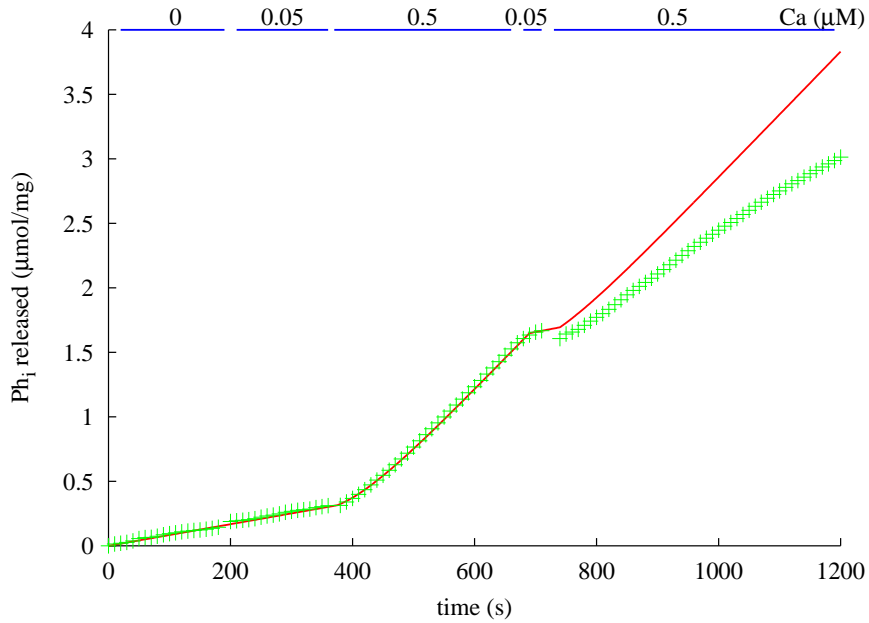


Figure 3.17: Time course of Ph_i production of the h2b isoform

The figure displays the theoretical (red line) and the experimentally measured (green crosses) time course of the Ph_i production during different calcium concentration exposures, shown on the top of the panel. The present calmodulin concentration was $0.117 \mu\text{M}$ during the experiment and the simulation. For the simulation a total pump concentration P_0 of $0.005 \mu\text{M}$ is used. The experiment was performed with the h2b isoform (with kind permission of Caride [1]).

In an experiment performed by Caride *et al.* [1] the tissue containing PMCA pumps has been exposed one after another to different calcium concentrations for various times. During that procedure the total amount of Ph_i has been recorded as a measure of changing calcium uptake activity. The time course of produced Ph_i is shown in figure 3.17 (green crosses). It was already pointed out that the Ph_i production rate directly corresponds to the calcium transport rate (see section 3.3.1). Utilising equation (3.59), it is possible to numerically integrate the time course of the Ph_i production by

$$\text{Ph}_i = \int_{t_0}^t (I_p + I_{\text{base}}) dt, \quad (3.61)$$

where I_{base} corresponds to a constant base level rate which respects the non-zero Ph_i production rate at $Ca = 0 \mu\text{M}$ for $0 \text{ s} < t < 187 \text{ s}$ in figure 3.17. Regarding our simulation, since the production rate I_p in equation (3.59) is equal to zero at $Ca = 0 \mu\text{M}$, Ph_i would remain constant without adding I_{base} in equation (3.61). This additional rate could be related to another source of Ph_i within the investigated

tissue. In fact, in the absence of calcium no ions can be transported, *i.e.* no ATP can be hydrolysed, no Ph_i produced.

The calcium exposure protocol in figure 3.17 starts with a raise of the calcium concentration from 0 μM to 0.05 μM at $t = 185$ s. At $t = 360$ s the calcium concentration was raised to 0.5 μM for 300 s. For $660 \text{ s} \leq t < 720$ s, the tissue was exposed to 0.05 μM calcium, again. From $t = 720$ s to $t = 1200$ s the calcium concentration was 0.5 μM . The same calcium protocol is used in the simulation. With the universal parameter set the simulation (red line in figure 3.17) is adapted to the experiment by adjusting the unknown surface density η of PMCA pumps. This yields a expression level of 7.5 % PMCA pumps of total membrane protein. The slope at 0 μM calcium at $0 \leq t < 185$ s corresponds to $I_{\text{base}} = 0.00082 \mu\text{mol}/(\text{mg} \cdot \text{s})$.

Attention should be drawn to the fact, that beside a shift in the total amount of Ph_i at $t = 720$ s at the beginning of the second exposure to 0.5 μM calcium the measured activity does not reach the same slope as during the previous exposure to high calcium. Actually the pumping activity significantly decreases under the same experimental conditions during the second exposure to 0.5 μM . This might be related to insufficient ATP availability or to the increasing significance of ATP and calcium diffusion during the experiment.

After 300 seconds at 0.5 μM calcium ($360 \text{ s} \leq t < 660 \text{ s}$), during which a PMCA pump fraction is stimulated ($f_{\text{stim}}^{(\text{h2b})} = 98.5 \%$ and $f_{\text{stim}}^{(\text{h4b})} = 24.3 \%$), the concentration was decreased to 0.05 μM calcium for different durations Δt_{low} and raised again to high calcium concentration. The turnover rate at the end of the second low calcium exposure $I_{0.05}^{(\text{second})}$ is, due to the gradual decay of stimulated pump form, dependent on the duration time at low calcium. The fraction of change in $I_{0.05}$,

$$f_{I_{0.05}} = \frac{I_{0.05}^{(\text{second})} - I_{0.05}^{(\text{first})}}{I_{0.5}^{(\text{first})} - I_{0.05}^{(\text{first})}} \quad (3.62)$$

is shown in figure 3.18 and 3.19. $I_{0.05}^{(\text{first})}$ refers to the pumping activity at the end of the first exposure to 0.05 μM calcium, $I_{0.5}^{(\text{first})}$ is the activity at the end of the first exposure to high calcium and $I_{0.05}^{(\text{second})}$ stands for the pumping rate at the end of the second time at 0.05 μM calcium. Note that this fractional description is an universal depiction for equal M_0/Ca_0 ratios of relaxation behaviour since it is independent of the expression level. Beside the deviation between simulation and experiment at large times of the h2b isoform, which could be related to the decreasing pump activity during the time course of the experiment (see figure 3.17), the temporal behaviour of pump function is quantitatively reproduced. Also the different isoform specific temporal relaxation characteristics suggested by the experimental data in figure 3.19 and 3.19, namely a faster decay of the stimulated h4b pump isoform, are reflected.

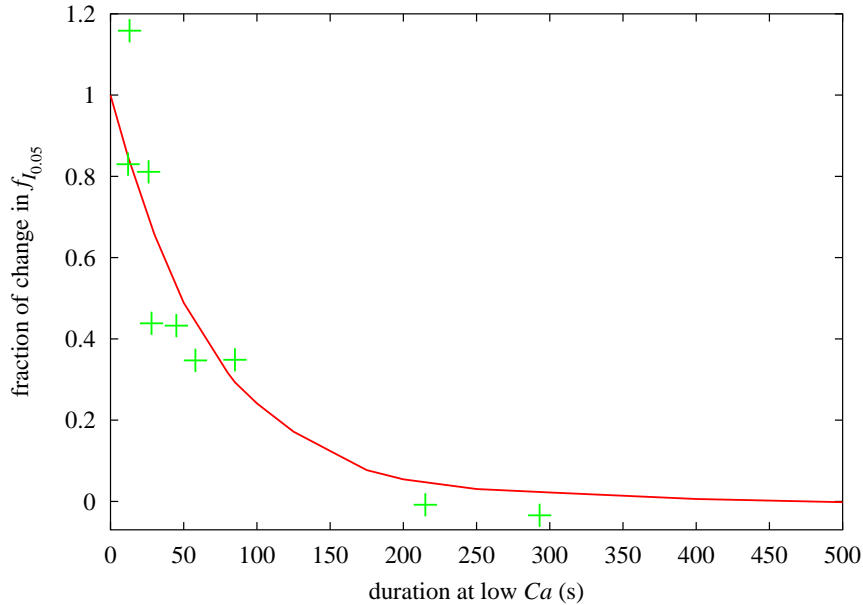


Figure 3.18: Fraction of change in $I_{0.05}$ of the h2b isoform after various durations at low calcium Δt_{low}

The fraction of change in $I_{0.05}$ (equation (3.62)) is shown as a function of time at low calcium Δt_{low} ($Ca = 0.05 \mu\text{M}$), experimentally measured (green crosses, with kind permission of Caride [1]) and theoretically predicted (red line). The present calmodulin concentration was $0.117 \mu\text{M}$. The simulations has been done with $I_{\text{base}} = 0.00082 \frac{\mu\text{mol}}{\text{mg s}}$.

3.7 Discussion of the PMCA pump model

The combined model of stimulation and pumping activity is able to reproduce the Plasma Membrane Calcium pump behaviour. With an analytical approach, starting from the stimulation model introduced by reaction equations (3.19) - (3.22) it is possible to reproduce the experimentally measured stimulation constants. The conjunction of the uptake behaviour characterisation and the stimulation model consistently describes the steady-state pump activity (figure 3.14, 3.15 and 3.16) and the time course of pump activity (figure 3.17, 3.18 and 3.19). Therefore the assumptions of the stimulation model could serve as a possible explanation for the underlying biological steps.

An essential element of the model is the separation between the attachment of the calmodulin-calcium complex to the pump (equation (3.19)) and the stimulation, which occurs in an additional step (equation (3.20)). The convergence of the stimulation constant $k_{\text{stim}}^{\text{exp}}$ at high calcium concentrations in figure 3.5 and 3.6 provides strong evidence for that assumption. Correspondingly the saturation at a maximum relaxation constant $k_{\text{unstim}}^{\text{exp}}$ in figure 3.7 and 3.8 at low calcium

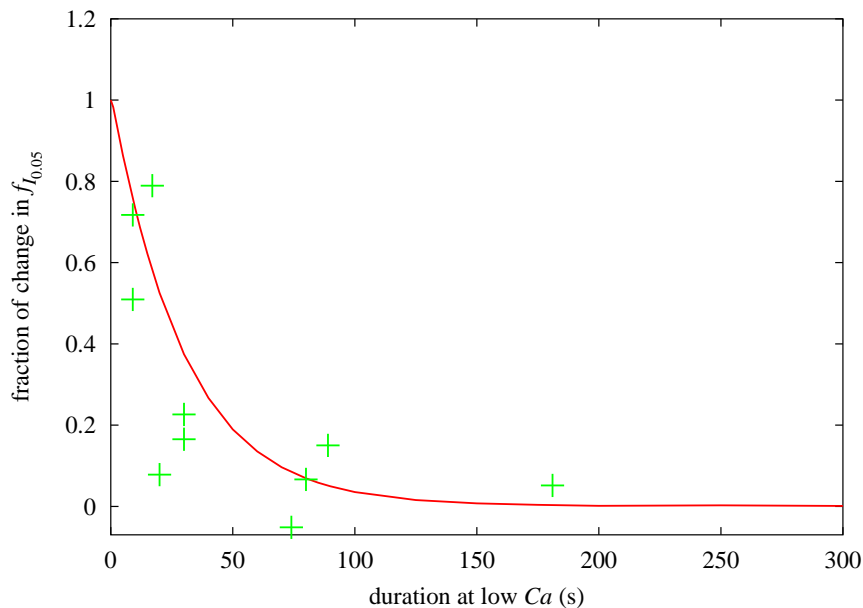


Figure 3.19: Fraction of change in $I_{0.05}$ of the h4b isoform after various durations at low calcium Δt_{low}

The fraction of change in $I_{0.05}$ (equation (3.62)) is shown as a function of time at low calcium Δt_{low} ($Ca = 0.05 \mu\text{M}$), experimentally measured (green crosses, with kind permission of Caride [1]) and theoretically predicted (red line). The present calmodulin concentration was $0.117 \mu\text{M}$. The simulations has been done with $I_{\text{base}} = 0.00082 \frac{\mu\text{mol}}{\text{mg s}}$.

concentrations gives reason for the same procedure with the relaxation cycle. The detachment of the calmodulin-calcium complex from the stimulated pump P_X^* is represented by reaction (3.21) and an additional limiting relaxation step is characterised by equation (3.22). In a corresponding manner an additional step exists in the pumping cycle in reactions (3.50), (3.53) and (3.54). These steps can be seen as an internal conformational change where its velocity cannot be further speeded up by concentration raises. In contrast to reaction (3.20) which is confined by the total available pump concentration P_0 and k_3 , the velocity of reaction (3.19) can be arbitrarily increased with higher calcium or calmodulin concentrations. That is, if the stimulation process is connected with equation (3.19), the stimulation constant k_{stim} would not saturate at high calcium concentrations as it is the case in Caride's model (see figure 3.4). Equivalently the relaxation velocity is confined by the total pump concentration and k_5 .

The rate constants k_2 and k_{-2} allow the quotation of the affinity of the unstimulated PMCA pump for the fully liganded calmodulin-calcium complex X_4 . Experimentally, a dissociation constant of $K_d = 5 \text{ nM}$ for the h4b isoform [32, 33, 35, 53] and a 5-10 times lower value for the h2b isoform are indicated [1, 19, 43, 48, 53].

This values are much higher as the affinities ($K_d = k_{-2}/k_2 = 0.00286$ nM for h2b, $K_d = 0.0202$ nM for h4b) delivered by the model. Even if k_2 and k_{-2} are only determined up to a range, the relation between these two parameter confines the value of K_d ($K_d \leq 0.0032$ nM for h2b, $K_d \leq 0.024$ nM for h4b). This problem is discussed further in section 4.1. Comparing the affinities of the new model to the dissociation constants delivered by Caride's approach [1], $K_d = 0.0001$ nM for h2b and $K_d = 0.00045$ nM, leads to two statements. Firstly, they are even significantly lower as the dissociation constants in the new model for PMCA pump stimulation. The reason for that is the additional step (3.20) in the new stimulation scheme, which does not permit the direct comparison between both. Secondly, the 10 times higher affinity for the calmodulin-calcium complex of the h2b isoform compared to the h4b isoform [19, 37, 43, 48] is suggested by the dissociation constants of the new model but cannot be seen in the dissociation constants of Caride's model. This feature is also a consequence of the separation between the attachment of the complex X_4 (3.19) and the stimulation step (3.20). The dissociation constant of the new model only contains informations about the attachment of the complex to the pump, whereas the dissociation constant of Caride's model describes the attachment together with the subsequent transformational change leading to stimulation.

The calmodulin dependence of the steady-state activity is shown in figure 3.16. A half activation concentration for such a plot of $K_{1/2} = 5...10$ nM for the h4b isoform and a 5-10 times lower value ($K_d = 0.5...1$) for the h2b isoform for calmodulin is stated in various publications [19, 33, 34, 37, 48, 49]. Since the half activation value of this plot $K_{1/2} \approx 15$ nM can be identified with the stated values in the publications, figure 3.16 is in good agreement. Concerning figure 3.16, it should be noticed that the depiction is universal for equal M_0/Ca_0 ratios, hence if this ratio changes the half activation concentration varies. But the half activation value in the steady-state calmodulin dependence cannot be equated with the dissociation constant of the PMCA pump for calmodulin K_d , since calmodulin attaches itself not directly to the pump. But the association rather is a two step process, *i.e.* the formation of the complex X_4 is followed by the attachment to the pump.

The separation between stimulation (equations (3.19) and (3.20)) and relaxation (equations (3.21) and (3.22)) enables to describe the different temporal behaviour independently which is required since for example isoforms h2b and h4b display opposed stimulation and relaxation pumping activity behaviour, *i.e.* the h2b isoforms stimulates faster than h4b but decays slower than h4b under the same conditions (see figure 3.9 and 3.10). Assuming the stimulation reaction (3.20) would become reversible, the formation and the degradation of stimulated pump form P_X^* could be described together by the first two reactions, (3.19) and (3.20) without the use of reactions (3.21) and (3.22). In such a case the calcium and calmodulin dependent stimulation and relaxation velocity could not be adjusted autonomously. The justification for two different pathways is a possible biological

differentiation of the underlying transformational changes.

In the stimulation model calcium and calmodulin are considered as both equally required for the stimulation of PMCA pumps. The only difference is the necessary quantity, *i.e.* four calcium ions and one calmodulin protein. For processes whose intermediate steps are suspected to show cooperative behaviour, the Hill coefficient n reflects the involved stoichiometry, *e.g.* a Hill function with Hill coefficient $n = 4$ fits best the experimentally measured stimulation constant for different calcium concentrations (see figure 3.5 and 3.6) reflecting the four involved calcium ions. Taking this into account, the raising face of the calcium dependence of the stimulation constant contains informations, if also calmodulin bound with three, two, one or none calcium ions can stimulate the pump. In such a case the stimulation constant fit function would be an accordant superposition of Hill functions with Hill coefficients $n = 3$, $n = 2$, $n = 1$ and $n = 0$. Additionally, the hypothetical calmodulin dependence of the stimulation constant in figure 3.16 describes a hill function with Hill coefficient $n = 1$ which can be related to the required number of one calmodulin protein. Regarding the stimulation model different types of calmodulin-calcium complexes, referred to as X_1 , X_2 , X_3 and X_4 , may be used for the stimulation of the PMCA pump. In such as case the quantity X_4 in reaction (3.19) has to be replace by a respective superposition of X_1 , X_2 , X_3 and X_4 . In figure 3.20 the connection between the formation of X_i ($i = 2, 4$) and the accordant Hill fit function is shown. It becomes evident that X_i mainly influences the shape of the calcium dependence plot of the stimulation constant $k_{\text{stim}}^{(3)}$ (equation (3.30)). Currently $k_{\text{stim}}^{(3)}$ (blue crosses) is almost exactly similar to a Hill function with Hill coefficient $n = 4$ (purple line), reflecting the assumption that only these calmodulin proteins bound with four calcium ions can stimulate the pump. Furthermore, this scenario fits best the experimental data, affirming the assumption of the model to only incorporate X_4 for the pump stimulation. Changing the required calcium quantity for the formation of X_i from four to two calcium ions, *i.e.* $i = 2$, the plot of the stimulation constant $(k_{\text{stim}}^{(3)})_{2\text{Ca}}$ (green crosses) resembles a Hill function with Hill coefficient two (cyan line). It was already pointed out in section 3.3.2 that the pump can also be stimulated only by the fully liganded amino- and carboxyl-terminal domain of calmodulin [31], *i.e.* with the required quantities of one calmodulin protein and two calcium ions. However, from figure 3.20 is becomes clear that a stimulation by X_2 compared to X_4 would not optimise the behaviour of the stimulation constant with respect to the experimental data. Therefore, the neglecton of the X_2 complex is justified. A biological reason for that might be the substantially larger affinity of the PMCA pump for the whole calmodulin protein as for the single C- or N-terminal (see section 3.1 on page 26).

Comparing the Hill fit function and the plot of $k_{\text{stim}}^{(3)}$ in figure 3.20 suggest an almost exact congruence. With regard to the nature of the Hill coefficient

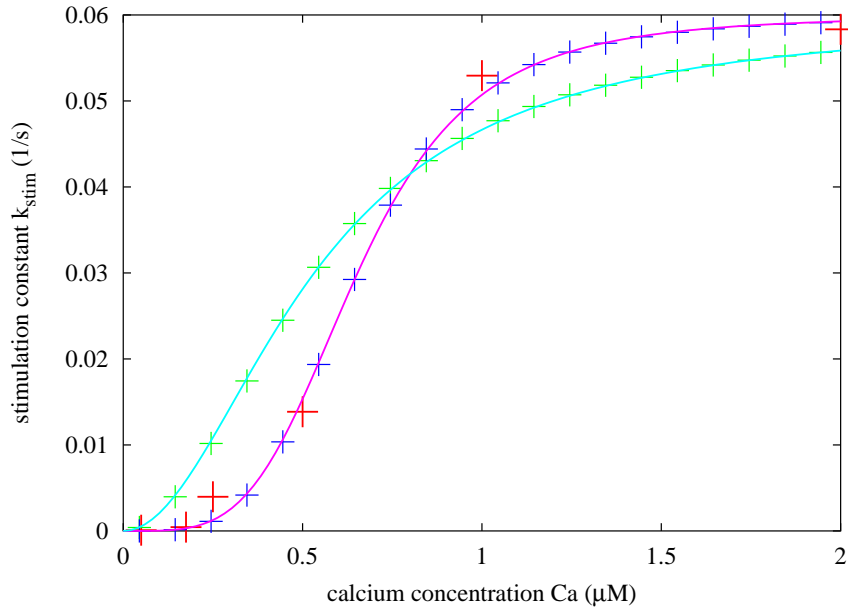


Figure 3.20: Connection between required quantity for pump stimulation and the Hill coefficient in case of $k_{\text{stim}}^{(3)}$ (h2b isoform)

The theoretical stimulation constant $k_{\text{stim}}^{(3)}$ (equation (3.30)) for changing calcium concentrations is depicted for two different stimulation cases. The blue crosses show $(k_{\text{stim}}^{(3)})_{4\text{Ca}}$ as used in the model with four calcium ions and one calmodulin protein forming X_4 . Corresponding to this the purple line depicts a Hill function with a Hill coefficient $n = 4$. Keeping the half maximum concentration and the saturation value constant the green crosses display $(k_{\text{stim}}^{(3)})_{2\text{Ca}}$ where X_4 is a complex formed by two calcium ions and one calmodulin protein. Again, this plot can also be described by a Hill function but with a Hill coefficient $n = 2$ (cyan line). The stimulation parameter in table 3.3 and 3.4 are used for both calculations of the stimulation constant $k_{\text{stim}}^{(3)}$. The red crosses are the experimentally measured stimulation constants (with kind permission of Caride [1])

this suggests a cooperative underlying process, namely the binding of calcium by calmodulin. Furthermore it can be deduced that the behaviour of $k_{\text{stim}}^{(3)}$ with the here employed parameterset is predominately influenced by the formation of the calmodulin-calcium complex, *i.e.* in the presented approach X_4 .

The aim to characterise pump isoforms by different universal parameter sets is achieved for the investigated h2b and h4b isoforms. The same way of function is assumed for all isoforms, hence these parameter express relevant differences in stimulation and pumping behaviour. With the concept of providing universal parametersets it is claimed for the sets to be applicable to other system simulations including hPMCA2b or hPMCA4b isoforms. Figure 3.16 shows an accurate prediction of the calmodulin dependence of the steady-state activity calculated out of the universal parameter of the h4b isoform.

Concerning the calcium pumping rates I_{max} and I_{max}^* , by using the expression level and the overall average protein mass, single pump turnover rates I_{single} and I_{single}^* are calculated ($I_{\text{single}} = 4.9$ Hz, $I_{\text{single}}^* = 10.3$ Hz for the h2b isoform and $I_{\text{single}} = 6.3$ Hz, $I_{\text{single}}^* = 31.3$ Hz for the h4b). Based on a measurement of Elwess *et al.* in 1997 [19] with the same approach but an accordant expression level of 0.2 % a turnover rate of 8.5 Hz for the rPMCA2b pump is computed. These calculated single turnover rates are of the same range as those of Blaustein who indicated a turnover of about 30 Hz without specifying the isoform ([41] and private communication). Note that I_{single} and I_{single}^* are calculated out of the steady-state activity measurements with a PMCA expression level of 5 % of total membrane proteins as indicated by Caride *et al.* [1]. However the adaption of these single turnover rates for the h2b isoform to the time course of Ph_i production shown in figure 3.17 yields an expression level of 7.5 %. It should be noticed that the expression level is liable to fluctuations in biological systems.

Therewith the isoform specific, universal set of parameter may be applied to different scenarios by incorporating the system specific expression level of PMCA proteins. However, alterations of the stimulation rate constants may occur under modified experimental conditions. Since proteins with polar binding sites are considered, a change of dynamical properties at different ionic strengths of the experimental solutions cannot be excluded. Corresponding experiments could elucidate the importance of such effects and also verify the theoretical predictions about the calmodulin dependence of the stimulation and relaxation constant.

Comparing the decay pathways of the new stimulation model (reaction (3.21) and (3.22)) with the respective steps in Caride's model (equations (3.16) and (3.17)), two different assumptions underlie these descriptions. Whereas in this work the calmodulin-calcium complex as a whole detaches from the stimulated PMCA pump form, Caride *et al.* describe the dissociation of the four calcium ions to occur firstly. The results of both theoretical models are not distinguishable for the relaxation pathway, the investigations even lead to the same rate constant for the irreversible relaxation step (compare (3.17) and (3.22)) $k_4^{(c)} \approx k_5$ (see table

3.2 and 3.3). Therefore, the actual biological procedure has to be elucidated by accordant experiments.

4 PMCA pump stimulation in presynaptic calcium dynamics

The effect of PMCA pump stimulation on intracellular calcium dynamics has been measured by Snitsarev *et al.* [54] and by Klishin *et al.* [55] in endothelial cells and by Bautista *et al.* [56] in human T cells. By blocking different components contributing to the intracellular calcium homeostasis they could show that the enhancement of calcium clearance kinetics can be related to the PMCA pump. The time scale of the observed facilitation of calcium extrusion after a sustained intracellular high calcium exposure is on the range of minutes as shown in chapter 3.

This section deals with the implementation of the comprehensive PMCA model [2] in the model of presynaptic calcium dynamics of the Research Group Theoretical Biophysics presented in section 2.2 [3, 4]. The addressed question is whether and under which conditions the pump stimulation has an impact on presynaptic calcium dynamics. Also the possibility of an engagement in long-term modifications or trigger mechanisms towards long-term effects is examined.

Since the h2b isoform of the PMCA splicing variants is predominately expressed in the brain [37, 42, 43, 44, 57, 58], the investigations concerning the implementation focus on that specific type.

4.1 PMCA pump affinity

Before the implementation in the presynaptic calcium dynamics model will be discussed in section 4.3, the interplay of calcium, calmodulin and the PMCA pump in real cells requires a deeper consideration.

In section 3.7 on page 62 the contradiction between the dissociation constant $K_d = k_{-2}/k_2$ deduced from the stimulation model and the values delivered from various publications has been mentioned. The high affinity of the PMCA pump for the calmodulin-calcium complex, arising naturally from the model approach, has to be reconciled with the stated affinity of 5 nM for the h4b isoform [32, 33, 35, 53] and 0.5 nM for the h2b isoform [1, 19, 43, 48, 53]. Otherwise under physiological conditions the high affinity directs the PMCA pump to a highly stimulated state at the resting intracellular calcium level. Since this is in turn not realistic the examinations in this section seek for explanations and different approaches.

Regarding the conditions in a neuron, the steady-state calcium concentration is about 0.1 μM [5, 6, 7] and can reach concentrations up to 100 μM during calcium

elevations, whereas the total available calmodulin concentration is approximately $30 \mu\text{M}$ [14, 18, 19]. During the experiments of Caride, under consideration in chapter 3 in order to determine the stimulation parameter, the total available calmodulin concentration was $0.177 \mu\text{M}$. The translation of the PMCA pump surface density in neurons $\rho_p = 3400 \mu^{-2}$ quoted in [4] into a concentration of PMCA pumps, available within the investigated volume with $r = 0.5 \mu\text{m}$, yields a concentration of $P_0 = 33.9 \mu\text{M}$. This translation is necessary since the calculation of the PMCA stimulation state requires a total available pump concentration as input parameter (see chapter 3.5.1). While the calcium concentration of the initial state is of the same range as considered in the previous chapter, the calmodulin and the PMCA pump concentrations are substantially higher. Normally, the PMCA pump stimulation model is scalable, but this requires the simultaneous increase in the concentrations of all the three participating reactants. The result of keeping the calcium concentration constant and increasing the calmodulin concentration about 200-fold and the PMCA pump concentration about 7000-fold can be seen in figure 4.7. There, the steady-state fractions f_{unstim} (red line) and f_{stim} (green line) of the PMCA pump calculated via equations (3.56) - (3.58) with $M_0 = 30 \mu\text{M}$ and $P_0 = 30 \mu\text{M}$ are shown for the h2b isoform. 80 % of the PMCA pump are already stimulated at the resting level calcium concentration of $Ca_0 = 0.1 \mu\text{M}$ (see black dotted line in figure 4.7). The binding constants of calmodulin for calcium K_i ($i = 1..4$) at $KCl = 150 \text{ mM}$ (see table 3.1) are chosen for that calculation. Note that the affinity of calmodulin for calcium at lower KCl concentrations increases, thus, since more complexes X_4 are available, the PMCA pump could even be stimulated to a higher degree at lower calcium concentrations as shown in figure 4.7 by the red and the green line.

The high fraction of stimulated PMCA pump form at a resting calcium level of $0.1 \mu\text{M}$ disagrees with the pump stimulation measurements in endothelial and T cells [54, 55, 56], where the pump stimulation only occurs when the free intracellular calcium concentration is significantly raised above a concentration of $0.1 \mu\text{M}$. Additionally, the investigations of Persechini *et al.* (1999) concerning the relationship between free calcium and free calmodulin-calcium complex concentrations within intact cells deliver further arguments against a high PMCA stimulation degree at low calcium concentrations [18]. They state that below a free Ca^{2+} concentration of $0.2 \mu\text{M}$ no detectable calcium-liganded calmodulin is produced, hence little or no global activation of calmodulin targets should occur.

Together, there is strong evidence, that the depicted scenario of almost complete PMCA pump stimulation at resting level calcium concentration does not reproduce the situation in real cells. Obviously, the reason for the highly stimulated state is the high affinity of the PMCA pump for the calmodulin-calcium complex which is the subject of further investigations. It has already been pointed out in section 3.7 on page 62 that the numerical values for $K_d = k_{-2}/k_2$ of both pump isoforms disagree with experimental data.

In the stimulation model represented by (3.1) and (3.19) - (3.22), the formation of P_X , which is required for the PMCA pump stimulation reaction (3.20), is a two-step process. After the subsequent binding of 4 calcium ions to the calmodulin protein (shown in reaction scheme (3.1)), the complex X_4 binds to the pump in step (3.19). So far the binding constants for the formation of X_4 are chosen on account of the statement from Caride *et al.* that the experimental conditions correspond to a KCl concentration of 150 mM [1]. Due to the low affinity of the calmodulin protein for calcium at this conditions, only small concentrations of X_4 complexes are available. Thus, the PMCA pump in the model has to express a high affinity for the X_4 complex in order to reproduce the measured stimulation behaviour. This is reflected in the high dissociation constants between the complex X_4 and the PMCA pump of $K_d = 0.0032$ nM for the h2b isoform and $K_d = 0.0202$ nM for the h4b isoform. Even if k_2 and k_{-2} are only determined up to a range, the dissociation constants of the model have an upper bound ($K_d \leq 0.0036$ nM for h2b, $K_d \leq 0.027$ nM for h4b). This limitation comes from the available calmodulin-calcium complex X_4 concentration and is reflected in equation (3.37). An expression for $K_d = k_{-2}/k_2$ can be deduced from this equation

$$K_d = \frac{k_{-2}}{k_2} = X_{4Ca_{stim}^{(1/2)}} - \frac{k_3}{2k_2}, \quad (4.1)$$

with $X_{4Ca_{stim}^{(1/2)}}(KCl = 150 \text{ mM}) = 3.58 \cdot 10^{-3}$ nM for the h2b isoform and $X_{4Ca_{stim}^{(1/2)}}(KCl = 150 \text{ mM}) = 2.67 \cdot 10^{-2}$ nM for the h4b isoform. k_3 is identified with the maximum stimulation constant $k_{stim}^{max} = 0.06 \text{ s}^{-1}$ for the h2b isoform and $k_{stim}^{max} = 0.024 \text{ s}^{-1}$ for the h4b isoform. By choosing k_2 high enough, $X_{4Ca_{stim}^{(1/2)}}$ confines the maximum possible dissociation constant K_d .

The free calmodulin-calcium complex concentration $X_{4Ca_{stim}^{(1/2)}}$ in dependence of the present KCl concentration delivered by equation (3.4) is shown in figure 4.1. For that plot the binding constants K_i provided by Linse *et al.* for a range of KCl concentrations from low ionic strength to 150 mM have been used (see table 3.1) [13]. To yield an appropriate dissociation constant of 0.5 nM for the h2b isoform [1, 19, 43, 48, 53] and 5 nM for the h4b isoform [32, 33, 35, 53], the corresponding KCl concentration, which determines via the binding constant K_i ($i = 1 \dots 4$) the available X_4 concentration, may not exceed $KCl < 50.2$ mM for the h2b isoform and $KCl < 36.2$ mM for the h4b isoform, respectively. This limitations correspond to the points of intersection highlighted by the dotted black lines in figure 4.1.

The further investigations restrict to the h2b isoform, since it is the predominantly expressed isoform in the brain [37, 42, 43, 44, 57, 58]. In order to be consistent with the experimental data suggesting a dissociation constant of $K_d = k_{-2}/k_2 = 0.5$ nM, a KCl concentration of 50 mM (see point of intersection in figure 4.1) is assumed to describe the calcium buffering by calmodulin during the measurements of Caride *et al.* [1]. With this different precondition the the

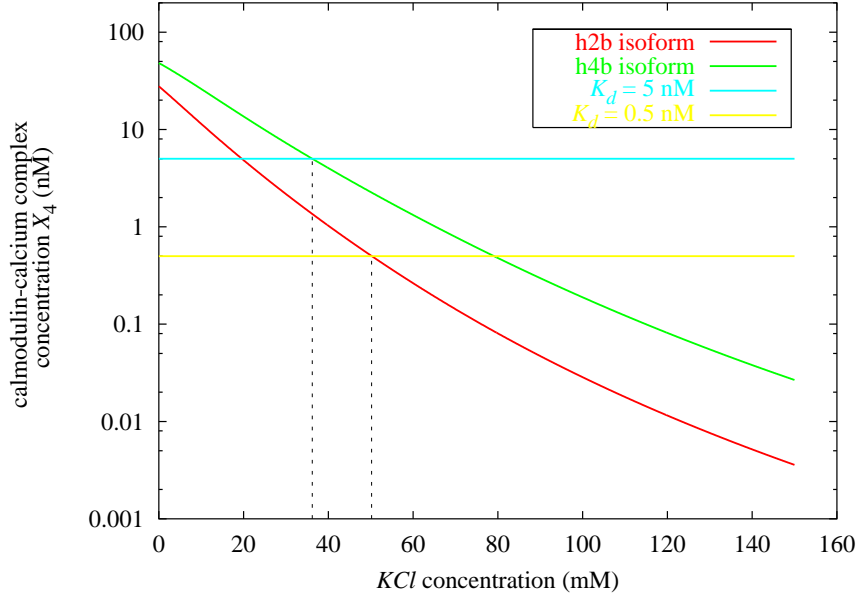


Figure 4.1: The available calmodulin-calcium complex concentration $X_4 C a_{\text{stim}}^{(1/2)}$ at various KCl concentrations

The $X_4 C a_{\text{stim}}^{(1/2)}$ concentration according to equation (3.37) is plotted against changing KCl concentrations, *i.e.* changing K_i 's, for the h2b (red line) and the h4b isoform (green line). The half stimulation concentrations of the h2b and the h4b isoform are $C a_{\text{stim}}^{(1/2)} = 0.653 \mu\text{M}$ and $C a_{\text{stim}}^{(1/2)} = 1.1 \mu\text{M}$, respectively. The calmodulin concentration in both calculations is $0.117 \mu\text{M}$. The dissociation constants K_i ($i = 1 \dots 4$) (see [13] and table 3.1) have been fitted by a quadratic function in dependence of the present KCl concentration in order to yield $K_i(KCl)$.

stimulation model parameters have to be redetermined, since the changed formation characteristics of the X_4 complex influences the choice of the stimulation parameter. By applying the same procedure as presented in section 3.4.1 for the stimulation and in section 3.4.2 for the relaxation and the use of the experimentally measured stimulation and relaxation constants by Caride *et al.*, respectively, a new parameterset can be quoted (see table 4.1). With the additional precondition of $K_d = 0.5 \text{ nM}$, k_2 and k_{-2} can be determined exactly from equation (3.37). With the available informations in section 3.4.1 they could only be fixed up to a range. On the contrary, k_4 and k_{-4} remain to be determined up to a range, since no informations concerning the complex detachment from the stimulated PMCA pump form P_X^* are available. It should be noticed that the dissociation constant between the calmodulin-calcium complex X_4 and the stimulated pump form P_X^* , $K_d = k_4/k_{-4} = 6.01 \cdot 10^{-4} \text{ nM}$ (step (3.21)), is substantially lower as it is the case for the unstimulated pump form P , $K_d = k_{-2}/k_2 = 0.5 \text{ nM}$ (step (3.19)).

parameter	h2b	unit	source
k_2	3504	$1/(\mu\text{M} \cdot \text{s})$	equation (3.37) with $K_d = 0.5 \text{ nM}$ and $\text{Ca}_{\text{stim}}^{(1/2)} = 0.653 \mu\text{M}$
k_{-2}	1.75	1/s	
k_3	0.06	1/s	$k_{\text{stim}}^{\text{max}}$
k_4	0.076	1/s	equation (3.46)
k_{-4}	126428	$1/(\mu\text{M} \cdot \text{s})$	
k_5	0.015	1/s	$k_{\text{relax}}^{\text{max}}$

Table 4.1: New rate constants for the h2b isoform at a KCl concentration of 50 mM

Since P and P* differ in their conformational composition they can exhibit different affinities for X₄, in principle. Note the the old parameterset of the h2b isoform implied also a significantly higher affinity of the stimulated pump form P_X*. The old parameterset determined in chapter 3 at with binding constants K_i ($i = 1\dots 4$) corresponding to $KCl = 100 \text{ mM}$ yields $K_d = k_{-2}/k_2 = 2.03 \cdot 10^{-6} \text{ nM}$ and $K_d = k_4/k_{-4} = 2.03 \cdot 10^{-6} \text{ nM}$ (see table 3.3 and 3.4).

As shown in section 3.4.1 and 3.4.2, the rate constants k_i with $i = \pm 2, 3, \pm 4, 5$ are deduced from experimentally measured stimulation and relaxation constants via the adaption of equation (3.30) and (3.42) to the data, respectively. The theoretical stimulation constant $k_{\text{stim}}^{(3)}$ (equation (3.30)) and the relaxation constant $k_{\text{relax}}^{(3)}$ (equation (3.42)) is plotted in figure 4.2 and 4.3, respectively, by utilising the new parameterset shown in table 4.1. The pumping activity parameters are not affected by a change in the formation of the calmodulin-calcium complex, since the calcium ions bind directly to the pump and the whole transportation process happens without the involvement of X₄. Thus, the pumping activity parameters in table 3.5 remain unchanged. Attention should be drawn to the discussed fact, that the choice of the stimulation parameter influence the shape of the steady-state pumping activity at lower calcium concentrations (see section 3.5.2). In figure 4.4 the calcium dependence of the steady-state activity for the h2b isoform in the absence and the presence of calmodulin is shown.

Apart from the later saturation of the theoretical stimulation constant in figure 4.2, the figures 4.2, 4.3 and 4.4 suggest that the experimental data can also be described by assuming the binding of calcium by calmodulin with dissociation constants K_i ($i = 1\dots 4$) corresponding to a present KCl concentration of $KCl = 50 \text{ mM}$.

Regarding equation (4.1) and the naturally arising high affinities of the PMCA pump for the X₄ complex in chapter 3 poses the question, if for any reasons the experimental conditions do not determine the calcium binding to correspond to $KCl = 150 \text{ mM}$. In this section this fact has been questioned. By assuming differ-

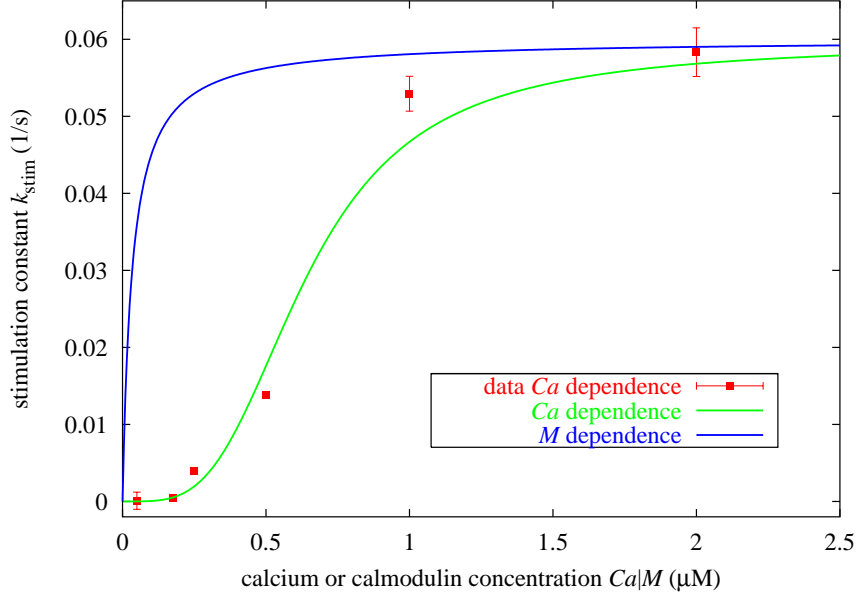


Figure 4.2: Stimulation constant $k_{\text{stim}}^{(3)}$ of the h2b isoform at $\text{KCl} = 50 \text{ mM}$

$k_{\text{stim}}^{(3)}$ according to equation (3.30) is plotted against calcium (green line) at constant calmodulin concentration of $0.117 \mu\text{M}$ utilising the new parameterset shown in table 4.1. The blue lines represent the $k_{\text{stim}}^{(3)}$ dependence on calmodulin at fixed calcium concentration of $1 \mu\text{M}$. The stimulation rate data (red squares) has been measured at various calcium concentrations with constant calmodulin concentration of $0.117 \mu\text{M}$ (with kind permission of Caride [1]). For comparison see also figure 3.5, displaying the same fit but with the old parameterset shown in table 3.3 and 3.4.

ing calmodulin - calcium buffering conditions, namely corresponding to $\text{KCl} = 50 \text{ mM}$, the experimental data can also be reproduced. Additionally, the dissociation constant $K_d = k_{-2}/k_2 = 0.5 \text{ nM}$ for the h2b isoform is assured. The therewith determined parameterset (table 4.1) will be used for further investigations, whereas the calmodulin - calcium buffering behaviour is determined by the present conditions and thus requires adaptation to the respective environment.

4.2 Intracellular calcium - calmodulin - target protein homeostasis

The considerations in chapter 3 and in section 4.1 where addressed to the reproduction of the PMCA pump stimulation behaviour during *in vitro* experiments of Caride *et al.* [1]. The implementation of the PMCA pump stimulation model in the presynaptic calcium dynamics raises the question which calcium buffering constant K_i ($i = 1..4$) of calmodulin should be employed in order to simulate

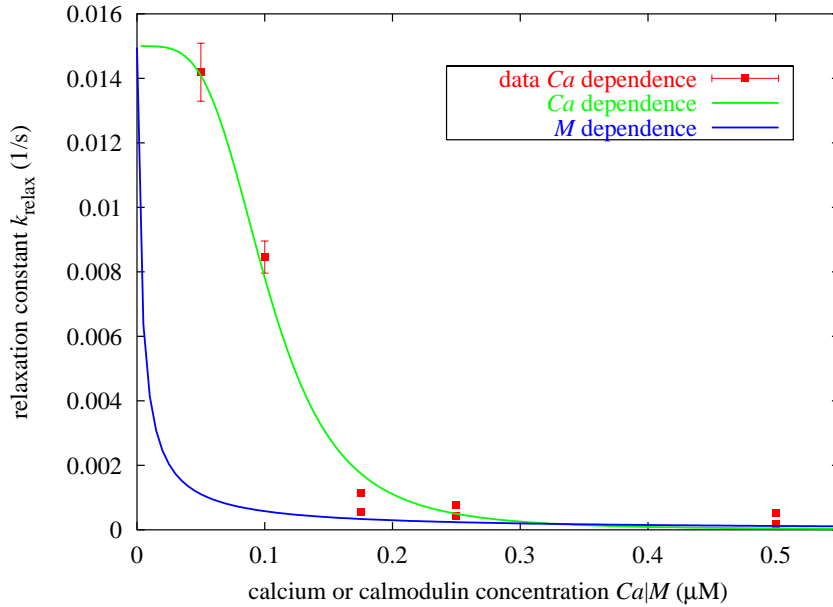


Figure 4.3: Relaxation constant $k_{\text{relax}}^{(3)}$ of the h2b isoform at KCl = 50 mM

The relaxation constant $k_{\text{relax}}^{(3)}$ according to equation (3.42) is plotted for changing calcium (green line) and calmodulin (blue line) concentrations whereas calmodulin ($M_0 = 0.117 \mu\text{M}$) and calcium ($Ca_0 = 0.25 \mu\text{M}$) are kept constant. The used parameter set is shown in table 4.1. The theoretical behaviour at changing calcium concentrations is shown in table 4.1. The theoretical behaviour at changing calcium concentrations is fitted to the experimental data (red squares) at $M_0 = 0.117 \mu\text{M}$ (with kind permission of Caride [1]). For comparison see figure 3.7, displaying the same fit but with the old parameter set shown in table 3.3 and 3.4.

the physiological calcium buffering by calmodulin in neurons. With regard to the large differences in the K_i 's shown in table 3.1 a correct description is of crucial importance. That question is addressed in this section. Note that the choice of the appropriate binding constants K_i is discussed in terms of a fictive present KCl concentration. Since the K_i 's vary under changing KCl concentrations (see table 3.1) the investigations in this section seek for an appropriate KCl concentration as a parameter which determines the calmodulin - calcium binding. However, that binding might also be influenced by other conditions, represented here by the KCl concentration adjustment.

In order to establish appropriate binding constants for the calcium buffering by calmodulin, statements of Persechini *et al.* (1999) [18] who investigated the relationship between free calcium and free calmodulin-calcium complex concentrations in intact cells are employed. In addition, Linse *et al.* provided the binding constants K_i for a range of KCl concentrations from low ionic strength to 150 mM (see table 3.1) [13].

The investigations of Persechini *et al.* lead to several interesting statements.

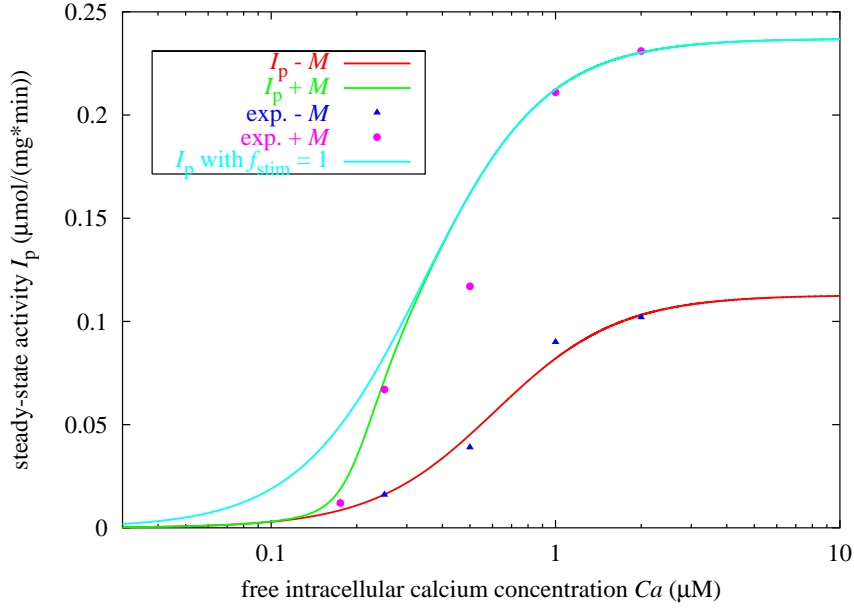


Figure 4.4: Steady-state activity of the h2b isoform at $KCl = 50$ mM

The measurements in the absence (blue triangles) and in the presence (purple circles) of $0.117 \mu\text{M}$ calmodulin have been kindly provided by Caride [1]. The red line depicts the fit of equation (3.55) with $f_{\text{stim}} = 0$, corresponding to no available calmodulin, to the experimental data. The green line shows the fit of (3.55) to data measured in the presence of calmodulin. The total pump concentration P_0 is taken from [1] to be $0.005 \mu\text{M}$. For more informations please refer to section 3.5.2 and figure 3.14. Note that the steady-state activity parameter I_{max} , I_{max}^* , H_p and H_p^* are not affected by the new stimulation parameters and are equal to the these stated in table 3.5 for the h2b isoform. Figure 3.14 displays the same plots but using the old stimulation parameterset in table 3.3 and 3.4.

They found that below a free calcium concentration of $0.2 \mu\text{M}$ little or no calcium-liganded calmodulin is detectable [18]. A maximum free X_4 concentration is produced at a calcium concentration of $3 \mu\text{M}$, while the half maximum concentration of X_4 is produced when the free Ca^{2+} concentration is $1 \mu\text{M}$. Attention should be drawn to the fact, that with a total physiological calmodulin concentration of $30 \mu\text{M}$ [14, 18, 19] only a minor fraction of produced calmodulin-calcium complexes remains free in cells. This underscores the importance of X_4 for target activation within cells. Furthermore, Persechini states that a maximum free X_4 concentration of about 45 nM is reached at a free calcium concentration of $3 \mu\text{M}$. In the following these statements are utilised to determine the appropriate binding constants which reproduce the measured scenario. In that consideration the KCl concentration is treated as a free parameter in order to fit the data of Persechini *et al.*.

For the purpose to qualitatively reproduce the physiological relationship between free calmodulin-calcium complexes and free calcium ions a simple model aimed to describe intracellular calcium buffering and calmodulin-calcium complex target activation is examined. Free calcium is buffered by calmodulin M. Equation (3.3) delivers a relation between free calmodulin and free complex X_4 . Again, only the X_4 complex is considered to be capable of protein target activation. The investigations in chapter 3 provide strong evidence for that assumption (see section 3.7 on page 64).

As mentioned in chapter 3.1, the calmodulin-calcium complex is responsible for the activation of a vast variety of target proteins, whereas the affinities of these target proteins for the X_4 complex differ on a range of $1 \text{ nM} < K_d < 100 \text{ nM}$ [1, 18, 19, 32, 43, 48, 53, 59]. Two representants, one high affinity target protein P ($K_d^{(p)} = 1 \text{ nM}$), representing the PMCA pump, and one low affinity protein Q ($K_d^{(q)} = 100 \text{ nM}$) is incorporated in the model, expressed by



P_X is X_4 bound to P, whereas calmodulin-calcium complex bound by Q is referred to as Q_X .

The whole process is considered to be in quasi-steady-state. With the protein mass conservations $P_0 = P + P_X$ and $Q_0 = Q + Q_X$ the calmodulin conservation law is given by

$$\frac{K_1 K_2 K_3 K_4}{C a^4} X_4 + \frac{K_2 K_3 K_4}{C a^3} X_4 + \frac{K_3 K_4}{C a^2} X_4 + \frac{K_4}{C a} X_4 + X_4 + P_X + Q_X = M_0, \quad (4.4)$$

where the X_i 's ($i = 1...3$) and M have been replaced utilising equation (3.4). M_0 stands for the total calmodulin concentration. This conservation equation leads to a cubic equation in X_4

$$\begin{aligned} 0 = & - X_4^3 \cdot A \\ & + X_4^2 \cdot \left[M_0 - (K_d^{(p)} + K_d^{(q)})A - P_0 - Q_0 \right] \\ & + X_4 \cdot \left[M_0(K_d^{(p)} + K_d^{(q)}) - K_d^{(p)} K_d^{(q)} A - K_d^{(q)} P_0 - K_d^{(p)} Q_0 \right] \\ & + M_0 K_d^{(p)} K_d^{(q)}, \end{aligned} \quad (4.5)$$

with

$$A = 1 + \frac{K_4}{C a} + \frac{K_3 K_4}{C a^2} + \frac{K_2 K_3 K_4}{C a^3} + \frac{K_1 K_2 K_3 K_4}{C a^4}. \quad (4.6)$$

The quasi-steady-state treatment reduces the rate constants in the reaction scheme 4.2 and 4.3 to the respective dissociation constants $K_d^{(p)} = k_-^p/k_+^p$ and $K_d^{(q)} = k_-^q/k_+^q$.

The total available calmodulin concentration in neurons is about $30 \mu\text{M}$ [14, 18, 19]. As already discussed, the PMCA pump surface density of $\rho_p = 3400 \mu\text{m}^{-2}$ quoted in [4] can be translated into a concentration of PMCA pumps of $P_0 = 33.9 \mu\text{M}$. For the simulation a value of $P_0 = 30 \mu\text{M}$ is used. Persechini *et al.* further indicate that the total concentration of calmodulin-calcium complex binding sites exceed the total concentration of calmodulin M_0 by a factor of about 2. Therefore the total concentration of the low affinity target protein Q_0 is chosen to be $30 \mu\text{M}$ [18]. With the use of equation (4.5) for the free intracellular X_4 concentration the KCl concentration can be adapted with the requirement to accomplish all the stated informations by Persechini *et al.* regarding the formation of free X_4 at the given calcium concentrations [18]. In figure 4.5 the free X_4 concentration is plotted against the free intracellular calcium concentration with binding constants K_i ($i = 1\dots 4$) corresponding to a KCl concentration of 100 mM , since this scenario fits best all the stated requirements. Only the real and positive solution of equation (4.5) which fulfils $0 \leq X_4 \leq P_0$ is considered here. It can be seen that the maximum free X_4 concentration strongly depends on the total available high affinity and low affinity calmodulin target concentrations P_0 and Q_0 , respectively. From this observation in figure 4.5 it can be reasoned that for the production of 45 nM free X_4 concentration the amount of high affinity target protein should have been significantly lower compared to the low affinity target protein during the investigations of Persechini *et al.*. Note that the sum of both is kept constant in order to fulfil $2M_0 = P_0 + Q_0$. Depending on the analysed cell type the occurrence and distribution of target proteins might vary leading to different saturation concentrations X_4 at $Ca = 3 \mu\text{M}$. However, the half maximum calcium concentration of about $1 \mu\text{M}$ remains relatively stable such as the production of the maximum free X_4 concentration at a free calcium concentration of $3 \mu\text{M}$ while varying the proportion of P_0 and Q_0 . These two facts are mainly influenced by the used dissociation constants K_i ($i = 1\dots 4$) and thus by the corresponding KCl concentration.

Furthermore one can pose the question for the remaining free calcium concentration during the simulation of calcium - calmodulin - target protein binding in relation to the total calcium load within the cell. This question is of interest since it is known that during calcium elevations only a minor fraction of 1 - 5 % of the total intracellular calcium remains free within the cytosol [12, 15]. In the introduced model, represented by the calcium buffering in reaction (3.1) and the target binding in reactions (4.2) and (4.3), bound calcium occurs in associations of X_1 , 2 X_2 , 3 X_3 , 4 X_4 , 4 P_X and 4 Q_X , where the numbers indicate the respective quantity of bound calcium. Therewith the fraction of free calcium concentration

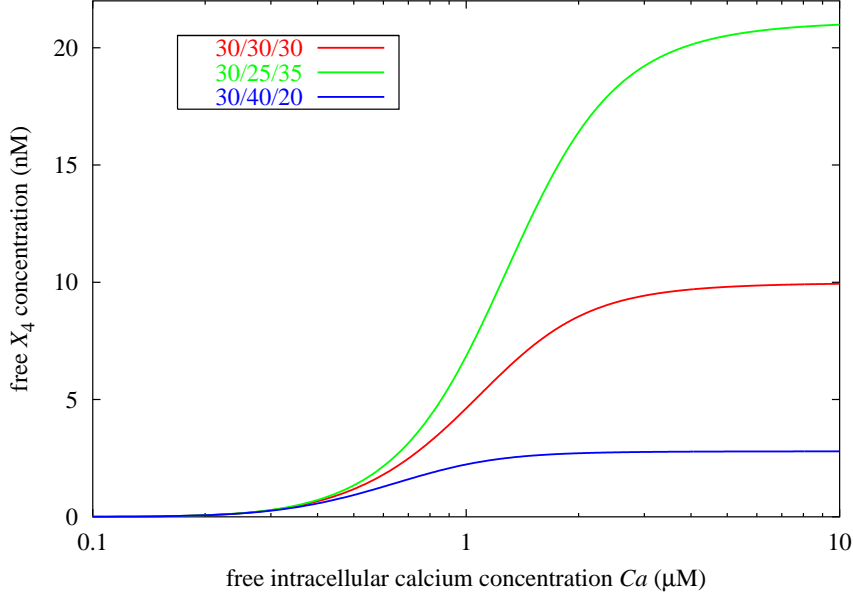


Figure 4.5: Changes in free intracellular X_4 concentration in dependence on the free calcium concentration at $KCl = 100$ mM

The solution of equation (4.5) is plotted against the free intracellular calcium concentration. The three numbers in the box characterising the different scenarios stand for the total calmodulin concentration M_0 , the total concentration of high affinity target protein P_0 and the total concentration of low affinity target protein Q_0 , *i.e.* $M_0/P_0/Q_0$. The binding constants K_i ($i = 1..4$) are taken at a concentration of $KCl = 100$ mM (see table 3.1 and [13]).

f_{freeCa} is given by

$$f_{\text{freeCa}} = \frac{Ca}{Ca + X_1 + 2X_2 + 3X_3 + 4X_4 + 4P_X + 4Q_X}. \quad (4.7)$$

The fraction of free calcium in relation to the free intracellular calcium concentration is shown in figure 4.6. The fraction of free calcium lies within the desired range from 1 - 5 % of the total intracellular calcium load. In figure 4.6 it becomes furthermore evident that the total quantity of bound calcium is mainly influenced by the total available calmodulin concentration, whereas at the same calmodulin concentration and differing low and high affinity target proteins, the plots show strong similarities. They only vary slightly at the peak of bound calcium in the vicinity of $0.5 \mu\text{M}$ free calcium.

Since the plot in figure 4.5 exhibits resemblance with the measured data of Persechini *et al.* and the fraction of free intracellular calcium accomplishes the expected conditions, the buffering constants K_i ($i = 1..4$) at a KCl concentration of 100 mM are used in the presynaptic calcium dynamics model for the description

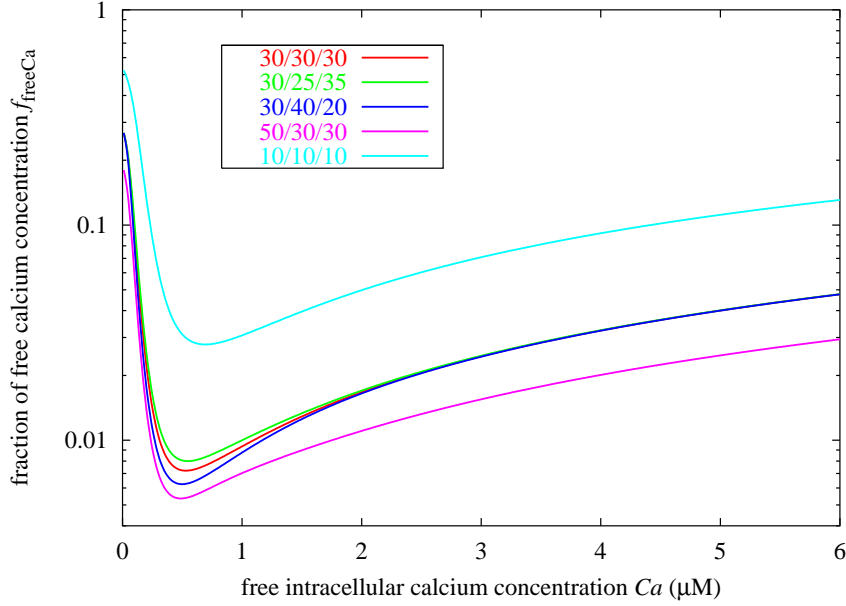


Figure 4.6: Fraction of free calcium concentration f_{freeCa}

f_{freeCa} according to equation (4.7) is plotted for total intracellular calcium loads. The three numbers in the box indicating the different plots refer to the total calmodulin concentration M_0 , the total concentration of high affinity target protein P_0 and the total concentration of low affinity target protein Q_0 , *i.e.* $M_0/P_0/Q_0$.

of calcium buffering by calmodulin. That is, the conditions in a real neuron determine that buffering as equivalently a solution of $KCl = 100$ mM would.

With the new parameterset for the h2b isoform (table 4.1) and the buffering constants K_i ($i = 1..4$) at $KCl = 100$ mM, the steady-state stimulation of the PMCA pump can be calculated again. The unstimulated pump fraction f_{unstim} (cyan line) and the stimulated pump fraction f_{stim} (grey line) in figure 4.7 suggest a level of stimulation of about 20 % at the resting level calcium concentration of $0.1 \mu\text{M}$. Beside that plots, the steady-state stimulation distribution at $KCl = 100$ mM computed with the old parameterset quoted in table 3.3 and 3.4 is shown (blue line for f_{unstim} , purple line for f_{stim}).

Using $KCl = 100$ mM and the new parameterset a stimulation degree of 20 % at $0.1 \mu\text{M}$ can be reconciled with the PMCA stimulation measurements in endothelial and T cells [54, 55, 56], where a raise of the intracellular calcium concentration above $Ca = 0.1 \mu\text{M}$ could measurably stimulate the extrusion pathway through PMCA pumps.

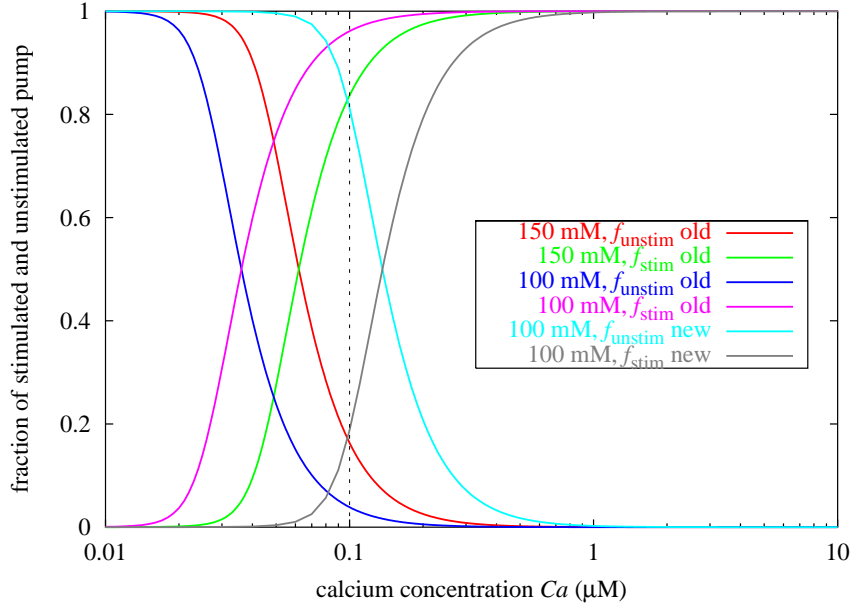


Figure 4.7: Steady-state fractions of unstimulated f_{unstim} and stimulated f_{stim} PMCA pump of the h2b isoform at various KCl concentrations and with different stimulation parametersets

The total available calmodulin and PMCA pump concentrations for all the shown calculations are $M_0 = 30 \mu\text{M}$ and $P_0 = 30 \mu\text{M}$. The concentrations in the box characterising the different plots refer to the KCl concentration which determines the used dissociation constants K_i ($i = 1\dots 4$) (see table 3.1). The red and the blue line depict f_{unstim} , the green and the purple line depict f_{stim} calculated via equation (3.56) - (3.58) and the use of the old parameterset for the h2b isoform shown in table 3.4 and 3.3 and the respective KCl concentration. The cyan and the grey line show f_{unstim} and f_{stim} , respectively, calculated via the same equations by using the new parameterset in table 4.1 and at a KCl concentration of 100 mM corresponding to conditions within a neuron (section 4.2). The black dotted line indicates the resting level calcium concentration of $0.1 \mu\text{M}$ in neurons.

4.3 Implementation in the presynaptic calcium dynamics model

Having determined the new stimulation parameters in section 4.1 and identified buffering constants K_i ($i = 1 \dots 4$) capable to describe intracellular calcium buffering by calmodulin in section 4.2 it is now possible to implement the new PMCA stimulation model in the theoretical description of presynaptic calcium dynamics, which has been introduced in section 2.2 [3, 4].

The presentation of the presynaptic calcium dynamics model [3, 4] in section 2.2 resulted in the quotation of a differential equation describing the sinks and the sources of intracellular free calcium concentration Ca

$$\frac{dCa}{dt} = \frac{G}{zF} \{J_v(U(t), Ca) - J_x(Ca) - J_p(Ca) + L\} \frac{1}{1 + \frac{dCa_{\text{bound}}}{dCa}}. \quad (4.8)$$

See section 2.2 for more details concerning this expression.

The comprehensive PMCA pumping activity model presented in chapter 3 determines the extrusion term $J_p(Ca)$ for calcium efflux through PMCA pumps. Furthermore the buffering of calcium ions has to be reconciled with the stimulation model, since calmodulin plays a key role in intracellular calcium buffering and at the same time acts in its fully liganded form on various target proteins, such as the PMCA pump.

PMCA pumping activity With equation (3.59) an expression for the calcium efflux through a single PMCA pump has been developed. This expression is in accordance with the architecture of the whole presynaptic calcium dynamics model which is based on single protein properties. The rate of transported calcium ions per second through a single PMCA pump protein corresponding to the term within the brackets in equation (3.59) can be translated into a current density of an ensemble of pumps by employing the Faraday constant F , the valence charge of calcium ions ($z_{Ca} = 2$) and the surface density of PMCA channels ρ_p

$$J_p(Ca) = \rho_p z_{Ca} F \left[f_{\text{unstim}}(t) \cdot \frac{I_{\text{single}} \cdot Ca^2}{H_{1/2}^2 + Ca^2} + f_{\text{stim}}(t) \cdot \frac{I_{\text{single}}^* \cdot Ca^2}{H_{1/2}^{*2} + Ca^2} \right]. \quad (4.9)$$

The fractions $f_{\text{unstim}}(t)$ and $f_{\text{stim}}(t)$ are determined via the stimulation model in dependence of the present free calcium and calmodulin concentration.

Calcium buffering The whole cascade of calcium buffering and calmodulin-calcium complex target attachment is crucial for the dynamics of intracellular calcium concentration since 95 - 99 % of the total intracellular calcium load is involved.

The cascade is triggered with the initial binding of calcium by free calmodulin (M). To assure a sufficient buffering of 95 - 99 % of the total intracellular calcium concentration and to reproduce the results in [3, 4] an additional endogenous buffer B^{en} beside the calmodulin protein M is introduced. This endogenous buffer comprises one binding site and effectively describes the buffering of calcium by other intracellular buffering proteins, such as parvalbumin, calretinin, calcineurin and calbindin-D_{26k} [12].

As described in section 4.2 on page 74, a low Q and a high affinity P target protein are included in the target activation cascade by X_4 complexes. The high affinity target is the Plasma Membrane Calcium pump, whereas the pump is described by the parameterset of the h2b isoform. This isoform displays an affinity of $K_d = 0.5$ nM for the calmodulin-calcium complex, whereas the low affinity target protein Q is characterised by an affinity of $K_d^{(q)} = 100$ nM.

Only considering the aspect of buffering and target protein activation, the processes together with the new PMCA stimulation model ((3.19) - (3.22)) is represented by the following system of coupled differential equations of first order

$$\begin{aligned} \frac{dCa}{dt} = & -k_1^m M Ca + k_{-1}^m X_1 - k_2^m Ca X_1 + k_{-2}^m X_2 - k_3^m Ca X_2 + k_{-3}^m X_3 \\ & - k_4^m Ca X_3 + k_{-4}^m X_4 - k_+^{\text{en}} Ca (B_0^{\text{en}} - B_{\text{Ca}}^{\text{en}}) + k_-^{\text{en}} B_{\text{Ca}}^{\text{en}}, \end{aligned} \quad (4.10)$$

$$\frac{dB_{\text{Ca}}}{dt} = +k_+^{\text{en}} Ca (B_0^{\text{en}} - B_{\text{Ca}}^{\text{en}}) - k_-^{\text{en}} B_{\text{Ca}}^{\text{en}}, \quad (4.11)$$

$$\frac{dM}{dt} = +k_1^m M Ca - k_{-1}^m X_1, \quad (4.12)$$

$$\begin{aligned} \frac{dX_4}{dt} = & +k_4^m Ca X_3 - k_{-4}^m X_4 - k_+^q (Q_0 - Q_X) X_4 + k_-^q Q_X \\ & - k_2 X_4 P + k_{-2} P_X + k_4 P_X^* - k_{-4} P^* X_4, \end{aligned} \quad (4.13)$$

$$\frac{dQ_X}{dt} = +k_+^q (Q_0 - Q_X) X_4 - k_-^q Q_X, \quad (4.14)$$

$$\frac{dP}{dt} = -k_2 X_4 P + k_{-2} P_X + k_5 P^*, \quad (4.15)$$

$$\frac{dP_X}{dt} = +k_2 X_4 P - k_{-2} P_X - k_3 P_X, \quad (4.16)$$

$$\frac{dP_X^*}{dt} = +k_3 P_X - k_4 P_X^* + k_{-4} P^* X_4, \quad (4.17)$$

$$\frac{dP^*}{dt} = +k_4 P_X^* - k_{-4} P^* X_4 - k_5 P^*. \quad (4.18)$$

Where M , X_1 , X_2 , X_3 and X_4 denote the concentrations of the calmodulin protein with none, one, two, three and four calcium ions bound, respectively. $B_{\text{Ca}}^{\text{en}}$ is endogenous calcium buffer bound with calcium and for the free endogenous buffer B^{en} the total mass conservation $B_0^{\text{en}} = B^{\text{en}} + B_{\text{Ca}}^{\text{en}}$ has been utilised. Q_X refers to the low affinity target protein of the calmodulin-calcium complex bound with

the complex X_4 . The free low affinity target Q can be replaced by the total mass conservation $Q_0 = Q + Q_X$. P , P_X , P_X^* and P^* denote the PMCA pump in its different stimulation states (see section 3.4). The superior letters in the rate constants refer to the involved buffer or target protein, only the rate constants belonging to the PMCA pump stimulation are not marked by an additional letter. They correspond to the rate constants introduced in the stimulation model ((3.19) - (3.22)) and quoted in table 4.1.

The single reaction rates with a superior letter are unknown but all the dissociation constants, determined by the ratio of the backward reaction rate to the forward rate, are given. The buffering dissociation constant of calmodulin $K_1 = k_{-1}^m/k_1^m$, $K_2 = k_{-2}^m/k_2^m$, $K_3 = k_{-3}^m/k_3^m$ and $K_4 = k_{-4}^m/k_4^m$ have been measured by Linse *et al.* [13] and are quoted in table 3.1. The dissociation constant for the low affinity buffer $K_d^{(q)} = k_-^q/k_+^q$ is fixed to 100 nM [1, 18, 19, 32, 43, 48, 53, 59]. The affinity of the h2b isoform can be found in various publications, $K_d = k_{-2}/k_2 = 0.5$ nM [19, 33, 34, 37, 48, 49] (see discussion in section 4.2).

The overall presynaptic calcium dynamics becomes with equation (4.10)

$$\begin{aligned} \frac{dCa}{dt} = & \frac{G}{zF} \left[J_v(U(t), Ca) - J_x(Ca) - J_p(Ca) + L \right. \\ & - k_1^m M Ca + k_{-1}^m X_1 - k_2^m Ca X_1 + k_{-2}^m X_2 \\ & \left. - k_3^m Ca X_2 + k_{-3}^m X_3 - k_4^m Ca X_3 + k_{-4}^m X_4 \right] \frac{1}{1 + \frac{dCa_{\text{bound}}}{dCa}}, \quad (4.19) \end{aligned}$$

and

$$\frac{dCa_{\text{bound}}}{dCa} = \frac{B_0^{\text{en}} K_d^{\text{en}}}{(K_d^{\text{en}} + Ca)^2}. \quad (4.20)$$

Note that for the endogenous calcium buffer B^{en} the fast buffer approximation presented in section 2.2 on page 15 has been employed with $K_d^{\text{en}} = k_-^{\text{en}}/k_+^{\text{en}}$.

The parameters which are not directly affected by the PMCA stimulation implementation are taken from [3, 4]. These include the parameters describing the Sodium-Calcium Exchanger, the Voltage Directed Calcium Channels and specifying the geometry as well as the membrane protein densities of the investigated presynaptic terminal. Further parameters have been previously stated. A collection of the used parameter for the simulation in the following section (4.4) is shown in table 4.2.

Note that in contrast to the calcium buffering by the endogenous buffer, the calcium buffering by calmodulin and the target binding of the calmodulin-calcium complex to Q is described dynamically. Hence the rate constants for the respective reactions and directions are required beyond the dissociation constants. These single rate constants are chosen sufficiently high to provide the buffering and target binding to occur fast with respect to the considered time scales.

value	source
calcium-calmodulin-target protein binding	
$K_d^{\text{en}} = 0.5 \mu\text{M}$	[3, 4, 12]
$B_0^{\text{en}} = 15 \mu\text{M}$	[3, 4, 12]
$K_1 = 11.68 \mu\text{M}$	[13]
$K_2 = 0.323 \mu\text{M}$	[13]
$K_3 = 46.98 \mu\text{M}$	[13]
$K_4 = 3.598 \mu\text{M}$	[13]
$M_0 = 30 \mu\text{M}$	[14, 18, 19]
$K_d^{(q)} = 100 \text{ nM}$	[18, 32, 59]
$Q_0 = 30 \mu\text{M}$	[18]
PMCA stimulation	
$k_2 = 3504 (\mu\text{M} \cdot \text{s})^{-1}$ $k_{-2} = 1.75 \text{ s}^{-1}$ $k_3 = 0.06 \text{ s}^{-1}$ $k_4 = 0.076 \text{ s}^{-1}$ $k_{-4} = 126428 (\mu\text{M} \cdot \text{s})^{-1}$ $k_5 = 0.015 \text{ s}^{-1}$	stimulation parameterset of the h2b isoform (table 4.1)
PMCA activity	
$I_p = 1.57 \cdot 10^{-21} \text{ C/ms}$ $I_p^* = 3.3 \cdot 10^{-21} \text{ C/ms}$ $H_p = 0.612 \mu\text{M}$ $H_p^* = 0.34 \mu\text{M}$ $n_p = 2$	steady-state activity parameterset of the h2b isoform (table 3.5)
NCX activity	
$I_x = 4.8 \cdot 10^{-19} \frac{\text{C}}{\text{ms}}$ $H_x = 1.8 \mu\text{M}$ $n_x = 1$	[3, 4]
VDCC activity	
$\bar{g}_v = 14 \text{ ps}$ $\bar{U}_{\text{Ca}} = 47 \text{ mV}$ $\tau = 1 \text{ ms}$ $\kappa = 6.3 \text{ mV}$ $U_H = -4 \text{ mV}$	[3, 4]
membrane protein densities	
$\rho_v = 3 \mu\text{m}^{-2}$ $\rho_p = 3000 \mu\text{m}^{-2}$ $\rho_n = 100 \mu\text{m}^{-2}$	[3, 4]
geometry and resting state	
$G = 3/0.5 \mu\text{m}$ $U_0 = -70 \text{ mV}$ $\text{Ca}_0 = 0.1 \mu\text{M}$ $\text{Ca}_{\text{ext}} = 1.5 \mu\text{M}$	[3, 4]

Table 4.2: Comprehensive collection of the parameter used in the presynaptic calcium dynamics simulations

In [3, 4] the simulation has been adapted to experimental fluorescence data of Koester and Sakmann (2000) [15] by fixing the surface densities of the membrane proteins. On account of that, the model in [3, 4] contains also a fluorescence buffer which is not considered here.

It has to be mentioned that apart from the PMCA pump stimulation and the calcium buffering the presynaptic calcium dynamics model has not gained adequate attention in this work. For further informations especially regarding the characteristics and the modelling of the action potentials please refer to Erler *et al.* (2003) and Meyer-Hermann *et al.* (2003) [3, 4].

4.4 Consequences of the pump stimulation for the calcium dynamics

The consequences of the PMCA pump stimulation in response to various stimulation protocols shall conclude the investigations presented in this work.

The translation of the PMCA pumps surface density of $\rho_p = 3000 \mu\text{m}^{-2}$ in a concentration yields $P_0 = 29.9 \mu\text{M}$. Hence with at total calmodulin concentration of $M_0 = 30 \mu\text{M}$ theoretically all the pump proteins can be stimulated. In figure 4.7 the resting level degree of PMCA stimulation is suggested to be 20 %. Together with an additional buffer B^{en} the initial state stimulation level is decreased to 10 % in the simulation of presynaptic calcium dynamics.

In figure 4.8 the dynamical calcium answer to similar action potentials in the resting level $f_{\text{stim}} = 0.1$, in almost fully stimulated state $f_{\text{stim}} = 0.83$ and in fully stimulated state $f_{\text{stim}} = 1$ is shown. Since the PMCA pump comprises a high calcium affinity and a low transport rate it is responsible for the fine tuning of the calcium extrusion. In contrast, the sodium-calcium exchanger (NCX) exhibits a low calcium affinity paired with a high calcium transport rate [41, 42]. Thus, the NCX is suitable for a rapid recovery from high calcium levels. This fact is reflected in the three calcium answers in figure 4.8. The stimulation of the PMCA pump (green and blue line) does not significantly affect the peak of the calcium transient, but accelerates the recovery to resting calcium levels at the relaxing face.

During an application of a 10 Hz train of action potentials, as it is used during potentiating stimuli, this faster recovery to the resting calcium level of $0.1 \mu\text{M}$ at highly PMCA pump stimulation degree significantly decreases the emerging new base line [3, 4] (see figure 4.9). This arising lower base line leads in turn to lower peak values of the calcium elevation since the amplitude in response to a single action potential remains constant but the starting point of the calcium peak is decreased due to the stimulated pumping rate of the PMCA extrusion pathway.

Considering the unstimulated case, during such a 10 Hz train of action potentials lasting for 1000 ms as shown in figure 4.9 the formation of stimulated pump form

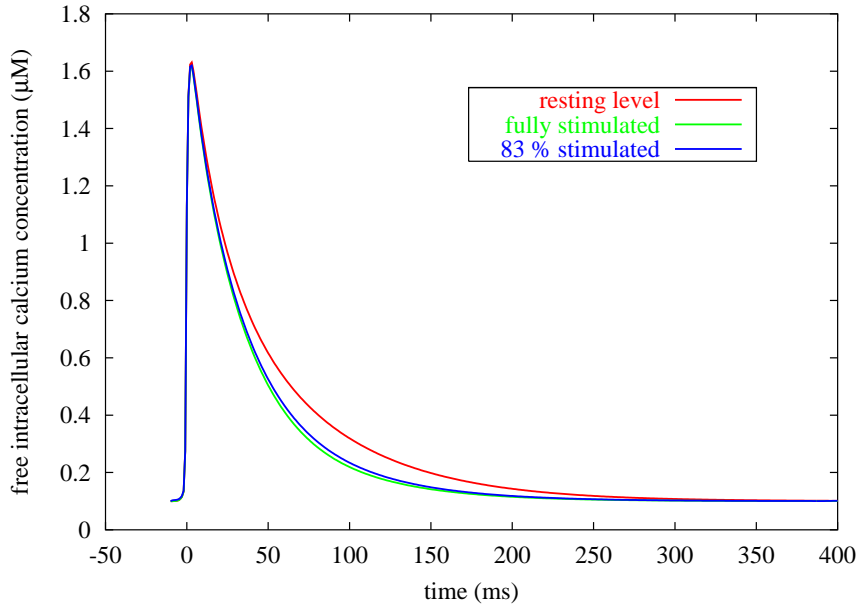


Figure 4.8: Presynaptic calcium answer to a single action potential

The calcium response to the application of a single action potential is plotted (equation (4.19)). The temporal evolution is depicted for three different stimulation levels of the PMCA pump. The simulation indicated by the red line started with the resting level stimulated PMCA pump fraction of about 10 %, *i.e.* $f_{\text{stim}} = 0.1$. At the beginning of the simulation portrayed by the green line, fully stimulated PMCA pumps have been assumed, *i.e.* $f_{\text{stim}} = 1$ at $t = -10$ ms. Whereas the blue line shows a simulation starting with $f_{\text{stim}} = 0.83$.

has no interactive relevance. Due to the limitation of the stimulation velocity reflected in the minimum half stimulation time of $t_{\text{minstim}}^{(1/2)} = 11.6$ s for the h2b isoform the pump is stimulated about 1 % during the 1 s calcium elevation shown in figure 4.9. Since high frequency trains characteristically last only for seconds, they are not capable to substantially increase the fraction of stimulated PMCA pump form f_{stim} . This argumentation holds also for the stimulation response to single action potentials as shown in figure 4.8 since the persistent time of the elevated calcium concentration is even shorter.

In contrast, low frequency trains of action potentials of about 2 Hz may be applied for up to minutes. Combined with the slow recovery of stimulated PMCA pump form, which also happens on a time scale of minutes (see figure 3.10), such a stimulation protocol evokes a measurable degree of PMCA stimulation. In figure 4.10 the model has been exposed to an action potential train of 2 Hz for 10 min. During that simulation the fraction of stimulated pump form f_{stim} could be increased from $f_{\text{stim}} = 0.1$ at resting level to $f_{\text{stim}} = 0.84$. During such a protocol of action potentials no emerging base line can be observed since after 500 ms, the

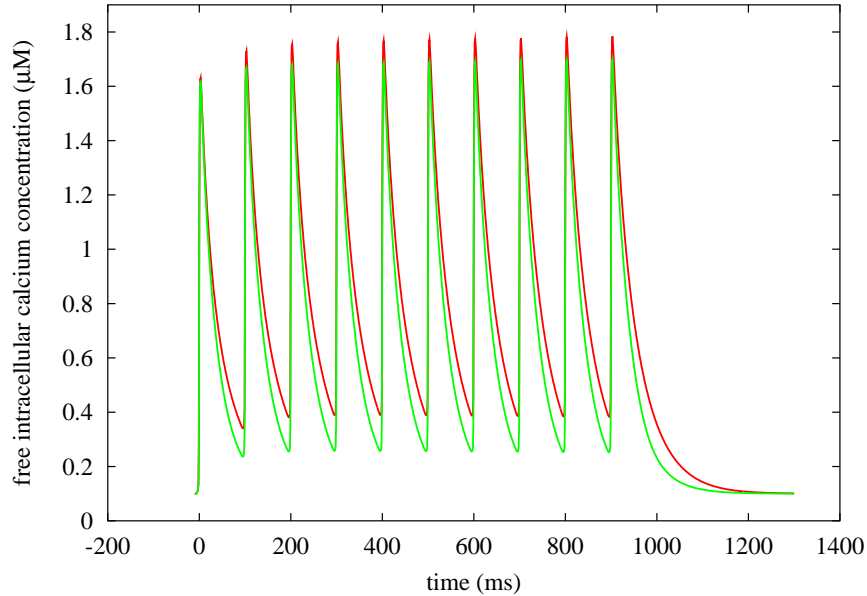


Figure 4.9: Presynaptic calcium answer to a 10 Hz train of action potentials

The calcium response to the application of a 10 Hz train of action potentials lasting for 1000 ms is shown (equation (4.19)). The temporal evolution is depicted for two different stimulation levels of the PMCA pump. The simulation indicated by the red line started with the resting level stimulated PMCA pump fraction of about 10 %, *i.e.* $f_{stim} = 0.1$. At the beginning of the simulation portrayed by the green line fully stimulated PMCA pumps have been assumed, *i.e.* $f_{stim} = 1$ at $t = -10$ ms.

time of the recurring stimuli, the intracellular free calcium concentration recovers completely to the resting level (see figure 4.8).

One can now address the question to the differences of the calcium answers to a single action potential before and after the presented stimuli. The red line in figure 4.8 depicts the reference calcium elevation, *i.e.* the calcium response to an action potential at resting PMCA pump stimulation level ($f_{stim} = 0.1$) prior to any stimulation protocol. The calcium response subsequent to a high frequency stimuli lasting for one second is not shown, since due to the 1 % stimulation of PMCA pumps the single action potential response after the protocol does not noticeably diverge from the reference response (red line in figure 4.8). On the contrary, the calcium transient at $f_{stim} = 0.83$ (blue line in figure 4.8) as it appears after a low frequency train of 10 min almost resembles the depicted fully stimulated PMCA pump (green line) scenario. The facilitated extrusion pathway by stimulated PMCA pump activity decays over a time range of minutes. Thus one can associate with the altered shape of the calcium response an expression of a short-term depression state at the presynaptic terminal related with PMCA pump stimulation. This result is consistent with the experimentally proven fact,

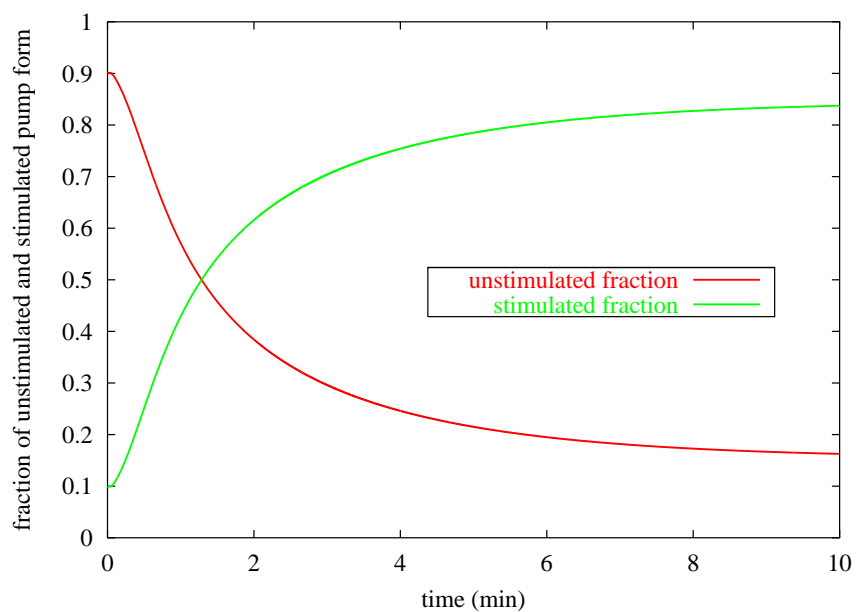


Figure 4.10: Stimulation of the h2b PMCA pump during a low frequency train of 2 Hz lasting for 10 min

The simulation started with the resting PMCA stimulation level of about 10 % stimulated pump form. The red and the green line depict f_{unstim} and f_{stim} , respectively, in response to the temporal intracellular calcium elevations evoked by the stimuli.

that low frequency stimuli occur to evoke short- and long-term depression of the synaptic signal transmission.

5 Discussion and Conclusions

The in chapter 3 presented comprehensive model for the PMCA pump stimulation and activity provides the opportunity to be implemented in simulation of various biological systems. For that purpose the architecture of the presented pump module distinguishes between universal and specific parameter classes. Universal parameters are postulated to have system-independent properties. These parameters comprise the described single membrane pump properties, such as the single pumping rates ($I_{\text{single}}, I_{\text{single}}^*$), the affinities of the pump for calcium (H_p, H_p^*) and the stimulation parameter set (k_i with $i = \pm 2, 3, \pm 4, 5$). Specific parameters depend on the system under consideration or on the details of the experimental setup and are the expression level (η) and the conditions of calcium buffering by calmodulin (K_i with $i = 1...4$). Since chapter 3 itself represents a concluded part of this thesis, a detailed discussion of the PMCA pump model is found in section 3.7 and will not be repeated here.

With the implementation of the PMCA pump stimulation model presented in chapter 4 of this work in the presynaptic calcium dynamics model of the Research Group Theoretical Biophysics [3, 4] a signature of the Plasma Membrane Calcium pump stimulation in a neuron could be acquired. However, it has to be mentioned that the results have a qualitative character. For the purpose of the addressed questions in this work, the parameter set, not affected by the PMCA stimulation, has just been taken over from [3, 4].

In section 4.1 the contradiction between the pump affinity for the calmodulin-calcium complex arising naturally from the approach in chapter 2 and the experimentally established value has been discussed. Starting with an affinity of the h2b isoform of $K_d = 0.5$ nM [1, 18, 19, 32, 43, 48, 53, 59] it is, however, possible to describe the measured stimulation data of the h2b isoform by presuming experimental conditions corresponding to a calmodulin-calcium binding at a KCl concentration of 100 mM (see figure 4.2, 4.3 and 4.4). The actual formation of the calmodulin-calcium complex remains to be questioned and deserves further investigations. The marked importance of the correct description is suggested in table 3.1. The macroscopic dissociation constants between the calmodulin-calcium complex and free calcium vary tremendously over a range of two decades in dependence of the present KCl concentration. Therefore, in the concerted interaction of calcium, calmodulin-calcium complexes and target proteins the correct description of calcium buffering by calmodulin is essential for the exact reproduction of the whole calcium-calmodulin dependent signal cascade.

Other possibilities to reconcile the PMCA pump stimulation model approach

with the given affinity of the pump for the X_4 complex is a higher total calmodulin concentration M_0 during the measurements of Caride *et al.*. But there are no obvious reasons not to rely on the stated concentration of $M_0 = 0.117 \mu\text{M}$. Also assuming a thermodynamical bath at M_0 cannot be justified regarding the experimental setup which suggests an equal total amount of calcium and calmodulin in the medium where the measurement took place ([1] and private communication with Ariel Caride). A thermodynamical bath at M_0 stands for a high total available calmodulin quantity compared to calcium such that M_0 is the available free calmodulin concentration throughout the whole measurement. This assumption conflicts with the addition of enough CaCl_2 to obtain the desired free calcium concentration, since by forming calmodulin-calcium complexes the free calmodulin concentration is reduced. This is the case if both reactants are available in similar quantities apart from the present concentrations.

The effect of calcium and calmodulin dependent facilitation and inactivation of Voltage Directed Calcium Channels (VDCC) resembles the here discussed phenomena of PMCA pump stimulation. Lee *et al.* (2000) and Zühlke *et al.* (1999) [60, 61, 62] measured a facilitation and later inactivation of P/Q- and L-type VDCC's as an effect dependent on the present calcium and calmodulin concentration. However, the modulation of Voltage Directed Calcium Channels is poorly understood and controversially discussed. Considering the overall transmembrane current, the PMCA pump stimulation meaning a facilitation of calcium extrusion would lead to the same outcome as an inactivation of VDCC's, *i.e.* a reduction of calcium influx current. This VDCC modulation can be blocked by buffering free intracellular calcium or calmodulin, as it is the case for the PMCA stimulation procedure. Nevertheless, the here presented investigations clearly exclude the PMCA pump stimulation as an alternative explanation for the facilitation of influx through Voltage Directed Calcium Channels. The involved time scales deliver the most striking argument against that comparison. While during the experiments of Lee *et al.* and Zühlke *et al.* the facilitation of calcium influx could be measured during the application of a 100 Hz action potential train lasting for one second, the limitation of the velocity of the PMCA channel stimulation would not allow a measurable effect within that time window of elevated calcium concentration. Even if the evoked free intracellular calcium concentration is substantially larger during a 100 Hz stimulus compared to a 10 Hz stimulus as shown in figure 4.9, the formation of stimulated pump form is confined by the minimum half stimulation time $t_{\text{minstim}}^{(1/2)} = 11.6 \text{ s}$ for the h2b isoform and $t_{\text{minstim}}^{(1/2)} = 28.5 \text{ s}$ for the h4b isoform as shown in section 3.4.3.

It can be stated that the modelling of an effective calcium buffering causes no problems. One simply has to assure a sufficient amount of calcium to be bound. The purpose of this work, however, is to examine a stimulation effect in the subsequent step beyond calcium buffering. Therewith the modelling of calcium buffering and target attachment has to become precise and has to account

for several aspects. Firstly, the challenge is to include other competing calcium buffering proteins beside calmodulin to obtain the actual available amount of calmodulin-calcium complexes at every present calcium concentration. Also the particular importance of a physiologically correct description of calcium buffering by calmodulin could be shown (see section 4.1 and 4.2). Secondly, the distributions and characteristics of X_4 complex target proteins strongly influence the kinetics of the calcium-calmodulin dependent target activation (see figure 4.5). The investigations in section 4.2 revealed that small deviations in the amount or affinity of either reactant cause tremendous differences in the resulting homeostasis of free and bound quantities. In conclusion, the whole signalling chain happens in a well concerted and fine tuned manner and deserves further investigations supported by experiments aiming to measure concrete aspects of the calmodulin-calcium dependent target activation cascade in real cells.

Taking this into account and regarding the attachment and the movement of the calmodulin-calcium complex and the pure calmodulin protein, diffusion receives a not negligible importance. Without much doubt, diffusion might significantly delay the whole process of target activation by calmodulin. With respect to that, the extension of the presynaptic calcium dynamics model in order to describe the spatiotemporal diffusion of the participating reactants is currently in progress.

With regard to the question addressed in this work, whether the stimulation of the Plasma Membrane Calcium pump plays a role as a possible expression state of short-term modifications or in the induction pathways towards long-term potentiation/depression the investigations enable to resume several statements. The defined model makes it furthermore possible to study the PMCA pump involvement in calcium transients evoked by LTP and LTD stimulation protocols

The connection between an increase in the postsynaptic calcium concentration and the triggering of long-term potentiation has been pointed out in section 2.3. This elevation can be induced by a number of ways. However, the most convenient way to induce LTP is to deliver a high frequency train of action potentials (typically a train of 50 - 100 action potentials at 100 Hz) to the presynaptic terminal [20]. Although the patterns of induction via this pathway to LTP can vary the persistent times need not to exceed the range of several seconds. The outcome of this work establishes that the PMCA stimulation neither affects the presynaptic signal transmission leading to exocytosis during such a high frequency train nor can the pump be stimulated to a significant degree within the seconds of higher calcium exposure.

In its stimulated form the facilitation of the calcium extrusion through PMCA pumps can lead to a measurable effect as shown in figure 4.8 and 4.9. Furthermore, it has been suggested that a recurring exposure to intracellular calcium accumulations over minutes can lead to significant formations of stimulated pump fractions (see section 4.3). Such low frequency trains of action potentials occur to be depressing protocols of the synapse, since during the signal transduction the

postsynaptic calcium concentration does not exceed the threshold for inducing LTP which can thus lead in turn to long-term depression (LTD) [21]. But beside a permanent train of low frequency stimuli the stimulation of PMCA pumps can be provoked by every sustained protocol of stimuli in which the interval between the calcium elevations is sufficiently short compared to the relaxation of PMCA pumps in order to accumulate stimulated pump form. That is, if the time gap is large, *i.e.* the emerged fraction of f_{stim} decays to resting stimulation level of 10 %, subsequent calcium concentration raises are faced with initial PMCA activity conditions. In contrast, if the action potential interval falls below a characteristic time the PMCA pump can display memory of past calcium spikes. Such a characteristic time is represented by the minimum half relaxation time of the PMCA pump ($t_{minrelax}^{(1/2)} = 45.6$ s for the h2b isoform and $t_{minrelax}^{(1/2)} = 20$ s for the h4b isoform).

The facilitation of the calcium extrusion from neurons influences the accumulation of intracellular presynaptic calcium quantities as response to single action potentials or during the application of a high frequency stimuli. Especially in the second case, if the emerging base line is responsible for the triggering of subsequent intra- and extracellular signal cascades at the presynaptic terminal, the decrease of the elevated calcium level might inhibit or even block the related mechanisms. Since the emerging base line is connected with LTP stimulation protocols, a high stimulation level of PMCA pumps could inhibit the induction of the potentiated state by these stimuli. In this regard, the PMCA pump stimulation seems to express a short-term depression state on the level of the presynaptic terminal. Even the calcium response to a single action potential is affected dependent on the degree of PMCA pump stimulation. If and how the modification at the relaxing face of a single calcium answer affects the molecular machinery of the synapse cannot be answered with the current knowledge of processes within the neuron.

However, since the molecular mechanisms associated with presynaptic calcium elevations are poorly understood the here discussed consequences of PMCA pump stimulation on the shape of intracellular calcium transients have to be seen as conjectures and suggestions. Corresponding experiments could elucidate the importance of the proposed effects for presynaptic calcium homeostasis and verify the theoretical predictions concerning the influence of PMCA stimulation on the shape of calcium elevations.

The capability of the Plasma Membrane Calcium pump to sense the frequency and intensity of calcium signals has been the subject of intensive investigations in this work. It has been shown that the PMCA pump uses this informations to determine its role in shaping subsequent presynaptic calcium signals. The presented lines emphasise the physiological relevance of the PMCA stimulation for plasticity effects on the level of synapses.

Acknowledgement

I would like to thank Prof. Dr. Gerhard Soff for offering me the opportunity to work in his group and supporting this work.

I am deeply grateful to Dr. Michael Meyer-Hermann who was always well disposed for discussions and questions on the field of theoretical biophysics. My work on this diploma thesis gained a lot from his comments, ideas and suggestions. Furthermore, I personally enjoyed very much the friendly and pleasant cooperation beyond physics with him. I want to express my gratitude to Frido Erler for teaching me neurobiophysics. I mainly owe him the understanding of neuronal processes and the C++ program code describing it. His friendly and bright mind delighted the interworking on neurons a lot. Not to mention the remaining members of the Research Group Theoretical Biophysics, I am thankful for helpful discussions on various subjects with them.

Furthermore I want to address my thanks to the staff of the Institute for Theoretical Physics. I especially appreciated the nice and friendly atmosphere with the secretaries Gundula Schädlich, Gudrun Latus and Ute Wächtler.

It was a pleasure for me to share the office with my friend Ingmar Glauche. We spent a lot of time discussing ad hoc networks - the topic Ingmar is working on -, neurobiophysics as well as everything which concerns the world. I would like to thank Ingmar for his support and for the great time together.

I am obliged to Jakob Schweizer and Mathias Kuhnt for encouraging me by their friendship which I very much appreciate. Jakob Schweizer furthermore always showed interest in my research work and helped me on diverse biophysical topics.

I want thank the German Federal Ministry of Education and Research for granting me during my whole studies.

Finally, I want to thank my parents Marianne and Klaus-Peter Graupner for making my studies possible, for always supporting me, mentally and financially, and encouraging me not only during my time at the Technische Universität Dresden.

These people and my friends which have not been mentioned here altogether contributed for letting become the time of my diploma thesis the most interesting and most beautiful time and conclusion of my physics studies at the Technische Universität Dresden.

Bibliography

- [1] A. J. Caride, A. R. Penheiter, A. G. Filoteo, Z. Bajzer, A. Enyedi, and J. T. Penniston, *J Biol Chem* **276**, 39797 (2001).
- [2] M. Graupner, F. Erler, and M. Meyer-Hermann, submitted, manuscript available at: [arXiv:physics/0306121] (2003).
- [3] F. Erler, M. Meyer-Hermann, and G. Soff, submitted, manuscript available at: [arXiv:physics/0203014] (2003).
- [4] M. Meyer-Hermann, F. Erler, and G. Soff, *Presynaptic calcium dynamics of neurons in answer to various stimulation protocols*, In: A. Deutsch, M. Falcke, J. Howard, W. Zimmermann (eds.), in press (Birkhäuser, Basel, 2003).
- [5] Z. W. Hall, *An introduction to molecular neurobiology* (Sinauer, Sunderland, 1992).
- [6] C. Hammond, *Cellular an molecular neurobiology* (Academic Press, Paris, 1996).
- [7] E. R. Kandel, J. H. Schwartz, and T. M. Jessell, *Neurowissenschaften - Eine Einführung* (Spektrum, Heidelberg, 1996).
- [8] L. G. Wu, J. G. Borst, and B. Sakmann, *Proc Natl Acad Sci U S A* **95**, 4720 (1998).
- [9] J. C. Magee and D. Johnston, *Journal of Physiology* **487** (1995).
- [10] F. Bezanilla, *Physiol Rev* **80**, 555 (2000).
- [11] B. Hille, *Ionic channels of excitable membranes* (Sinauer, Sunderland, 1992), 2nd ed.
- [12] W. J. Pottorf, S. P. Duckles, and J. N. Buchholz, *J Auton Pharmacol* **20**, 63 (2000).
- [13] S. Linse, A. Helmersson, and S. Forsen, *J Biol Chem* **266**, 8050 (1991).
- [14] A. Schiegg, W. Gerstner, and J. L. v. Hemmen, *J Neurphysiol* **74**, 1046 (1995).

- [15] H. J. Koester and B. Sakmann, *J Physiol* **529**, 625 (2000).
- [16] K. Luby-Phelps, M. Hori, J. M. Phelps, and D. Won, *J Biol Chem* **270**, 21532 (1995).
- [17] M. G. Tansey, K. Luby-Phelps, K. E. Kamm, and J. T. Stull, *J Biol Chem* **269**, 9912 (1994).
- [18] A. Persechini and B. Cronk, *J Biol Chem* **274**, 6827 (1999).
- [19] N. L. Elwess, A. G. Filoteo, A. Enyedi, and J. T. Penniston, *J Biol Chem* **272**, 17981 (1997).
- [20] T. V. P. Bliss and G. L. Collingridge, *Nature* **361**, 31 (1993).
- [21] R. C. Malenka and R. A. Nicoll, *Science* **285**, 1870 (1999).
- [22] M. Frerking and M. Wilson, *Curr Opin Neurobiol* **6**, 395 (1996).
- [23] D. K. Patneau, *J Neurosci* **10**, 2385 (1990).
- [24] A. K. McAllister and C. F. Stevens, *Proc Natl Acad Sci U S A* **97**, 6173 (2000).
- [25] J. Lisman, *Trends Neurosci* **17**, 406 (1994).
- [26] J. H. Williams, *J Lipid Mediat Cell Signal* **14**, 331 (1996).
- [27] K. M. Turner, R. D. Burgoyne, and A. Morgan, *Trends Neurosci* **22**, 459 (1999).
- [28] A. Lewit-Bentley and S. Rety, *Curr Opin Struct Biol* **10**, 637 (2000).
- [29] D. Chin and A. R. Means, *Trends Cell Biol* **10**, 322 (2000).
- [30] S. W. Vetter and E. Leclerc, *Eur J Biochem* **270**, 404 (2003).
- [31] H. Sun and T. C. Squier, *J Biol Chem* **275**, 1731 (2000).
- [32] T. Meyer, P. I. Hanson, L. Stryer, and H. Schulmann, *Science* **256**, 1199 (1992).
- [33] A. R. Penheiter, A. J. Caride, A. Enyedi, and J. T. Penniston, *J Biol Chem* **277**, 17728 (2002).
- [34] H. P. Adamo and M. E. Grimaldi, *Biochem J* **331**, 763 (1998).
- [35] A. J. Caride, A. G. Filoteo, N. L. Elwess, A. K. Verma, A. Enyedi, Z. Bajzer, and J. T. Penniston, *J Biol Chem* **274**, 35227 (1999).

- [36] H. Bisswanger, *Enzyme kinetics* (Wiley, Weinheim, 2002), 3rd ed.
- [37] J. T. Penniston and A. Enyedi, *J Membr Biol* **165**, 101 (1998).
- [38] E. Carafoli, *Annu Rev Physiol* **53**, 531 (1991).
- [39] A. Persechini, P. M. Stemmer, and I. Ohashi, *J Biol Chem* **271**, 32217 (1996).
- [40] A. Persechini, K. Yano, and P. M. Stemmer, *J Biol Chem* **275**, 4199 (2000).
- [41] M. Juhaszova, P. Church, M. P. Blaustein, and E. F. Stanley, *Eur J Neurosci* **12**, 839 (2000).
- [42] L. Zylinska and M. Soszynski, *Acta Biochim Pol* **47**, 529 (2000).
- [43] D. Guerini, *Cell Tissue Res* **292**, 191 (1998).
- [44] T. P. Stauffer, D. Guerini, and E. Carafoli, *J Biol Chem* **270**, 12184 (1995).
- [45] E. Carafoli, *J Biol Chem* **267**, 2115 (1992).
- [46] C. Tanford, J. A. Reynolds, and E. A. Johnson, *Proc Natl Acad Sci U S A* **84**, 7094 (1987).
- [47] M. R. Webb, *Proc Natl Acad Sci U S A* **89**, 4884 (1992).
- [48] W. Ba-Thein, A. J. Caride, A. G. Filoteo, A. Enyedi, K. Paszty, C. L. Croy, and J. T. Penniston, *Biochem J* **356**, 241 (2001).
- [49] A. K. Verma, A. Enyedi, A. G. Filoteo, E. E. Strehler, and J. T. Penniston, *J Biol Chem* **271**, 3713 (1996).
- [50] J. Keener and J. Sneyd, *Mathematical Physiology*, vol. 8 (Springer, New York, 1998).
- [51] H. Hilfiker, D. Guerini, and E. Carafoli, *J Biol Chem* **269**, 26178 (1994).
- [52] B. Alberts, D. Bray, J. Lewis, M. Raff, K. Roberts, and J. D. Watson, *Molekularbiologie der Zelle* (VCH, Weinheim, 1995), 3rd ed.
- [53] A. Enyedi, A. G. Filoteo, G. Gardos, and J. T. Penniston, *J Biol Chem* **266**, 8952 (1991).
- [54] V. A. Snitsarev and C. W. Taylor, *Cell Calcium* **25**, 409 (1999).
- [55] A. Klishin, M. Sedova, and L. A. Blatter, *Am J Psychol* **274**, C1117 (1998).
- [56] D. M. Bautista, M. Hoth, and R. S. Lewis, *J Physiol* **541**, 877 (2002).

- [57] T. P. Stauffer, H. Hilfiker, E. Carafoli, and E. E. Strehler, *J Biol Chem* **268**, 25993 (1993).
- [58] A. G. Filoteo, N. L. Elwess, A. Enyedi, A. J. Caride, H. H. Aung, and J. T. Penniston, *J Biol Chem* **272**, 23741 (1997).
- [59] M. N. Teruel, W. Chen, A. Persechini, and T. Meyer, *Curr Biol* **10**, 86 (2000).
- [60] A. Lee, T. Scheuer, and W. A. Catterall, *J Neurosci* **20**, 6830 (2000).
- [61] R. D. Zühlke, G. S. Pitt, K. Deisseroth, R. W. Tsien, and H. Reuter, *Nature* **399**, 159 (1999).
- [62] A. Lee, R. E. Westenbroek, F. Haeseleer, K. Palczewski, T. Scheuer, and W. A. Catterall, *Nature Neurosci* **5**, 210 (2002).

Declaration

This diploma thesis is the result of my own work except where explicit reference is made to the work of others. This work has not been submitted for another qualification to this or any other examination board.

Michael Graupner

Dresden, July 31th 2003

Erklärung

Hiermit bestätige ich, dass ich diese Diplomarbeit ohne unzulässige Hilfe Dritter und ohne die Benutzung anderer als der angegebenen Hilfsmittel angefertigt habe. Die aus fremden Quellen direkt oder indirekt übernommenen Gedanken sind als solche kenntlich gemacht. Die Arbeit wurde bisher weder im Inland noch im Ausland in gleicher oder ähnlicher Form einer anderen Prüfungsbehörde vorgelegt.

Michael Graupner

Dresden, 31. Juli 2003